



Norwegian University of
Science and Technology

Wind Powered Water Injection Systems for Oil and Gas Applications

Jesus Ernesto Silva Diaz

Master of Science in Electric Power Engineering

Submission date: June 2016

Supervisor: Elisabetta Tedeschi, ELKRAFT

Norwegian University of Science and Technology
Department of Electric Power Engineering

SUMMARY

The project is focused on the modelling and control of water injection systems (WIS) in oil and gas (O&G) facilities powered by wind turbines. The use of wind power for WIS has been presented by DNV-GL as an sustainable, environmentally friendly solution, while at the same time keeping is economic feasibility according to initial findings [1]. The fundamental assumption for presenting this concept is related to the flexibility of WIS to increase and decrease the load demand depending on the available power. Some of challenges identified are the frequency and power balance, wind intermittency and impacts on the system stability and the effective load control. This work addressed these challenges by a mathematical modelling of the system components and by testing the assembled configurations in different wind scenarios, exploring the systems response on the mentioned variables of interest.

The first part of the thesis works with two models. The hybrid WIS model and the stand-alone WIS model. The hybrid WIS configuration is a representation of a dual system that uses a gas turbine and a wind turbine. In other words, the hybrid model is a representation of an O&G platform that integrates wind power. The use of wind power for WIS in O&G platforms is an alternative used proposed here for reducing CO_2 emissions, increasing installed capacity and wind penetration without compromising the system operation. The ordinary approach has been to assume an inflexible load and a predominance of gas units. The gas turbines must be able to provide for the demand at each instant in case of wind power deficit, leading to large dependency and frequent on and off cycles on the generators. The new approach developed here, is to incorporate load control on the existing system and to understand the advantages of load management, when dealing with wind power fluctuations. The load control is applied to specific equipment as for example, injection pumps or non-priority loads. The hybrid model is composed of four subsystems. The wind turbine, the gas turbine, the fixed and flexible loads and the dump load subsystem. The wind turbine subsystem is composed of a wind turbine, made of a direct-drive permanent magnet synchronous generator (PMSG), a rectifier, a crowbar protection circuit, an inverter and a filtering inductance. The gas turbine subsystem drives a synchronous generator with an excitation circuit. The fixed load is a three-phase balance load defined in terms of active and reactive power and a flexible load controlled by an external power balance loop. Finally, the dump load subsystem is represented by a regulating resistor bank. The second dynamic model is composed of five subsystems, it is called here stand-alone WIS configuration. The wind turbine, the synchronous flywheel, the fixed load, the dump load and

a variable speed drive connected to an induction motor. This configuration is a double back-to-back system proposed in a previous specialization project. The new component is the synchronous flywheel that sets the system frequency, and is also responsible for providing active and reactive power to balance the network. Another project contribution is the full implementation of the VSD with pump torque profile as mechanical load.

The generalized VSC control framework is used for developing control of the different IGBTs. Firstly, a simplified control of rotor speed and maximum power extraction from the wind turbine on the rectifier is implemented. Secondly, the inverter control objective is on the DC voltage and to be compliant with the grid requirements. Thirdly, the dump load control was based on frequency measurement and varying conductance changes in the ballast load. Finally, the second back-to-back converter (VSD) implements an improved field-oriented control strategy with respect to the specialization project. The improvement consists of the installation of front-end rectifier that allows a bidirectional power flow.

The second part of the thesis implements an energy model in HOMER (Hybrid Optimization of Multiple Energy Resources) Energy™. This model was developed as a validation for long-term assessment in a different time scale, wind resource evaluation in a specific region near to Trondheim, and as a feasibility test of load management for WIS. The dynamic simulations confirmed that it is possible for the load to *follow* the wind generation within its permissible operating range. This software is specialized in microgrids and energy studies. The study uses real wind profile downloaded from NASA surface meteorology database. The wind speed was measured at 50m above the earth surface, and it was corrected to the hub height. The measurements were monthly average values in a 10-year period. The system simulated consists of a wind turbine, a flexible load and a battery bank. The wind turbine is a 6MW turbine, with a load of 3.5MW of peak demand and a 500kW battery bank. The load profile was synthesized following the generation curve of the wind turbine, representing an adaptable load. Two cases were run on HOMER, one for high wind (12m/s) and another for low wind condition (8.66m/s). The simulations consisted in sensitivity and optimization analyzes. Under the user-specified constraints, the program optimized at the lowest total net present cost, varying fuel cost, number of batteries, number of wind turbines, etc. and then selects the best configuration. Besides obtaining useful technical information, long-term energy assessment studies are required for determining the economics of a particular project. However, due to lack of investment costs, economic analyses are out of scope in this report.

ACKNOWLEDGEMENTS

I would like to express my gratitude to Professor Elisabetta Tedeschi for her support, guidance and comments throughout this project. I would also like to thank my parents Jesús and Milagros for their help and unconditional support in any goal I set in my life. Finally, I dedicate this work to my beloved sister Sorgalim that watches upon me from heaven.

Jesús Silva Diaz

Trondheim, Norway

14th June, 2016

CONTENTS

SUMMARY	I
ACKNOWLEDGEMENTS	III
LIST OF FIGURES	VII
LIST OF TABLES	X
1 INTRODUCTION	1
1.1 PROBLEM BACKGROUND.....	1
1.2 MOTIVATION	2
1.3 MAIN OBJECTIVE.....	4
1.4 SPECIFIC OBJECTIVES.....	4
1.5 METHODOLOGY.....	5
1.6 LIMITATION OF SCOPE.....	7
1.7 REPORT OUTLINE.....	8
2 SYSTEM COMPONENTS	9
2.1 WIND TURBINE.....	9
2.2 WATER INJECTION SYSTEM.....	11
2.2.1 <i>Water Injection Methods</i>	12
2.2.2 <i>Water injection pumps</i>	14
2.3 GAS TURBINE (GT)	15
2.4 LOADS	15
2.5 SUBSEA POWER SYSTEM	16
3 SYSTEM CONFIGURATIONS	18
3.1 HYBRID WIS CONFIGURATION	18
3.2 STAND-ALONE WIS CONFIGURATION	20
4 SYSTEM MODELLING	23
4.1 OIL AND GAS PLATFORM.....	23
4.2 FIXED PQ LOAD	23
4.3 FLEXIBLE LOAD.....	23

4.4	SUBMARINE CABLE	24
4.5	OIL PLATFORM SYNCHRONOUS GENERATOR	25
4.6	OIL PLATFORM GAS TURBINE	26
4.7	DUMP LOAD	26
4.8	WIND TURBINE	28
4.9	PITCH CONTROL	29
4.10	PERMANENT MAGNET SYNCHRONOUS GENERATOR (PMSG).....	30
4.11	GENERATOR SIDE CONTROL	32
4.12	CROWBAR PROTECTION.....	33
4.13	GRID SIDE CONTROL	33
4.14	INDUCTION MOTOR	34
4.15	PUMP LOAD PROFILE	35
4.16	VARIABLE SPEED DRIVES	35
4.16.1	Control schemes of Induction Motor Drives	36
4.16.2	Field Oriented Control (FOC)	36
4.16.3	Grid Side Rectifier.....	37
4.16.4	Motor Side Inverter	38
4.16.5	Control of back-to-back VSD: Test Case.....	39
5	STUDY CASES: HYBRID WIS MODEL.....	43
5.1	CASE 1: FIXED LOAD	43
5.1.1	Wind Turbine (WT): Hybrid WIS	43
5.1.2	Gas Synchronous Generator (GT)	45
5.1.3	Active and reactive power	47
5.1.4	Overall Stand-Alone System. Case 1	48
5.2	CASE 2: FIXED AND FLEXIBLE LOAD	49
5.2.1	Gas Synchronous Generator	50
5.2.2	Overall Stand-Alone System. Case 2	51
5.3	DISCUSSION OF RESULTS	53
6	STUDY CASES: STAND-ALONE WIS TOPOLOGY.....	54
6.1	CASE 1: FIXED LOAD AND FLEXIBLE LOAD	54
6.1.1	Wind Turbine Stand-Alone.....	54

6.1.2	<i>Synchronous Flywheel Stand-Alone</i>	56
6.1.3	<i>Active and reactive power</i>	57
6.1.4	<i>Overall Stand-Alone System. Case 1</i>	60
6.2	CASE 2: FIXED LOAD AND VSD PUMP	61
6.2.1	<i>Variable Speed Drive (VSD)</i>	61
6.2.2	<i>Overall Stand-Alone back-to-back System. Case 2</i>	63
6.3	DISCUSSION OF RESULTS	65
7	ENERGY WIS MODEL	66
7.1	SYSTEM OVERVIEW	66
7.2	WIND TURBINE.....	67
7.3	WIND PROFILE.....	68
7.4	LOAD PROFILE.....	70
8	ENERGY WIS STUDY CASES	73
8.1	CASE 1: HIGH WIND SCENARIO (12M/s).....	73
8.1.1	<i>Wind Turbine</i>	73
8.1.3	<i>Dumped Load (Excess Energy)</i>	77
8.1.4	<i>System overall results</i>	78
8.2	CASE 2: NORMAL WIND SCENARIO (8.66M/s)	79
8.2.1	<i>Wind Turbine</i>	79
8.2.2	<i>Dump Load (Excess Energy)</i>	82
8.2.3	<i>System overall results:</i>	84
9	CONCLUSIONS AND FURTHER WORK	86
9.1	HYBRID WIS MODEL	86
9.2	STAND-ALONE WIS MODEL	86
9.3	ENERGY WIS MODEL.....	87
9.4	FURTHER WORK.....	88
10	BIBLIOGRAPHY	90
11	APPENDICES	93

LIST OF FIGURES

Figure 1.1 Cost comparison of stand-alone system with gas raw seawater injection [11].....	3
Figure 1.2 Cost of traditional sol. including pipeline for injecting processed water [11]......	3
Figure 2.1 Foundation Deep Water [14].....	10
Figure 2.2 Hywind Scotland Pilot Park [15].....	11
Figure 2.3 WT Dimensions of Hywind Scotland [15]	11
Figure 2.4 Water injection methods [19].....	12
Figure 2.5 Water injection template Tyrihans Field [2]	13
Figure 2.6 Reservoir pressure development simulation [2].....	13
Figure 2.7 DNV-GL WinWin powered water injection [12].....	14
Figure 2.8 Sub-sea pumps types [20].	15
Figure 2.9 Subsea power system types and configurations [20].....	16
Figure 2.10 Subsea Power System [20].....	17
Figure 3.1 Hybrid system Oil and Gas platform connected to a wind offshore turbine.....	18
Figure 3.2 Single back-to-back detailed topology	20
Figure 3.3 Double back-to-back detailed topology.....	21
Figure 4.1 PI cable line model [22].....	24
Figure 4.2 Control block diagram SG Oil Platform	25
Figure 4.3 Speed controller of the thermal generator.....	26
Figure 4.4 Control scheme of dump load	27
Figure 4.5 Internal structure of dump load	27
Figure 4.6 Dependencies C_p of λ with different values β [25]	29
Figure 4.7 Power turbine characteristics with pitch angle ($\beta = 0^\circ$)	29
Figure 4.8 Block diagram of pitch controller.....	30
Figure 4.9 a) d-q system from abc system b) d-q axis of rotating machine [27]	31
Figure 4.10 Mechanical speed ω_{ref} reference block diagram.....	32
Figure 4.11 Control block diagram generator side converter	33

Figure 4.12 Control block diagram grid side converter	34
Figure 4.13 FOC high-level schematics [24]......	37
Figure 4.14 Block diagram FOC [24]......	38
Figure 4.15 Field Oriented control principle [24]......	38
Figure 4.16 VSD Dynamic Performance FOC	40
Figure 4.17 VSD Active and Reactive Power	41
Figure 4.18 VSD back-to-back DC Link.....	41
Figure 5.1 Hybrid Topology for WIS.....	43
Figure 5.2 PMSG stator currents and rotor speed.....	44
Figure 5.3 PMSG electromagnetic torque and wind speed	44
Figure 5.4 Wind turbine DC link voltage and control signal.....	45
Figure 5.5 Gas synchronous generator $V_{terminal}(pu)$ and $V_{fieldpu}$ voltages. Case 1	46
Figure 5.6 Gas synchronous generator $P_{gen}(pu)$ and $Q_{gen}(pu)$. Case 1	46
Figure 5.7 Active and reactive power wind turbine	47
Figure 5.8 Active and reactive gas turbine. Case1	48
Figure 5.9 Power Curves with Fixed Load. Case 1.....	48
Figure 5.10 System Frequency. Case 1	49
Figure 5.11 Gas synchronous Generator $V_{terminal}(pu)$ and $V_{fieldpu}$ voltages. Case 2 ...	50
Figure 5.12 Gas synchronous generator $P_{gen}(pu)$ and $Q_{gen}(pu)$. Case 2	50
Figure 5.13 Active and Reactive Power Gas Turbine. Case 2.....	51
Figure 5.14 Power Curves with Fixed Load. Case 2.....	52
Figure 5.15 System Frequency. Case 2	52
Figure 6.1 PMSG stator currents and rotor speed.....	54
Figure 6.2 PMSG electromagnetic torque and wind speed.	55
Figure 6.3 Wind turbine DC link voltage	56
Figure 6.4 Synchronous flywheel $P_{sg}(pu)$, $\omega_{sg}(pu)$ and wind speed. Case 1	57
Figure 6.5 Wind Turbine active and reactive power. Case 1.....	57

Figure 6.6 Flywheel $V_{terminal}(pu)$ terminal and field $V_{fieldpu}$ voltages. Case 1.....	58
Figure 6.7 Flywheel active and reactive power. Case 1	59
Figure 6.8 Dump load power and control. Case 1.....	60
Figure 6.9 Power curves with flexible load. Case 1	60
Figure 6.10 Variable Speed Drive curves.....	62
Figure 6.11 VSD Power curves.....	63
Figure 6.12 Power curves with VSD implementation. Case 2	63
Figure 6.13 System frequency with VSD implementation. Case 2.....	64
Figure 7.1 Project Location	66
Figure 7.2 System components	67
Figure 7.3 Wind turbine power curve.....	67
Figure 7.4 Monthly average wind speed data	68
Figure 7.5 Wind annual profile	68
Figure 7.6 Wind speed monthly averages.....	69
Figure 7.7 Wind speed histogram	69
Figure 7.8 Wind speed daily profile.....	70
Figure 7.9 Annual Load Profile	71
Figure 7.10 Generation-load tracking.....	71
Figure 7.11 AC primary load daily profile	72
Figure 7.12 AC primary load monthly averages.....	72
Figure 8.1 Electrical summary. Case 1.....	74
Figure 8.2 Monthly power output. Case 1	75
Figure 8.3 Power Output daily profile. Case 1	75
Figure 8.4 Power Output Cumulative Frequency. Case 1	76
Figure 8.5 Power Output Duration curve. Case 1	76
Figure 8.6 Excess electrical production monthly averages. Case 1	77
Figure 8.7 Excess electrical production cumulative frequency. Case 1	77

Figure 8.8 Excess electrical production duration curve. Case 1	78
Figure 8.9 Yearly power curves: power output, load and dump load. Case 1	79
Figure 8.10 Electrical summary. Case 2.....	80
Figure 8.11 Monthly power output. Case 2	80
Figure 8.12 Power Output daily profile. Case 2	81
Figure 8.13 Power Output Cumulative Frequency. Case 2	81
Figure 8.14 Power Output Duration curve. Case 2	82
Figure 8.15 Excess electrical production monthly averages. Case 2	83
Figure 8.16 Excess electrical production cumulative frequency. Case 2	83
Figure 8.17 Excess electrical production duration curve. Case 2	84
Figure 8.18 Yearly power curves: power output, load and dump load. Case 2.....	84
Figure 11.1 Clarke and Park Transformations [33].....	93
Figure 11.2 Schematic of the general system [34].....	94
Figure 11.3 Vector control principle [34].....	94
Figure 11.4 Stand Alone Complete Model	95

LIST OF TABLES

Table 2-1 System component for each studied case	9
Table 4-1 Medium Voltage VSD [29].....	36
Table 4-2 Comparison between control schemes [29].	36
Table 7-1 Load main characteristics	70
Table 8-1 Wind turbine simulation summary. Case1	73
Table 8-2 Wind turbine simulation summary. Case 2.....	79

1 INTRODUCTION

1.1 PROBLEM BACKGROUND

The oil and gas industry is facing numerous challenges mainly in terms of remaining hydrocarbon reserves, low product prices and compliance with stricter environmental regulations. In the North Sea, oil companies are in active search for improving production techniques and increasing the rate of oil recovery. Numerous fields have been operating for several decades, and their production is declining, making it difficult to keep their economic viability. As a response, different secondary recovery methods have been developed one is water injection. The objective of a WIS is to provide energy to the feeble marginal field, extending its productive lifespan or productivity by recovering as much oil as possible by injecting water and pushing oil out. However, these injection templates must be specifically placed in order to provide the expected results. The conventional way of injecting pressurized water is through large controlled motors. These machines are usually on the O&G platform or sometimes placed on the sea bottom. In either case, kilometers of pipelines must be laid down if treated water is required. If raw seawater is allowed, long cables should be connected from the host platform to the injection site. For example, the Tyrihans field developed by Statoil [2] in the Norwegian Continental Shelf injects raw seawater, but a long cable with a step-out distance of 31km is connected from the host platform. Long subsea cables confront various technical challenges and they are extremely costly investments.

Offshore O&G facilities are conventionally powered by gas turbines. They release annually thousands of tons of CO_2 and oxides nitrates SO_x to the atmosphere. Offshore gas turbines have low efficiency and are a main source of this type of emissions in Norway [3]. Maintenance costs and in many cases short remaining lifetime are issues of main importance among O&G operators. Simultaneously, more energy is needed as result of expanding operations or because of the implementation of enhanced recovery methods, all of which are highly energy intensive. Another structural problem for adding additional gas turbines units on the existing platforms are space and weight limitations. Therefore, cleaner, compact and scalable solution are called for in the industry.

On the other hand, offshore facilities in the North Sea are located in areas with abundant and constant wind resources. Some studies [4]–[8], have determined that is suitable to integrate

wind power to O&G platforms. A key technological aspect is the development of floating wind turbines as the Hywind from Statoil [9]. These structures can be used in water depths between 100-200m, which is typical in platform depths [8]. Among other technology drivers pushing forward this innovation are the high power rating of electronic converters, MW direct drive permanent magnet synchronous generators (PMSG), new light materials and optimized design for large offshore wind turbines. From the economic point of view, large turbines are more profitable for offshore applications instead of several turbines of smaller rating due to the capital expenditure (CAPEX) and operation and maintenance expenditure (OPEX) [1]. Operational and maintenance costs are huge in conventional gas turbines due mainly to fuel prices and frequent unit maintenance. In addition, different positive incentives exist, for example, the CO_2 tax and stricter policy regarding prohibition of processed water disposal directly to the sea.

Another aspect of vital importance for the concept proposed here is the flexibility of WIS. By coupling variable speed drives (VSD) to induction motors is possible to vary the load. In fact, pressurization of reservoirs can take up weeks; therefore, a fixed injection rate is not mandatory. When using a non-dispatchable source of energy as wind power, is advantageous to have ways of controlling the load instead of only controlling the generation. This has been the foundation for DNV-GL WinWin [10] proposal of using wind power for WIS.

The power system of this application is defined as islanded or stand-alone solution. Stand-alone systems are off-grid networks. As such, they must set their own system frequency and voltage, which is challenge in terms of system operation and control. Another, key aspects include active and reactive power balance, frequency stability and control. This project addresses power system requirements, pump system flexibility and operation of the combined wind/water injection configuration under realistic scenarios. Modelling and test cases are presented in dynamic and long-term energy simulations as to assess technical feasibility of this innovation.

1.2 MOTIVATION

According to DNV-GL technical and economic feasibility study reported in [11], a base system which consisted of a 6MW floating wind turbine, and costs of operation and maintenance during a 10-year period was compared to the costs of a conventional raw seawater injection supplied from a gas turbine via an umbilical at various step-out distances. The investigation indicated that the main CAPEX (capital expenditure) contributor for the traditional system was the cable cost, and during its lifetime, the OPEX (operation expenditure) was essentially fuel costs and

maintenance costs to a lesser extent. The break-even distance was approximately 30 km, as seen from the business case results in Figure 1.1.

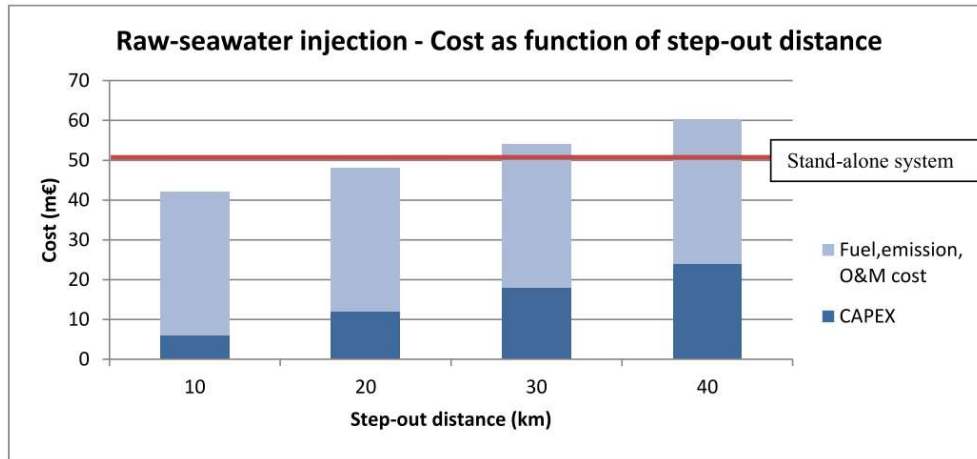


Figure 1.1 Cost comparison of stand-alone system with gas raw seawater injection [11]

A second business case was also presented in [11], considering a pipeline with processed water from the host platform to the injection site. As mentioned before some formations required injection of processed water from the water treatment plant on the host platform, requiring several kilometers of costly pipelines. When considering the pipeline cost, the investment was estimated to be 150 million €, Figure 1.2 [11]. Resulting in almost three times the amount compared to the stand-alone solution, not considering the expenses of a subsea water treatment plant.

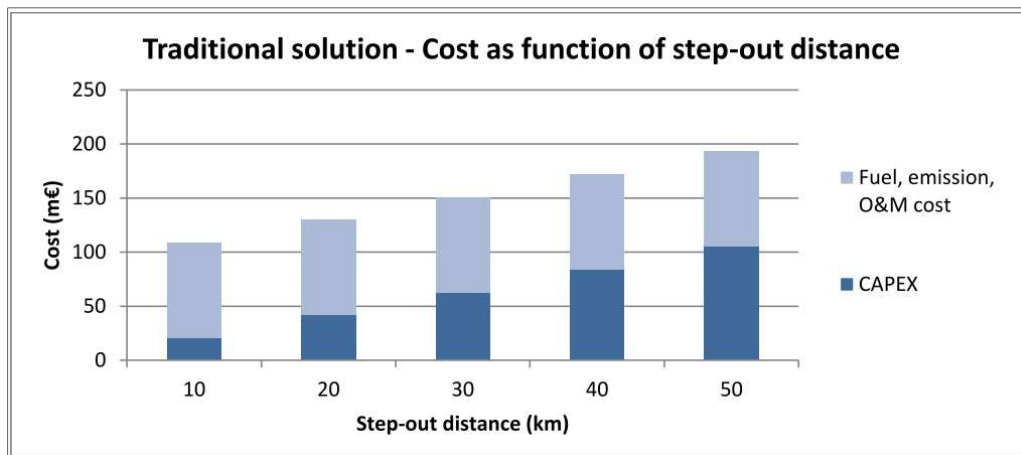


Figure 1.2 Cost of traditional sol. including pipeline for injecting processed water [11].

These promising economical figures in the business cases, along with the results of the initial technical assessment, has prompted DNV-GL and their collaborators to revise this project in more detailed, leading to this work.

1.3 MAIN OBJECTIVE

The main objective of this thesis is to develop dynamic and energy models for evaluation of water injection systems (WIS) powered by a wind turbine or by a suitable combination of thermal and wind power.

1.4 SPECIFIC OBJECTIVES

Hybrid WIS Model

- To build and implement a model of a variable speed wind turbine based on steady state power curves. Including a direct-drive permanent magnet synchronous generator with several poles and gearless mechanism.
- To control dynamically the rotor speed and to calculate a reference speed for maximum power extraction according to power curves, limiting the mechanical and power output from the wind turbine through a proportional pitch controller. Including regulation of the rotor-side converter by controlling the active rectifier through PI speed and current PI controllers.
- To protect the *DC*-link using a crowbar circuit, limiting overvoltages during transient or wind gust conditions. To control the grid-side converter by regulating the *DC*-link using a PI voltage regulator, and a PI regulator to control transferred current to the system.
- To implement a gas turbine model, an exciter circuit type 1 IEEE for active and reactive power control of a synchronous generator.
- To balance the system active power and frequency by adjusting the impedance/conductance of a dump load. Including the definition of a fixed load and a flexible controllable load based on energy balance loops.

Stand-Alone WIS Model

- To create voltage and frequency reference through a synchronous flywheel, and contributing to balance the system through active and reactive power absorption and injection.
- To define a Variable Speed Drive (VSD) with an active-front-end rectifier control strategy with bi-directional energy exchange and regenerative braking. This comprises the implementation of field-oriented control strategy on the VSD, with decoupled torque

and speed loops. Finally, definition of a pump load profile is required to emulate mechanical torque of a centrifugal injection pump.

Energy WIS Model

- To define a stand-alone WIS system for long-term energy studies consisting of a wind turbine, a flexible load and a battery bank.
- To synthesize load profile based on generation follow-up strategy.
- To process wind data for resource assessment in terms of daily, monthly averages and annual profile and speed histogram.
- To determine wind turbine power curves, daily, monthly and cumulative frequency curve.
- To compare energy produced, consumed and dumped for system overall evaluation.

1.5 METHODOLOGY

The models developed have been as realistic as possible in order to reflect the system behavior accurately. In order to achieve the research goals, two different kinds of programs were used. The first set of models were developed in MATLAB ®/Simulink™ using the power system toolbox. This programming language is based on graphical building blocks, within the MATLAB ® environment; some functions were developed in order to assist in formatting the signals generated on the models.

The approach has been to split up the entire system into smaller subsystems. Afterwards, they were tested individually and later integrated, in a bottom-up strategy. There are five recognizable parts, the wind turbine subsystem, the gas turbine subsystem, the dump load and conventional loads (fixed or flexible), and finally the variable speed drive subsystem. All of the basic components were available in the Power System Simulink™ library.

The variable speed WT subsystem was tuned by setting up the base wind speed, generator power, mechanical power and base rotational speed. The inputs were wind speed, generator speed and pitch angle. The pitch controller was a proportional regulator that works in the event of sudden rotor speed acceleration during wind gusts or by limiting the rotor speed due to a sudden load shedding. The rotor-side controller was implemented with two control loops. The reference rotor speed was calculated as proportional to base wind speed as to maximize power extraction following the wind turbine power curves. The reference speed was measured against the measured speed, and it is fed into a PI controller, which in turn generated the reference

stator current in the dq -plane. The second control loop is a faster PI current controller measuring the stator current against its reference value.

The crowbar protection circuit consisted of an on-off relay with upper and lower threshold values for the DC -link. The acceptable band was 15%, higher values triggered an ideal switch connected in series with a low impedance path. This overvoltage protection was meant to be activated during transients or when the voltage was out of valid range.

The grid-side converter was regulated using two cascaded control loops. The first loop was a voltage PI regulator that generated a quadrature stator current reference, the direct component was set to zero for avoiding reactive power injection and keeping voltage close to unity on the DC link. The second loop was a faster PI current controller, which injected power to the system under the voltage and frequency requirements by synchronizing the pulses.

The second subsystem was the gas turbine composed of the gas turbine itself, a synchronous generator and a type 1 IEEE exciter. The GT implemented was based on a thermal generator transfer function. Synchronous generator and exciter were available on the power system library in per unit. Some parameters were changed as to dimension to the power requirements.

The third subsystem was the dump load. The dump load acted as a balancing element burning excess of energy by measuring the system frequency. A phase lock loop (PLL) measured the system frequency generated a cumulative signal that triggered different admittance values, as to increase or decrease a bank of resistors. Some mechanical power conditions from the gas turbine also triggered or dampened the dump load.

The system loads were classified as fixed and flexible load. The first was modelled as a three-phase balanced active and reactive power load. The flexible load was a varying demand component controlled externally by a vectorized P and Q signal. The active power P was determined by the measured wind power and limited by a maximum power of $P_{max} = 3MW$.

The variable speed drive (VSD) was built in the specialization project. However, a chopper was used to dissipate energy during accelerations or decelerations. A new approach was applied here, a front-end rectifier that allowed a bidirectional energy flow, injecting power to the grid during braking or absorbing during accelerations. Power fluctuations are expected to be frequent; therefore, a versatile solution with fewer losses and heating was preferred.

On the other hand, the second part of the project was developed in HOMER. The HOMER® energy model was defined by a wind turbine, a flexible load and a battery bank. A wind profile extracted from the software database in a 10-year period from NASA meteorological service,

corrected to the hub height 100m. The wind resource was assessed for daily profile, annual profile, monthly averages, and speed histograms. Additionally, several calculations were made for the 6MW wind turbine as power curves, monthly and daily power output, cumulative frequency, duration curve and dumped load. The load profile was synthesized following the generation, which has been proved feasible as demonstrated in the dynamic simulations. Economic simulations were possible but lack of investment costs limited the model scope.

1.6 LIMITATION OF SCOPE

The project focus is on the system level, therefore component-level considerations e.g., design, sizing, tuning, harmonics, and switches losses have been excluded. Power electronic components are based on voltage source converters (VSC). The VSC in the wind turbine and variable speed drives are modelled as universal three-phase bridge with ideal switches. The control strategies are based on existing control methods and they are implemented in the subsystems. Much of the background knowledge as power wind technology, power electronic converters, generator technologies and overview of isolated power systems, as well as different suitable topologies have been treated in detailed the specialization project [12] and they are not further treated here.

It is assumed that the magnetic material in the synchronous machines are linear. Therefore, there have not been modelling for magnetic saturations and hysteresis effects. The stator winding are assumed to be uniformly distributed and with a sinusoidal excitation. Friction and damping effect on the machines have been neglected. The exciter used an IEEE 1 model, available in Simulink without the exciter's saturation function. A simplified gas turbine model based on second order transfer function was implemented, and thermodynamic processes were disregarded. An ideal flexible load has been modelled in some study cases representing an injection pump. However, this is an idealization because the load cannot make instantaneous changes on its demand, since there are time constants and mechanisms associated to the injection process neglected in this study.

On the other hand, the pulse width modulation (PWM) has been assumed to work in the linear range. Limitations regarding saturations, anti-windup and protection system have been excluded, assuming a safe operating range.

Finally, in the Energy WIS model, due to lack of costs data, economic analyses were out of scope in this section.

1.7 REPORT OUTLINE

In Chapter 1, Introduction, the project has been introduced. The problem background and motivation, limitation of scope, research objectives and methodology have been presented.

In Chapter 2, System Components, information regarding the basic components of a WIS are qualitatively described in this section, including generalities on wind turbine, water injection system, gas turbine, loads and subsea power system.

In Chapter 3, System components, the two dynamic models: hybrid and stand-alone are explained in a more detailed manner, considering the interaction and control between the different parts, subsystems, topology and high-level understanding of both configurations.

In Chapter 4, System Modelling, the constitutive parts of both configurations are mathematically modelled and control strategy for each component is explained, which is the basis for testing the assembled configurations in chapter 5 and 6.

In Chapter 5 and 6. Hybrid and Stand-alone WIS models are simulated in SimPowerSystem® for investigating the dynamic behavior of both systems, with special emphasis on frequency and power balance, through particular study cases.

In Chapter 7 Energy WIS model, the energy model composed of a wind turbine, a flexible load and a storage unit. Wind turbine power curves, load profile and wind profile are calculated, among other quantities.

In Chapter 8 Energy WIS study cases, model simulations on HOMER are investigated, including two different high and normal wind scenarios. Wind energy production, energy dump and several other statistical wind and energy curves are determined.

In Chapter 9, 10 and 11 Conclusions, further work, bibliography and appendices are presented.

2 SYSTEM COMPONENTS

This project is concerned with stand-alone and isolated power systems. An isolated power system refers to a power network, which it is not connected to the main power grid. As such, it should be able to be self-controllable given its isolated nature. An example of this type of system is an offshore Oil and Gas platform. There are two configurations developed in this work in order to analyze the use of wind power for water injection systems. It is assumed that both are off-grid models. These are:

- Hybrid Water Injection System (WIS)
- Stand-alone Water Injection System (WIS)

Both configurations are composed of different electrical subsystems, some of which are common between the two. For example, wind turbine, PMSG, crowbar protection, loads. Other parts are unique for the specific application. Hybrid WIS for instance works in parallel with a gas turbine. This section explains qualitatively the basic building blocks of both configurations. Table 2-1 includes the subsystem components for each model and case developed. It is worth noticing that flexible and VSD loads, refers ultimately a centrifugal pump.

Component	Hybrid WIS Case 1	Hybrid WIS Case 2	Stand-alone WIS Case 1	Stand-alone WIS Case 2
Wind Turbine	X	X	X	X
Gas Turbine	X	X		
Fixed Load	X	X	X	X
Flexible Load		X	X	
VSD				X

Table 2-1 System component for each studied case

2.1 WIND TURBINE

Wind power has become a mature technology and in the last twenty years, the installed capacity has grown fast. As indicated in [13], during the year 2014, wind power represented 43.3% (11.7GW) of the new installed power in Europe. Offshore deployments have been favored because of constant and high winds, public acceptance, low visibility and technological developments to MW rating turbines. Offshore wind turbines have evolved continuously and they are constantly finding different applications in deeper waters due to improved materials

and anchoring structures, as shown in Figure 2.1. Offshore structures can be fixed or floating. Floating wind turbine can be installed in depths between 95-120m, according to Statoil Hywind prototype. The capacity factor, which refer to energy produced compared to the rated energy, has been close to 60% [8]. This has led Statoil to further develop its technology and in 2015, the Hywind project was extended to supply power to Kvitbjørn through a 10km submarine cable, reducing 11000 tons of CO_2 per year [9].

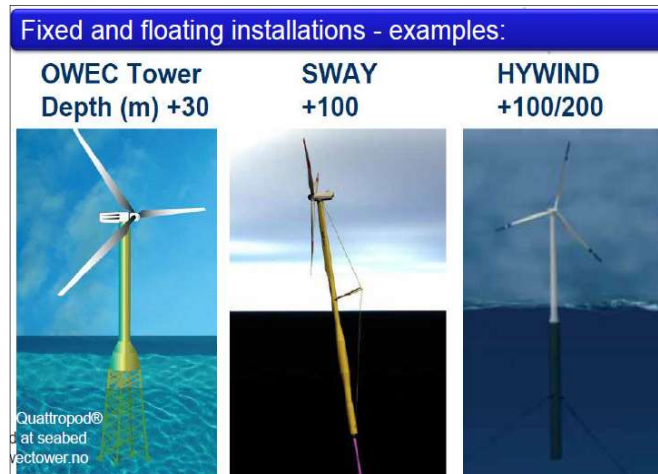


Figure 2.1 Foundation Deep Water [14].

In 2016, Statoil won a project to build a 30MW wind park consisting of five floating turbines of 6MW. See Figure 2.2. The first floating wind park will be located off the Scottish coast, near Buchan Deep, approximately 25-30km off the coast of Peterhead in Aberdeenshire. According to Statoil webpage, the pilot project objectives is to demonstrate cost efficient and low risk commercial parks in deep water with strong winds. The wind turbines are designed to be 258m in height, 178m above and 80m below water, Figure 2.3 [15]. On the other hand, in May 2016 Statoil has signed with DNV-GL a Joint Industrial Project to developed the second phase of the WinWin2 project, which is the base for this research [16].

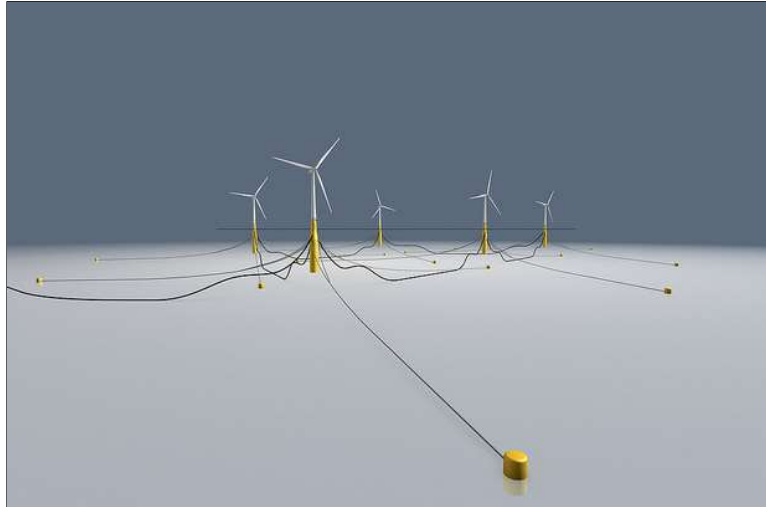


Figure 2.2 Hywind Scotland Pilot Park [15]

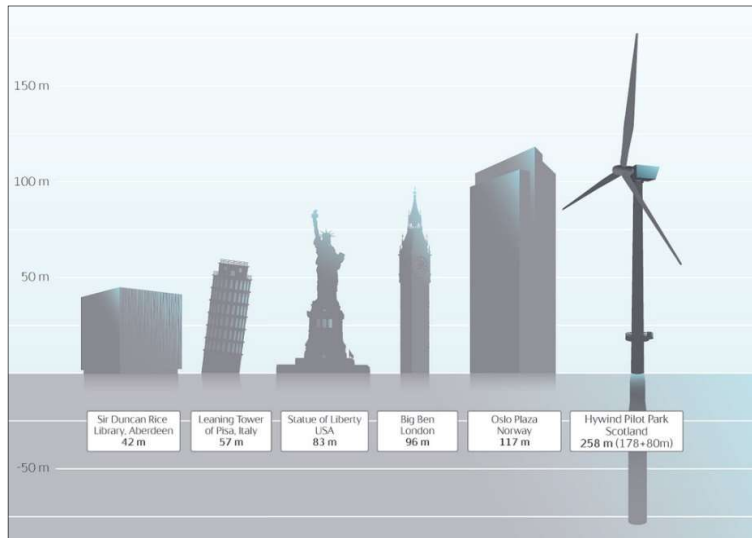


Figure 2.3 WT Dimensions of Hywind Scotland [15]

2.2 WATER INJECTION SYSTEM

When an oil well is discovered oil flows naturally out of the reservoir during the first exploitation phase. As time passes the pressure starts to decline and the production decreases. The well must then be intervened for pressure support. This is called secondary recovery or enhanced oil recovery (EOR), and the objective is to provide energy artificially to boost a declining production in a mature field. There are two techniques for secondary EOR process, water injection or gas lift. The last technique consists of injecting gas instead of water and it depends on the physical characteristics of the formation, and it is attractive when high-pressure

gas is available without compression or when gas cost is low. Compressors are sensitive to downtime and are not suitable for a fluctuating power source. Water injection is not a viable option for natural occurring gas wells [17].

Water injection is used in onshore and offshore developments. The introduction of water besides encouraging oil production it helps to move the oil in place. In some instances, the water must be suitable for the formation. Filtration and water processing are required to ensure no clogging and bacteria growth. In an effort to reduce corrosion within the reservoir, oxygen is removed from the water. Primary production recovers only 30 to 35% of the oil in place. Water injection effectiveness varies according to the formation characteristics, it can recover anywhere from 5% to 50% of the remaining oil, enhancing the well economics. When the water cut or water content in relation to oil reaches 90 to 99%, the process becomes uneconomical [17]. As indicated in [17] some water injections takes up to two years before the production is increased. Another form of water injection consists of introducing heated water. This is attractive for reservoirs with heavy oil content. Heat helps decreasing oil viscosity and making it more fluid [18].

2.2.1 Water Injection Methods

As indicated in Figure 2.4 [19], there are two common types of water injection methods. The traditional solution and the raw-seawater injection. The third solution called stand-alone is the new method proposed on this thesis based on DNV-GL idea [11].

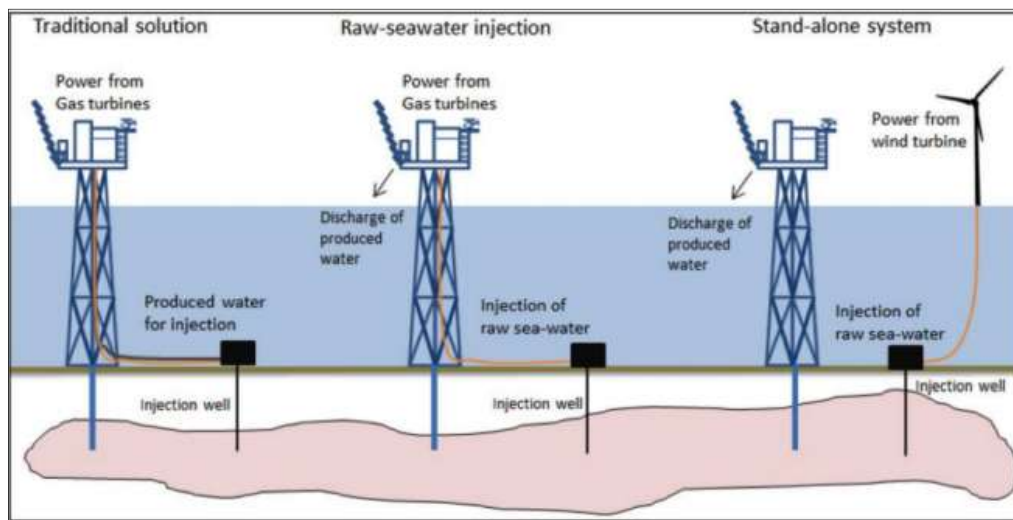


Figure 2.4 Water injection methods [19].

The first solution consists of a long pipeline extended from the host platform to the injection well. The water produced on the platform is pumped in through the pipeline to the injection site. In some instances, the pipeline has to be extended kilometers to the injection well. The pumps are usually located on the platform or they can be installed on the sea bottom over the well. If the latter is the case, a submarine cable that might require kilometers from the platform to the injecting well have to be connected. The second solution is based on a water injection subsea template as seen in Figure 2.5[2]. For example, the Tyrihans oil field developed by Statoil [2] is based on this idea, and it was taken as a reference case in DNV-GL for developing the concept of raw-seawater injection. In this system, a long cable of 31km was installed from the host platform to the injection site.

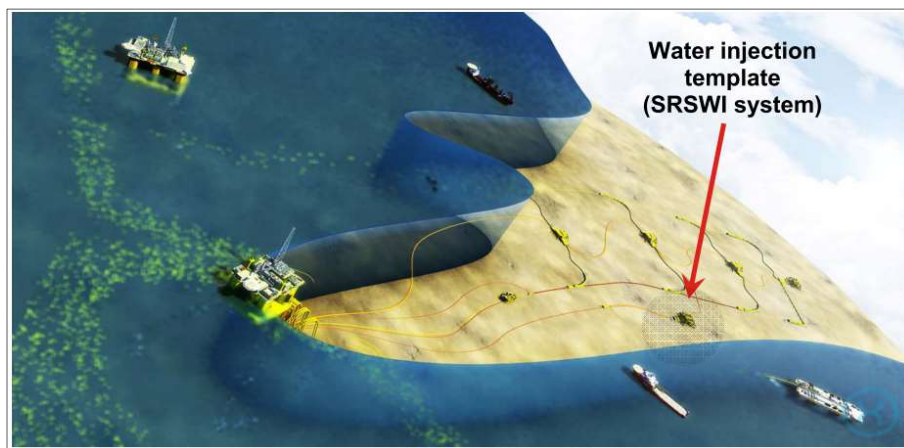


Figure 2.5 Water injection template Tyrihans Field [2]

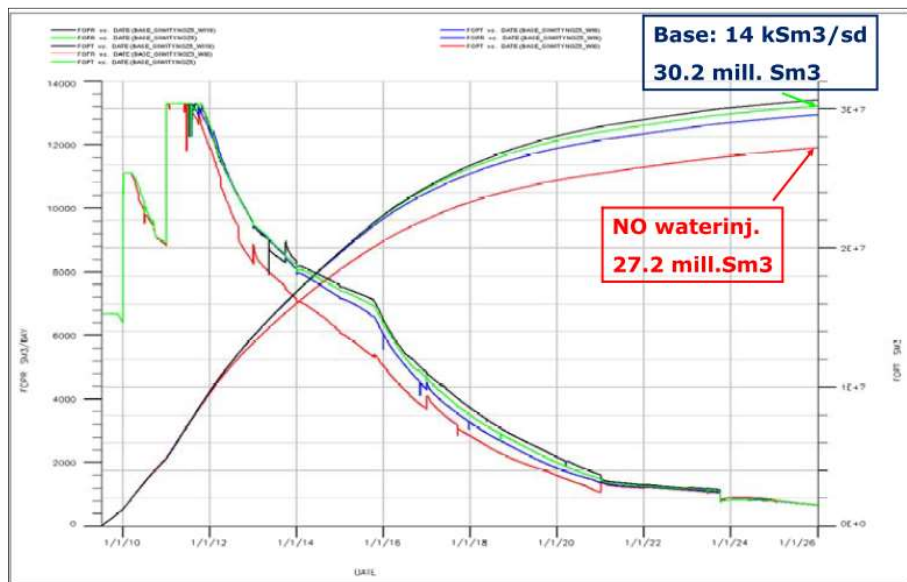


Figure 2.6 Reservoir pressure development simulation [2]

Figure 2.6 shows the results of an increased oil recovery on a reservoir at different water injection rates. By injecting seawater at a rate of $14000 \text{ Sm}^3/\text{day}$, represented by the green curve, the estimated gain is 3 million Sm^3 , in other words an increase of about 10% in total production compared to no water injection (red line). An injection rate of $19000 \text{ Sm}^3/\text{day}$, represented by the black curve will able to recover more oil on site. However, according to [2], a second injection well would have to be drilled, and consequently more costly. Therefore, the best present net value is achieved with an injection rate of $14000 \text{ Sm}^3/\text{day}$.

Finally, the new method proposed by DNV-GL called stand-alone system in its simplest form considers a subsea pump with a local offshore wind turbine that floats. As seen in Figure 2.7, a floating structure anchored to the seabed works where the hub of the wind turbine is mounted. Inside the hub or on a small platform, various electrical components can be installed, for the example a battery bank or auxiliary services of the wind turbine, including the power electronics devices required for the variable speed drives that ultimately controls the pump. A different configuration might include multiple smaller turbines whose representation was proposed in the specialization project [12], where high level qualitative analyses were given. Nevertheless, the use of MW wind turbine allows a system simplification and due to economics of the floating structure, the option considered for further revision in this project is the single turbine.

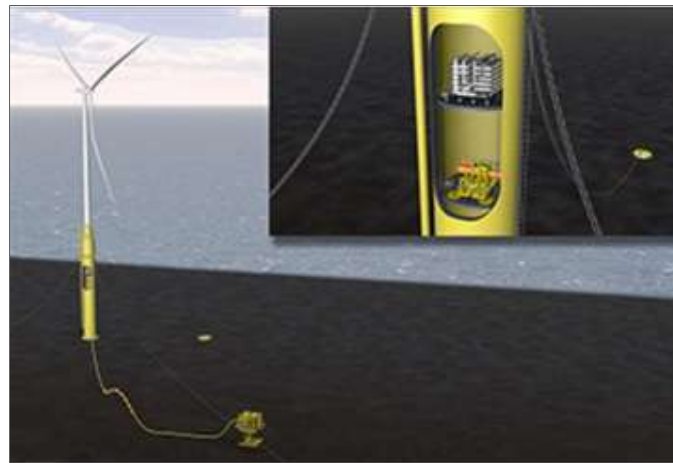


Figure 2.7 DNV-GL WinWin powered water injection [12]

2.2.2 Water injection pumps

There are several types of pumping technologies depending on their specific application. A quantity called gas-volume fraction (GVF) indicates the amount of gas in relation to the amount of liquid. Water injection pumps have a very low GVF, ranging from 0 to 15% as seen in Figure

2.8 [20]. In other words, the suitable option when liquid at high pressure is required is the centrifugal type. The differential pressures can be as high as 350 bars or 5100 psi. Naturally, this has been the option selected for subsea water injection wells as the case of Tyrihans field. This pump arrangement has a differential pressure of 296 bars and it is considered the most powerful water injection subsea system in operation, with two 2.5MW motors installed in a redundant configuration [2].

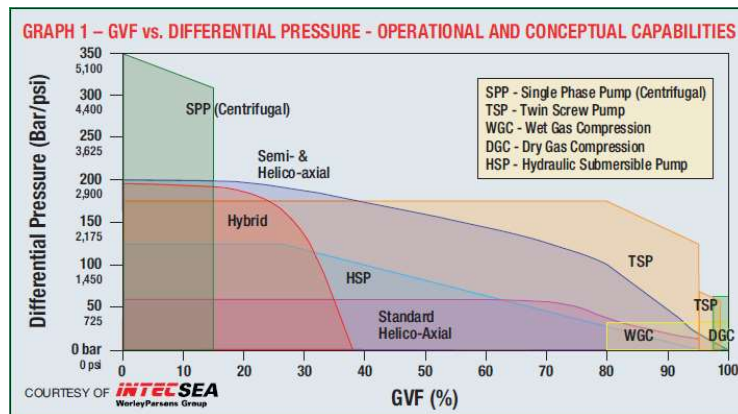


Figure 2.8 Sub-sea pumps types [20].

2.3 GAS TURBINE (GT)

The conventional power supply for O&G platforms come from gas turbines. They are closely integrated with the electric generator. Their thermal efficiency is low, around 30%. In some occasions, they are equipped with secondary recovery apparatus to extract residual energy normally in form of heat. If the wasted heat is recovered, the efficiency can go up to 60% by a steam engine. However, this is not the kind of solutions found in O&G. In 2008 the O&G installations emitted 27% of CO_2 , from which 80% came from gas turbines in Norway [8]. This has led to efforts in reducing these emissions, which also justifies this project realization.

2.4 LOADS

There are different power loads, which are part of the electrical system studied here. Fixed load, flexible load (idealization of a VSD) and VSD connected to pumps. The fixed loads include priority services, lighting, emergency and critical process services, as the case of main oil pumps or equipment. Flexible loads are defined as those that can be regulated, and whose active and reactive power can be defined. An ideal flexible load is a simplified version of a VSD in this project, because it does not consider time delays or electromechanical phenomena associated with the actuation time of the controllers. On the other hand, if a VSD is connected

to an induction motor, it is assumed that it corresponds to a more realistic approach when modelling the WIS. Both types of flexible loads are discussed further in the study cases.

2.5 SUBSEA POWER SYSTEM

There are four zones for subsea power systems as shown in Figure 2.9 [20], depending on the step-out distance. Each configuration is characterized by different specifications in terms of voltage, frequency, power and variable speed drive type. These configurations are standard according to [20]. Subsea power systems connected to Oil and Gas platforms tend to be similar as to benefit for equipment standardization.

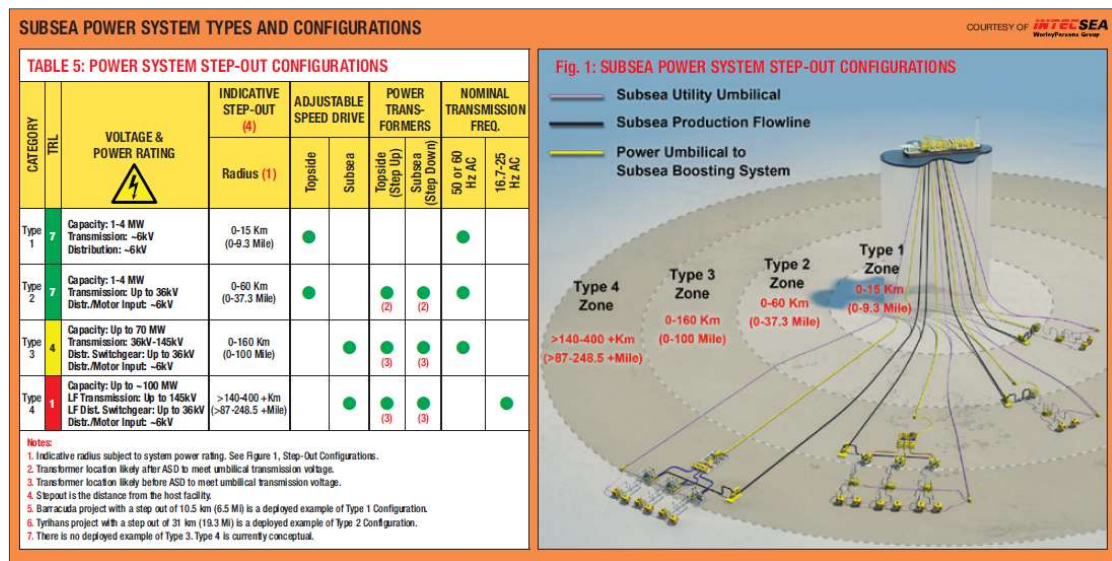


Figure 2.9 Subsea power system types and configurations [20].

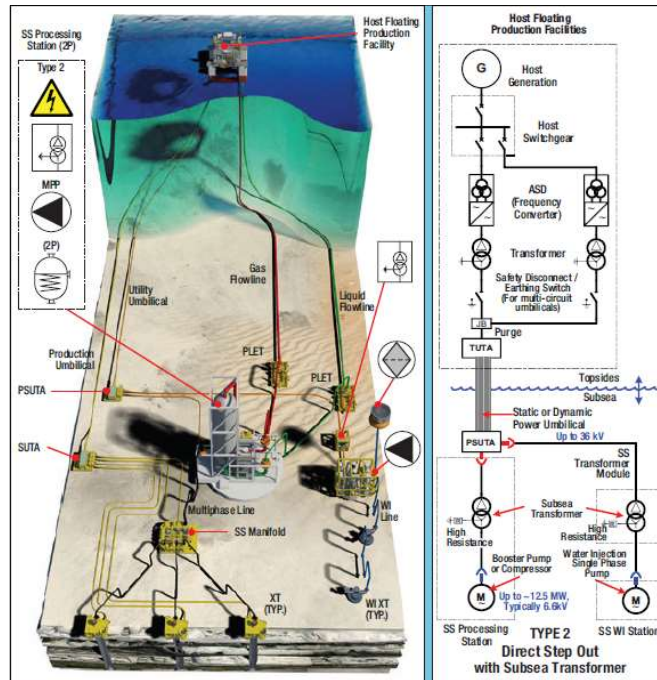


Figure 2.10 Subsea Power System [20].

Figure 2.10 [20] shows a host floating production facility that connects a subsea template with step-out distance of 31km. This configuration type was used for Tyrihans field, and was composed of a host generator, a switchgear, two frequency converters, two topside step-up and two subsea step-down transformers. The umbilical power cable of 36kV is connected from the platform to the injection well site, where it is reduced to 6kV to feed the pumps or compressors. Finally, the system has double redundancy for maintenance and operational purposes.

3 SYSTEM CONFIGURATIONS

There are two system configurations, the hybrid WIS and the stand-alone. The first is going to be used to analyze the O&G platform integrated with the wind turbine and the second configuration is used for simulations of the stand-alone WIS with only wind power.

3.1 HYBRID WIS CONFIGURATION

The system depicted in Figure 3.1 is a hybrid system composed of a wind turbine using a PMSG with a back-to-back converter, a gas turbine with synchronous generator and the loads. The wind turbine permanent magnet synchronous generator (PMSG) operates in parallel with the gas turbine synchronous generator. The main advantage of using a PMSG is a more reliable construction, because it does not require windings and slip rings on the rotor, though, the converter has to be fully rated. The wind turbine has two power electronic converters.

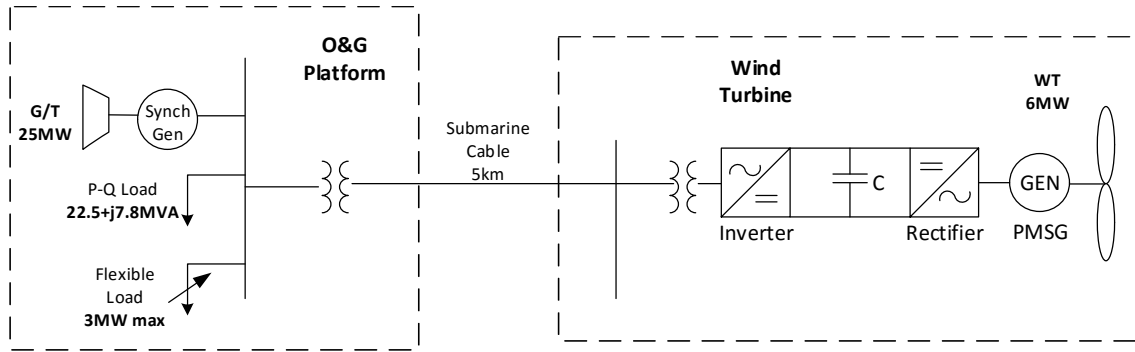


Figure 3.1 Hybrid system Oil and Gas platform connected to a wind offshore turbine.

The first converter is a front-end three-phase rectifier. The voltage induced in the PMSG is rectified with force-commutated switching devices, commonly IGBTs. The PMSG rotor speed is controlled by the rectifier. By measuring the wind speed is possible to calculate the optimal rotational speed, this reference speed is sent to the controller and the control speed ω_{sg} is generated. Voltage source converters are controlled in this project using voltage control, whose principles are explained in the appendix in section 11.1. Briefly said, the sinusoidal abc quantities are transformed to a simplified dq frame, which behave as DC quantities. Generally, the stator direct current component is set as $I_{gd} = 0$, and the speed controller output determines the values for I_{gq} . Both I_{gd} and I_{gq} are aligned to the rotor position θ_{sg} .

Before the second converter, a capacitor C is put in between. The inverter purpose is to transfer power to the network. The DC voltage is an indicator of power transfer, the voltage remains equal to the reference U_c by changing the current component I_{vd} , and the quadrature component

is $I_{qw} = 0$. This permits the alignment with the voltage space vector U_v , and consequently a lower current magnitude thanks to a zero reactive component on the grid side. In parallel to the capacitor, not shown on this figure, a limiting circuit is set that protects the *DC* link against overvoltages, for example in case of wind gust and it can be regarded. Finally, the inverter is connected to the system through an inductance L_v , not represented in figure.

The hybrid system is more intricate when a gas turbine sets the voltage and frequency in comparison to a grid connected situation. Since the wind power output wants to be optimized, the gas turbine power output depends on the dynamic relationships between the wind speed and load demand. For example, if the wind power is less than the load demand the gas turbine provides the missing power. When the wind speed rises and generates more power than needed, the gas turbine is supposed to turn off. However, in practical terms, the gas turbine cannot be turned-off and it keeps working with the minimum permissible loading of 10%, and it simultaneously provides a spinning reserve.

When there is an excess in generation, the grid voltage and frequency are affected. The gas turbine is capable of controlling the reactive balance and therefore the system voltage. Excess of generated power leads to frequency rise, but there are different methods to limit the frequency. For example, useful loads as pumps, energy storage elements as flywheels or batteries. Another alternative is the use of a dump load or automatic pitch control.

Here the system loading includes a fixed load and a flexible load. The idea behind this classification is to present a system that has both a priority load that must be supplied at all time, and a controllable or flexible load that can be shed if needed. A flexible load is a load idealization, whose active and reactive power are set at will. A non-ideal flexible load is a water injection pump controlled by a variable speed drive, which adds more complex and non-linear dynamics to the model.

The following chapter 4, explains concisely the modelling of hybrid system parts. This chapter includes concepts related to the integration of wind offshore power to an oil and gas platform to a greater level of detailed than the one presented in the specialization project. For instance, the variable speed wind turbine considered here is completely modelled, instead of the aggregated wind turbine represented by an ideal *DC* source behind a voltage source converter. The different subsystems developed in this thesis are more realistic. Finally, the entire configuration is assembled and tested under different wind conditions, for two study cases in chapter 5.

3.2 STAND-ALONE WIS CONFIGURATION

The topology presented in Figure 3.3 has been chosen based on the specialization project and on DNV-GL technical assessment report [10]. The report proposed two different topologies, the single back-to-back Figure 3.2 and double back-to-back Figure 3.3

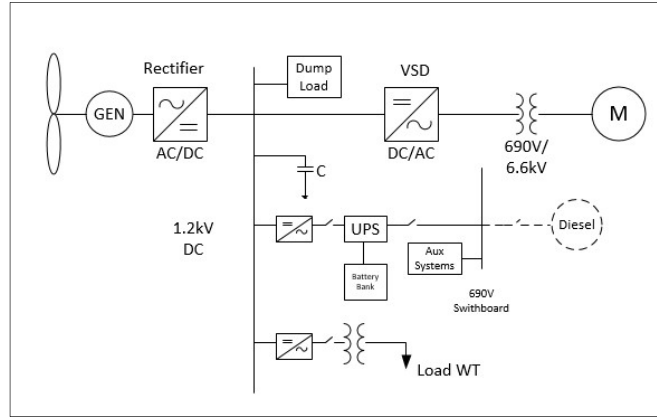


Figure 3.2 Single back-to-back detailed topology

The single back-to-back topology in Figure 3.2 has two converters, the rectifier and the VSD. The wind turbine generates power, which is rectified and sent to the DC link. The U_{dc} varies depending on the generation and demand. The turbine works at its maximum power tracking with blades fully pitched. The regulation occurs on the DC link, if the power generated is higher than the power consumed the voltage increases and will trigger the dump load, adding an extra load, keeping the system balance and avoiding excessive overvoltages in the DC system. The second converter is an inverter whose purpose is to control energy transferred to the load by speed regulation. An UPS (uninterruptible power supply) is added for serving auxiliary loads, including control systems, yaw, pitch drives, lighting, communication and pump services. An optional diesel generator shown in dashed lines can be added as back-up for these auxiliary loads. Finally, the water treatment plan can also be controlled depending on the water required for injection.

The single back-to-back topology has three operating modes: star-up, normal operation and shutdown. These modes were explained in detailed in the specialization project [12]. The star-up begins when the wind speed is above the cut-in speed, for example 5 m/s and the blades start to rotate. The wind turbine yawing and pitch systems try to capture the maximum power and the DC link is energized. The dump load is activated to control the voltage balance and the initial power fluctuations. The current flows from the stator to the capacitor creating and opposite torque to the rotor torque. The rotor speed increases until it stabilizes. The transformer

is energized through the inverter, which in turn feeds the pump in a controlled manner. The second mode is normal operation. The system will deliver power to the load according to the available supply. For example, an excess in generation will be dissipated in the dump load and generation deficit is controlled by reducing the pump injection rate. Finally, the shutdown mode can occur under two conditions, a high wind speed (25 m/s) will force the wind turbine to a controlled stop in order to preserve the system integrity and avoid excessive mechanical and electrical loads. The second condition is a low speed situation for example below (4 m/s). For extremely low speed, the losses are greater than the energy produced or the system efficiency is very low forcing a shutdown.

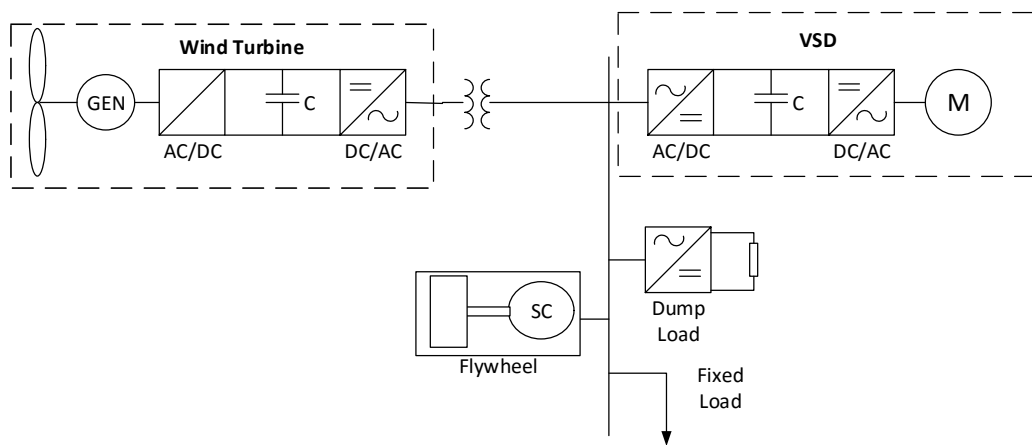


Figure 3.3 Double back-to-back detailed topology

The second topology depicted in Figure 3.3 is a more complex topology, and it is further investigated in this project. It is also made up of more components. However, the system can be considered an off-the-shelf solution. For example, contrary to the single back-to-back configuration, the double back-to-back is built on constitutive blocks, they can be close together or connected through a long submarine cable. This implies that it is not required the modification of the internal structure of the wind turbine or the variable speed drive, which according to DNV-GL report faces strong opposition from the manufacturers [10]. Another advantage of the double back-to-back is the addition of physical inertia by incorporating a flywheel. The objective of the flywheel is to provide active and reactive power to the system during fluctuations, and it works as an automatic power factor regulator. Additionally, the flywheel is coupled with a large rotating mass acting as a spinning reserve. The estimated spinning reserve is 10%. This added mechanical package will influence the system energy losses but will help to dampen out the system power fluctuations. The dump load controls the

synchronous flywheel, as the rotating speed increases beyond the allowed range the balancing load introduces an extra load to decelerate the machine.

On the other hand, the flywheel-synchronous generator offers inertia, voltage and frequency reference, which simplifies the control strategy of the inverter. Reactive support is another advantage added, since in a wind turbine it is limited to the converter current rating. A different effect is in the increase of short circuit capacity, important for avoiding destructive currents in case of short circuits due to the possible built-up of high voltages [12].

The double back-to-back system has three operating modes as well. Once the wind speed is above 4 *m/s*, the star-up mode is initiated by the AC/DC/AC converter, which accelerates the synchronous flywheel until it stabilizes. Then the flywheel establishes the grid voltage and frequency references. Once the references are set, the wind turbine is synchronized by means of a PLL controller that matches the grid. Then the fixed load is energized and the motor is slowly accelerated. The normal operation mode consists of keeping the energy balance through all the system components. The dump load plays an important role by controlling the system frequency by adding or subtracting resistors. A different approach can be achieved through a more sophisticated pitch control limiting energy output leading to less dissipation on the resistor bank. Finally, the shutdown mode follows the same criteria as the previous topology for high wind or low wind condition, stopping the system due to excessive mechanical loads or extremely low efficiency. The double back-to-back subsystem parts are explained in the chapter 4. At the end, the system is tested under different operating conditions in chapter 6.

4 SYSTEM MODELLING

4.1 OIL AND GAS PLATFORM

Power systems in oil and gas platforms are complex. Typical loads are electric motors for compressors, pumps and general processing equipment, auxiliary machinery, heaters for production processes [21]. As mentioned in [21], the loading in a platform depends on many factors: the kind of processes, the amount of oil and gas processed, field capacity, method of transportation for the hydrocarbons, and if it is serving as host for other neighboring smaller platforms, etc. Gas injection requires compressors that are driven by synchronous motors, a more general platform will include these type of loads but they are not included here. In this thesis, interest is on water injection systems fed by induction motors. Another type of loads are lighting and heating comfort. In this case, a concentrated P-Q load is used for modelling passive elements.

4.2 FIXED PQ LOAD

A lumped PQ load results from a total RLC combination of different elements. The resulting impedance is modelled as a constant load at a given frequency. A three-phase balanced load with not capacitive elements can be represented as,

$$Z_{load} = R_{load} + j\omega L_{load} \quad (4.1)$$

The load consumes active and reactive power, the relationships are described by,

$$P_{load} = \frac{V_p^2}{R_{load}} \quad (4.2)$$

$$Q_{load} = \frac{V_p^2}{\omega L_{load}}$$

Besides lighting, heating, conform loads, a fixed load can also represent systems losses and other passive elements.

4.3 FLEXIBLE LOAD

A flexible load is a controllable load whose active and reactive power can be changed over time according to the generation profiles. This is modelled ideally by a Simulink block that allows decoupled control in both P_{flex} and Q_{flex} , also referred in this project as dynamic load. The reactive component, however, is set to be zero. Then only control is actually made on the active

power consumption. This load represents a pump that can be controlled through for example a variable speed drive, as a result this might be understood as a simplification.

4.4 SUBMARINE CABLE

Submarine cables transmit energy underwater from the source to the loads. Wind offshore systems are connected through cables in different configurations. Cables are defined by their capacitive and inductive properties. In offshore systems, capacitive elements are predominant. The conductor length has an enormous effect on the system capacitance. There are two different models for representing cables: the distributed and the lumped parameters model [21]. That level of accuracy varies and depends on the length and type of study to perform. The distributed parameters model is used for frequency and wave propagation analyses. On the other hand, the lumped parameters model is suitable for power systems analysis as the one treated on this project, since no harmonics and frequency studies are considered. Additionally a relative short cable length is considered.

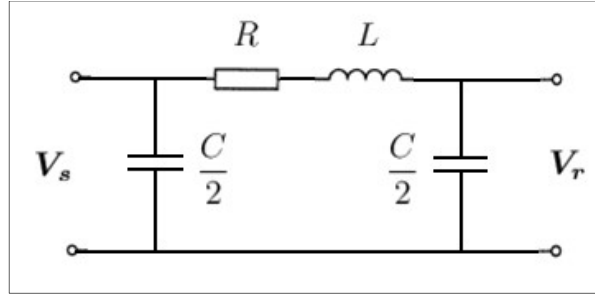


Figure 4.1 PI cable line model [22].

Figure 4.1 [22] shows a π -section of a balanced transmission line. This model lumps the inductive, capacitive and resistive parameters in equivalent impedances,

$$Z = R + j\omega L \quad (4.3)$$

$$\frac{Y}{2} = j\omega \left(\frac{C}{2} \right) \quad (4.4)$$

Where Z is the equivalent resistive and inductive impedance, and Y is the shunt impedance that is modelling the capacitive line effect. The circuit solution expressed in matrix form can be formulated as [9],

$$\begin{bmatrix} V_s \\ I_s \end{bmatrix} = \begin{bmatrix} (1 + \frac{ZY}{2}) & Z \\ Y(1 + \frac{ZY}{4}) & (1 + \frac{ZY}{2}) \end{bmatrix} \begin{bmatrix} V_r \\ I_r \end{bmatrix} \quad (4.5)$$

The subscripts s and r refer to the sending and receiving terminal respectively.

4.5 OIL PLATFORM SYNCHRONOUS GENERATOR

A complete mathematical development of the gas turbine synchronous generator on the O&G platform is out the scope of the project. In section 4.10, the WT PMSG modelling is briefly explained and fundamental expressions are considered, which are also valid for the synchronous generator connected to the GT. However, it is important to remember a couple of formulas required to understand key concepts related to active and reactive power of the generator, if the rotor resistance R is neglected the simplified relations yield [23],

$$P_{gen} = \frac{E_f V_t \sin \delta}{X} \quad (4.6)$$

Where P_{gen} , represents the active power. The reactive power is given by,

$$Q_{gen} = \frac{V_t E_f \cos \delta - t}{X} \quad (4.7)$$

The back-induced voltage is E_f , V_t is the terminal voltage and δ is known as the power angle. Finally, X is the reactance between the inducted E_f and terminal V_t voltage.

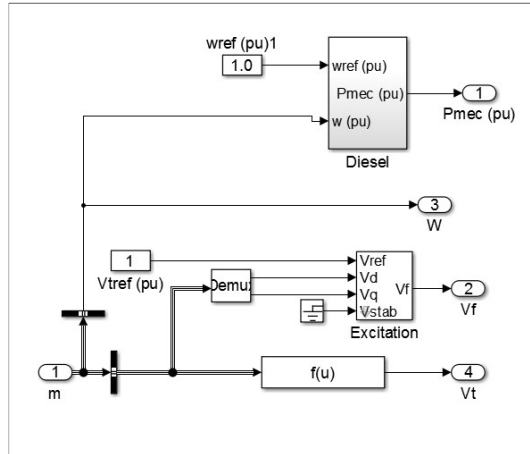


Figure 4.2 Control block diagram SG Oil Platform

Another subsystem of the synchronous generator is the excitation circuit or exciter, Figure 4.2 in Simulink. This part consists of an external controllable DC source that feeds the rotor winding and creates a controllable magnetic field. The modelled implemented is based on an excitation block integrated in Simulink® without the exciter's saturation function. The block implements an IEEE type 1 synchronous machine voltage regulator combined to an exciter [24]. The main function of this element is to provide excitation for the machine and regulate the terminal voltage in generating mode. The block inputs are the direct voltage V_d and quadrature voltage V_q of the synchronous machine. The voltage terminal reference is set to $V_{tref} = 1 pu$.

The output of the block is the field voltage V_f , which is applied to the synchronous machine that ideally ensures unity at the machine terminals.

4.6 OIL PLATFORM GAS TURBINE

Gas turbines are the standard generation units in O&G platforms. The block diagram of a thermal generator is illustrated in Figure 4.3. The model is developed in [25], is a simplified version of an emergency thermal generator developed in Matlab.

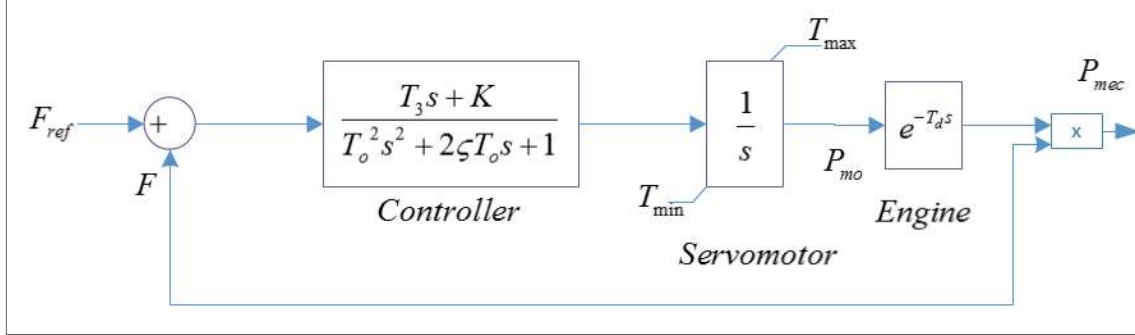


Figure 4.3 Speed controller of the thermal generator

The speed controller contains a high order transfer function. The values considered are $T_o = 0.02s$, $\xi = 0.3$ and $T_3 = 5s$. The reference frequency F_{ref} is set to 1pu (50Hz). When the actual frequency F is compared and a mismatch is found, an error signal is generated and fed into the controller. This controller acts as the machine governor, indicating that the fuel tank should be open or closed depending on the system frequency or in other words on the synchronous machine speed. The output is integrated in a servomotor or actuator that will open or close the fuel valve for more or less fuel respectively, within a torque range: T_{min} and T_{max} . Finally, the engine process time delay modelled is by $e^{-T_d s}$, is multiplied by the ω_{sg} that in pu is identical to F and will create the corresponding mechanical power that the synchronous machine needs.

4.7 DUMP LOAD

The dump load is an auxiliary and controllable load. The dump load control system described in [25] is shown in Figure 4.4. The dump load is activated if some conditions are satisfied. A phase locked loop (PLL) measures the grid frequency in the grid voltage U_v . The reference frequency is compared to the measured frequency and enters a dead-zone block ($\pm 0.2Hz$).

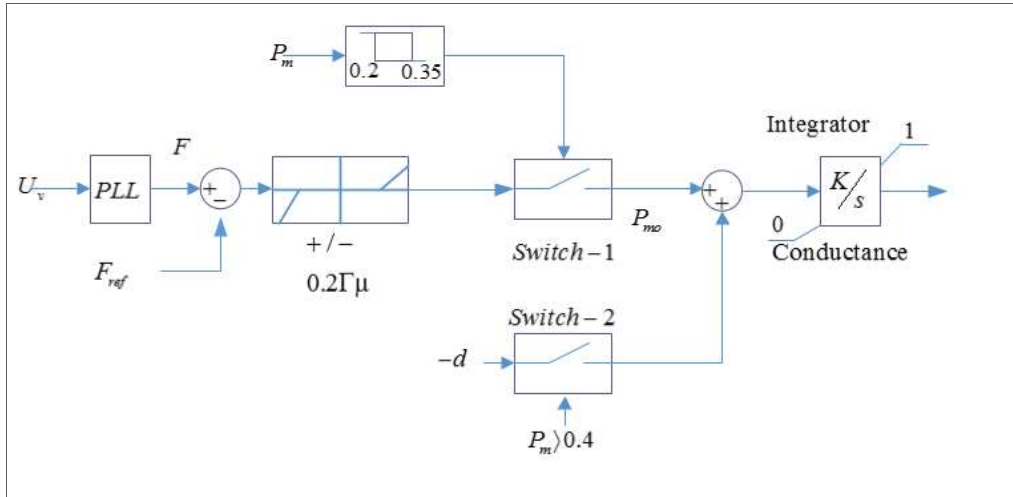


Figure 4.4 Control scheme of dump load

This dead-zone block inhibits the signal; the objective is to avoid unnecessary dump load activation within the defined frequency range. Switches 1 and 2, measures the mechanical power of the gas engine, if they are above the set threshold they generate error signals that are integrated providing a control signal with a value between 0-1. If the frequency increases above the permissible threshold, then the conductance of the load decreases and consequently the power absorbed by the dump load rises and conversely.

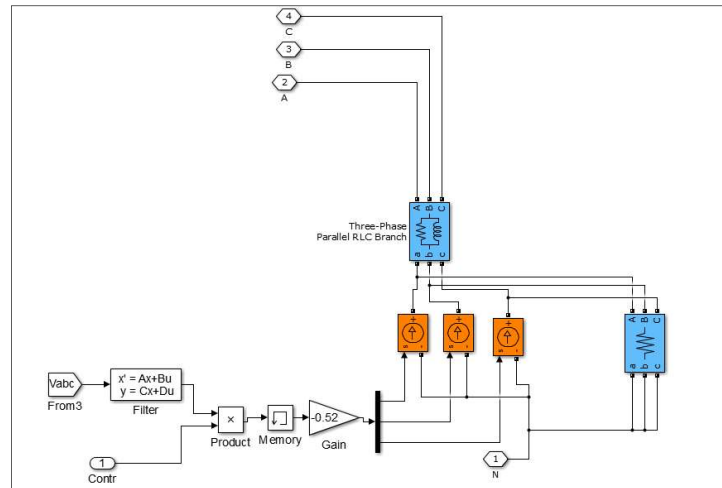


Figure 4.5 Internal structure of dump load

The dump load internally is composed by three controlled current sources. They draw currents from the point of common coupling. The currents are in phase with the phase voltages and their values are defined and the conductance factor that changes from 0 to 0.52. The filter and the inductance are intended for decoupling of the algebraic loop between voltage and the current

as explained in [25]. The current sources in other words change the equivalent resistor bank, increasing and decreasing its value acting a ballast or balancing element.

4.8 WIND TURBINE

When the wind blows, the rotor blades are turned creating a torque in the direction of the rotation. The fundamental equation for the wind turbine describes the relation between the mechanical power P_{mech} and the wind speed v is given by,

$$P_{mech} = T_{mech} \cdot \omega_m = \frac{1}{2} C_p(\lambda, \beta) \rho A v^3 \quad (4.8)$$

Where $A = \pi R^2$ is the rotor area and ρ is the air density and R is the rotor radius. T_{mech} is the mechanical torque acting on the blades and ω_m is the rotational speed (rad/s) [26]. The performance coefficient C_p is a function of the rotor blade tip speed $\lambda = R\omega_m/v$, and it is usually between $2 < \lambda < 13$. In order to get the maximum power extraction, the rotational speed ω_m should be changed such that $\lambda = \lambda_m$. The blade pitch β , must be as small as possible and will increase in the occurrence of large wind speed as to limit the power generation and mechanical stress on the turbine.

There are several analytic formulations for $C_p(\lambda, \beta)$. This project takes the description from SimPowerSystems [24]:

$$C_{p(\lambda, \beta)} = c_1 \left(\frac{c_2}{z} - c_3 \beta - c_4 \right) e^{-c_5/z} + c_6 \lambda \quad (4.9)$$

$$\frac{1}{z} = \frac{1}{\lambda + 0.08\beta} - \frac{0.035}{1 + \beta^3}$$

$$c_1 = 0.5176, c_2 = 116, c_4 = 5, c_5 = 21, c_6 = 0.0068.$$

The dependencies C_p of λ with different values β are illustrated in Figure 4.6. The maximum C_{pmax} is reached when $\lambda = 8$ and the blades have a pitch angle $\beta = 0^\circ$, when the energy capture is greatest.

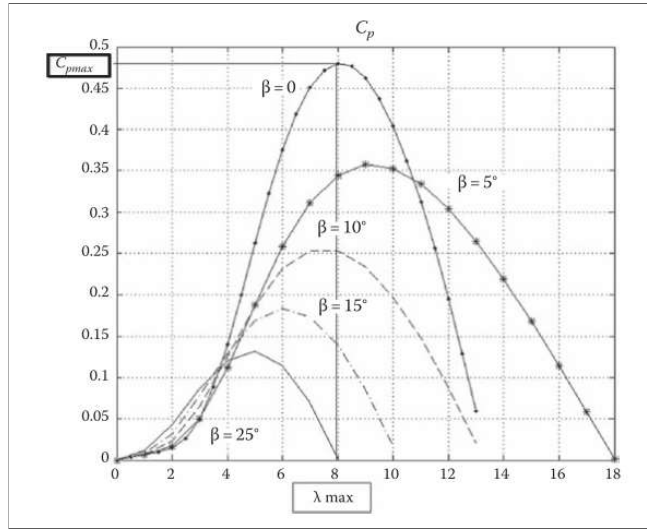


Figure 4.6 Dependencies C_p of λ with different values β [25]

The turbine power characteristics is indicated for different wind speeds ranging from 5 m/s to 11 m/s in Figure 4.7. These limits have been assumed considering a conservative speed range. The power output when the wind speed is 11 m/s is 6 MW .

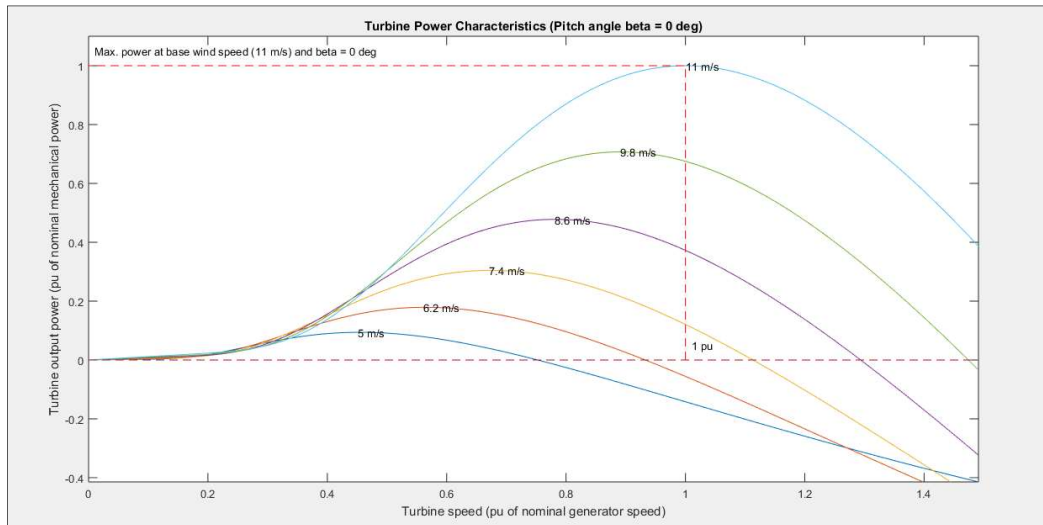


Figure 4.7 Power turbine characteristics with pitch angle ($\beta = 0^\circ$)

4.9 PITCH CONTROL

Pitch control is the more extended method for adjusting the aerodynamic generation in wind turbines. Almost all variable speed wind turbines use pitch control. The pitch has two main purposes: to extract as much power as possible in the low wind range and to keep a constant generation in the high wind range to avoid exceeding mechanical and electrical design limits [27]. The pitch angle β in this model is between 0° and 18° . The mechanical torque will

decrease with increasing β , until it reaches zero with blades fully pitched and breaking mechanisms act. However, there is a limitation in how fast the blades can be turned and it depends on the manufacturer. The pitch control can be implemented in different ways. In this project, a simple proportional controller is used. The simple structure is described in the block diagram in Figure 4.8.

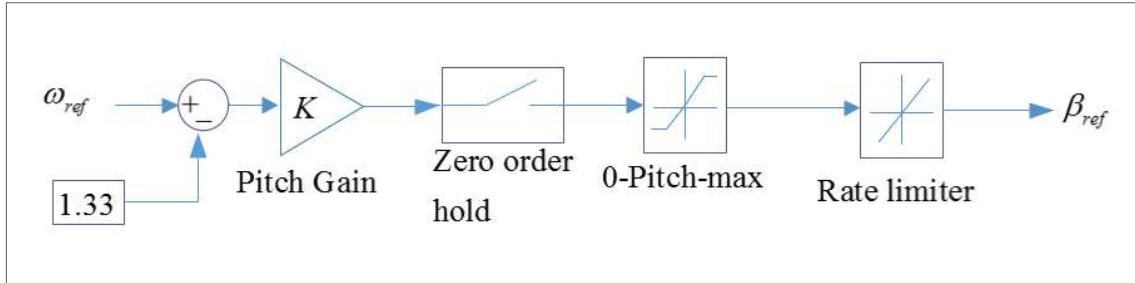


Figure 4.8 Block diagram of pitch controller

The reference rotor speed must be synthesized depending on the wind speed for maximum power extraction, therefore, ω_{ref} , changes dynamically. An error signal takes the difference between the reference speed and a maximum allowable speed $\omega_{max} = 1.33pu$, if the difference is positive meaning a large rotor speed, the pitch control actuates to decrease the speed. The error is amplified in a pitch gain block. After holding the gain value, the signal enters a saturation zone limiting the angle variation β between 0° and 18° . The rate of change is not arbitrary and the rising and falling slew rate is set as $\pm 4 m/s^2$. The final pitch angle β is fed into the wind turbine block to revolve the blades accordingly. It is worth mentioning that if an automatic pitch control is installed, the power output can be fully controlled, which can help reducing the dump load size or power system fluctuations.

4.10 PERMANENT MAGNET SYNCHRONOUS GENERATOR (PMSG)

The PMSG does not have a DC-excitation circuit as a regular synchronous machine. Instead, permanent magnets are placed in the rotor. An advantage in this machine is that it does not have wires supplying the magnetic field to the rotor, which means less electrical losses and improved mechanical reliability [27]. The direct drive PMSG offers significant advantages over conventional gearbox wind turbines. For example, fewer components and higher availability, lower maintenance costs, higher energy production 5-7% due to permanent excitation, low speed and voltage, reduced noise level for fewer moving parts. However, it requires a larger rotor diameter and a higher hub height [28].

A dynamic PMSG model is simplified when it is built in the synchronous dq reference rotating frame as shown in Figure 4.9. The q_{axis} is ahead 90° from the d_{axis} . The abc phasors and direction of the rotation speed through the angle Φ are illustrated. In addition, in b) it can be observed that the dq axis is in aligned position referred to the rotor and stator axis [27].

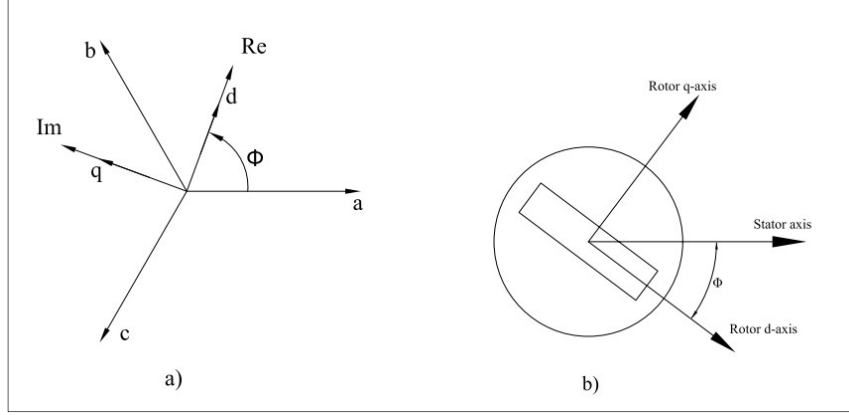


Figure 4.9 a) d-q system from abc system b) d-q axis of rotating machine [27]

The voltages are defined by applying the Clarke and Parks transformations to phase voltages as explained in appendix 11.1. The electrical model of the PMSG in the dq frame is defined by the next equations [27]:

$$v_d = i_d R_s + L_d \frac{\partial i_d}{\partial t} - \omega_r L_q i_q \quad (4.10)$$

$$v_q = i_q R_s + L_q \frac{\partial i_q}{\partial t} + \omega_r (L_d i_d + K_e) \quad (4.11)$$

$$T_e = \frac{3}{2} p i_q \left((L_d - L_q) i_d + K_e \right) \quad (4.12)$$

For a round rotor machine, the inductances on the d and q axis are the same and the torque equation reduces to,

$$T_e = \frac{3}{2} p i_q K_e \quad (4.13)$$

where v_d and v_q are the voltages transformed to $d-q_{axis}$, i_d and i_q are the currents, the stator resistance is R_s , the inductances are L_d and L_q , the rotational speed is given by ω_r , and K_e represents the permanent magnetic flux given by the magnets and p is the number of pole pairs.

The mechanical system is based on the following relations[24],

$$\frac{d\omega_r}{dt} = \frac{1}{J} (T_e - F\omega_m - T_m) \quad (4.14)$$

$$\frac{d\theta}{dt} = \omega_m, \quad (4.15)$$

Where J is the combined inertia of rotor and load, F the combined viscous friction, ω_m angular velocity of the rotor, T_m shaft mechanical torque and θ is the rotor angular position.

4.11 GENERATOR SIDE CONTROL

The generator has an electrical synchronous speed of $\omega_{gen} = 166.66 \text{ rad/s}$. This rotational speed is still high for large offshore turbines, a gearbox can be included or more magnetic poles added to the generator. The generator consists of 18 pair of poles, then the resulting nominal speed is $\omega_{nom} = 22 \text{ rad/s}$.

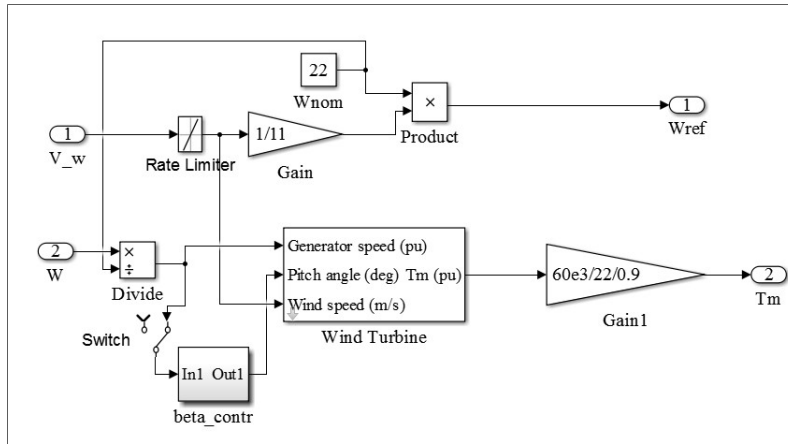


Figure 4.10 Mechanical speed ω_{ref} reference block diagram

The principal function of the rectifier is to control the rotor speed of the generator for maximum power extraction. This optimal reference speed is calculated as follows. The measured wind speed enters a rated limited block with slew raising and falling rate of $\pm 4 \text{ m/s}$, avoiding changes provoked by wind gusts. Afterwards, it is normalized dividing it by the base wind speed 11 m/s . The relationship is proportional and the nominal speed is multiplied by a correction factor varying with the wind speed. For example, if a wind speed of 9.8 m/s is considered, the rotor reference speed should be $\omega_{ref} = 0.9 \omega_{ref}$ for maximum power extraction, as indicated in the wind power curves characteristics Figure 4.7.

As seen in the control block of Figure 4.11 developed in [25], the reference speed enters a saturation and rate limiter as to ensure values within physical limits that can be handled by the generator. The measured speed ω_m is compared with the reference speed ω_{ref} , the error signal enters a PI controller, which calculates the quadrature current component I_{gqref} . The reference current direct component, is set as $I_{gdref} = 0$, which will minimize the total current and

resistive losses in the stator, ensuring maximum power extraction. The current magnitude I_{gqref} is checked for avoiding overcurrent.

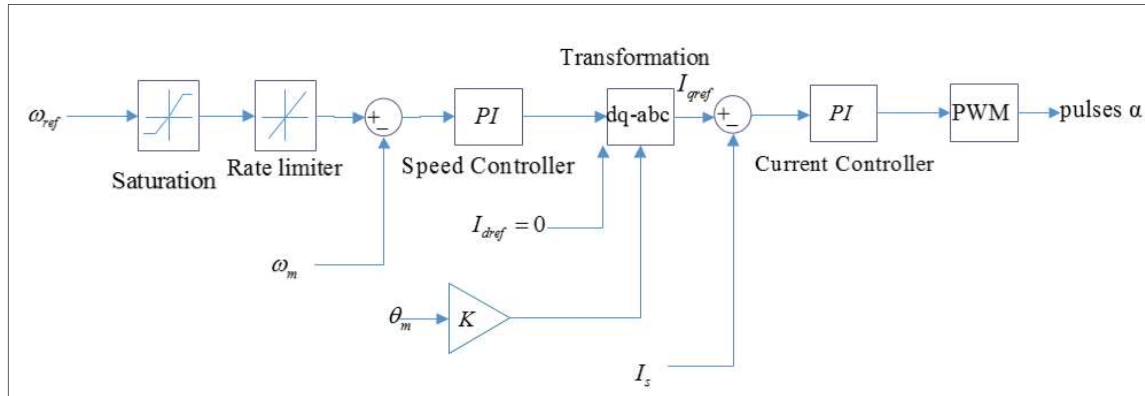


Figure 4.11 Control block diagram generator side converter

The rotation angle of the rotor θ_m is divided by the number of pole pairs and both references are created to enter the $dq - abc$ Parks inverse transform. A PI current stator regulator takes the current references in the abc frame, and compares it with the stator phase currents. Finally, the current regulator sends the signals to a PWM blocks that generates the pulses in the converter with a modulation frequency of 3240Hz.

4.12 CROWBAR PROTECTION

The DC side has a simple protection device to prevent overvoltages and possible circuit damage. It works by putting a low resistance path to ground through a resistor in series. The circuit consists of a switch that measures the voltage. In a range between 1.1 and 1.15 U_{dc} the switch is not activated. If the voltage exceeds 1.15 U_{dc} the switch is turned on and it is connected in series to a resistor to regulate the overvoltage by introducing a voltage drop. For example, in case of a sudden rotor acceleration an overvoltage is built up in the DC due to a wind gust, or if there is a massive load lost, the crowbar acts during the transient condition and once the U_{ref} is regained it is turned off.

4.13 GRID SIDE CONTROL

The converter control diagram is depicted in Figure 4.12. The control system is standard for this application and explained in [25]. The main objective of the inverter is to transfer maximum power and ensure compliance with the grid requirements. The voltage in the DC link is measured U_c and compared with the reference U_{ref} , a PI voltage controller generates a reference current I_{dv} after comparing with the actual current in the d-axis. A reactive PI

controller is set such that $Q_{ref} = 0$, then only active power is injected and I_{qv} is generated. Both dq current references enter a current controller that actuates on a transfer function TF with compensating decoupling terms not shown in figure, in order to determine the voltage references. The signals are sent to an inverse Park transformation block to generate the abc voltages. The reference angle is extracted from the grid voltage U_l using a PLL block. Finally, a PWM takes these values and sends pulses to the IGBT's.

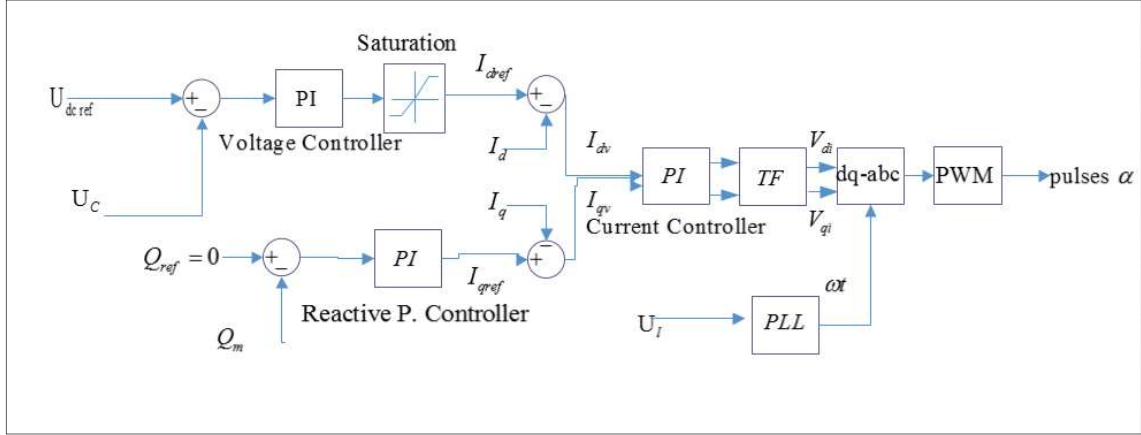


Figure 4.12 Control block diagram grid side converter

4.14 INDUCTION MOTOR

Induction motors are found in many applications in oil and gas offshore facilities. Typically, they represent the largest part of the total load along with synchronous motors. These machines play an important role in the overall dynamic response and system stability. Most of induction motors for water injection purposes are connected to variable speed drives (VSD), in order to control the water flow injected. VSD allows a soft motor starting, and then large currents are avoided by controlling the initial torque and speed. Both torque and speed can be controlled independently by using an appropriate control scheme. Induction motors are complex machines and a simplified version is always advantageous for analysis and control.

A common and convenient approach is to transform the classical primitive three-phase circuit or space vector formulation to the dq -axis reference. The decomposed d and q axis equations with prime sign shown below are referred to the stator [23].

The voltages referred to the stator are given by:

$$V_{qs} = R_s + d\phi_{qs}/dt + \omega\phi_{ds} \quad (4.16)$$

$$V_{ds} = R_s i_{ds} + d\phi_{ds}/dt - \omega\phi_{ds} \quad (4.18)$$

The fluxes established and inductances are calculated by:

$$\varphi_{qs} = L_s i_{qs} + L_m i'_{qr} \quad (4.19)$$

$$\varphi_{ds} = L_s i_{ds} + L_m i'_{dr} \quad (4.20)$$

$$L_s = L_{ls} + L_m \quad (4.21)$$

The electromagnetic torque is expressed by the following equation:

$$T_e = 1.5p(\varphi_{ds} i_{qs} - \varphi_{qs} i_{ds}) \quad (4.22)$$

On the other hand, the mechanical system is represented by:

$$d\omega_m/dt = 1/2H (T_e - F\omega_m - T_m) \quad (4.23)$$

Where T_e is the electromagnetic torque, T_m is the mechanical torque and F is the combined rotor and load viscous friction coefficient.

4.15 PUMP LOAD PROFILE

Induction motors can work with several load torque profiles, depending on the given application. Motors on platforms are connected to water, process pumps or gas compressors. Other pumps are used as cooling medium, lift sea water pumps or for crude oil export through pipelines [21]. Centrifugal pumps and ventilation equipment have a mechanical torque described by the torque equation 4.24,

$$T_m(\omega) = a + b\omega^2 \quad (4.24)$$

where a and b are constants that referred to the pump characteristics and proportional to the squared of the motor mechanical speed ω . For modelling purposes, this profile is taken as reference.

4.16 VARIABLE SPEED DRIVES

Water injection and pump processes in oil and gas installations are controlled by drives connected to induction motors. These drives are known as variable speed drives (VSD). Control of the pump rotational speed means control of the water injected or the oil pumped through a pipeline. Given the changing conditions on the fields, the inductor motor speed is changed accordingly to meet the pressure and flow requirements. Numerous VSDs exist in the market, technologies and ratings are particular for a given application. For medium voltage or high power applications, there are three common technologies of VSD, three-Level Neutral Point

Clamped, the Four-Level Flying Capacitor, and the cascaded H-Bridge[29]. A summary of manufacturers, power range and topologies is shown in Table 4-1 [29].

Manufacturer	Type	Power (MVA)	Topology
ABB	ACS 1000	0,3-5	Three level neutral point clamped
	ACS 5000	5,2-24	Multilevel cascaded H-bridge inverter
	ACS 6000	3,0-27	Three level neutral point clamped
Allen Bradley	Power Flex 7000	0,15-6,7	Current source inverter (CSI)
Alstom	VDM 5000	1,4-7,2	Two level voltage source inverter
	VDM 6000	0,3-8	Four level flying capacitor
	VDM 7000	7-9,5	Three level neutral point clamped
General Electric	Dura-Bilt5 MV	0,3-2,4	Three level neutral point clamped
	MV-GP Type H	0,45-7,5	Multilevel cascaded H-bridge inverter
Siemens	Perfect Harmony	0,2 - 31	Multilevel cascaded H-bridge inverter
	Simovort-MV	0,6 - 7,2	Three level neutral point clamped
	Simovort-S	≥ 10	Load commutated inverter

Table 4-1 Medium Voltage VSD [29].

4.16.1 Control schemes of Induction Motor Drives

Two well-accepted control schemes for medium voltage variable speed drives are: Field oriented control (FOC) and direct torque control (DTC). Based on the results of [29] for PWM modulation, the two classical control methods were slightly modified as Indirect Field Oriented Control (IFOC) and modified torque control (MDTC), and as indicated in the comparison table 4-2. Torque ripple was identified in [11] as a potential problem when intermittent power is feed into the system. Therefore, FOC is chosen in this project, in order to reduce mechanical oscillations on the pumps, because this control scheme has the lower ripple content in comparison to the direct torque control method.

Comparison	IFOC	MDTC
Motor parameters required	$R_s, L_{ls}, L_{lr}, L_m, R_r$	R_s
Sensitivity to motor parameter variations	Very sensitive	Not sensitive
Speed controller response	0,16 s	0,2 s
Phase Voltage THD	9 %	8,40 %
Torque ripple	2,50 %	10 %

Table 4-2 Comparison between control schemes [29].

4.16.2 Field Oriented Control (FOC)

The field oriented control (FOC) technique was developed by F.Blaschke in 1971 for induction motors. Many manufacturers have been using it for several decades. Therefore, it is considered a mature and reliable technology. The advantage of this technique is that it makes the induction

motor resemble a separately excited dc motor, and consequently torque and flux work as decoupled quantities, which allows an excellent dynamic response [29]. In the specialization project [12], the VSD modelled was composed of a three-phase diode rectifier, a braking chopper and a three-phase inverter. The control blocks implemented on the motor side were a speed controller and a field-oriented control loop. The braking chopper or resistor was used for reducing the overvoltage in the DC link, but it has some disadvantages. If frequent accelerations and decelerations are expected, which is the case for a variable energy source the resistor turns out to be too large. Therefore, instead of using a diode rectifier it is possible to use an active front-end rectifier in the standard back-to-back configuration, with a bidirectional power flow.

4.16.3 Grid Side Rectifier

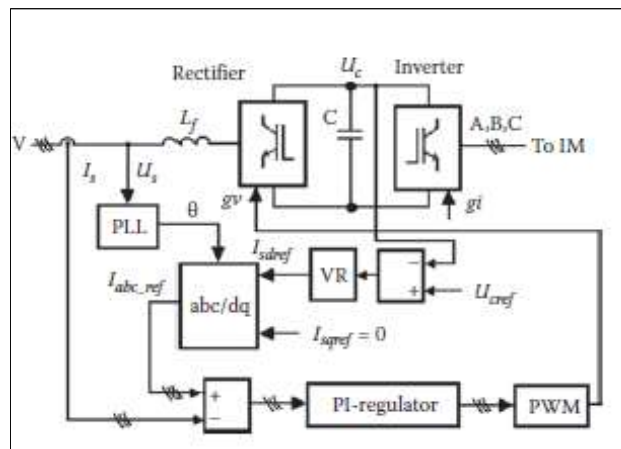


Figure 4.13 FOC high-level schematics [24].

The control system of the rectifier is shown in Figure 4.13. The objective of this rectifier is to keep the DC voltage constant. The reference value $I_{sqref} = 0$, implies that there is not phase shift between the supply voltage and the current. The reference value I_{sdref} defines a power value and its direction, which comes from measuring the voltage on the DC side and uses a voltage regulator VR with PI controllers. This control method allows two different operating modes: motor or generator. In the motor mode, U_c tries to decrease and the control system responds by increasing I_{sd} . In the generator mode, U_c tries to rise and I_{sd} is reduced and even changes its sign because the power must be transferred from the motor to the supply. The reference values I_{sdref} and I_{sqref} are transformed to abc quantities that are feed to a current loop with PI regulators and PWM modulation for pulse control of the IGBTs.

4.16.4 Motor Side Inverter

The schematics of the motor side inverter is shown on Figure 4.14 [24]. The block diagram is a representation of Field Oriented Control. The reference speed is fed to the loop control ω^* , the error signal is processed by the speed PI controller to produce a torque command T_e^* . The reference torque T_e^* and flux calculation ψ^* are required to calculate the stator direct current component i_{ds}^* .

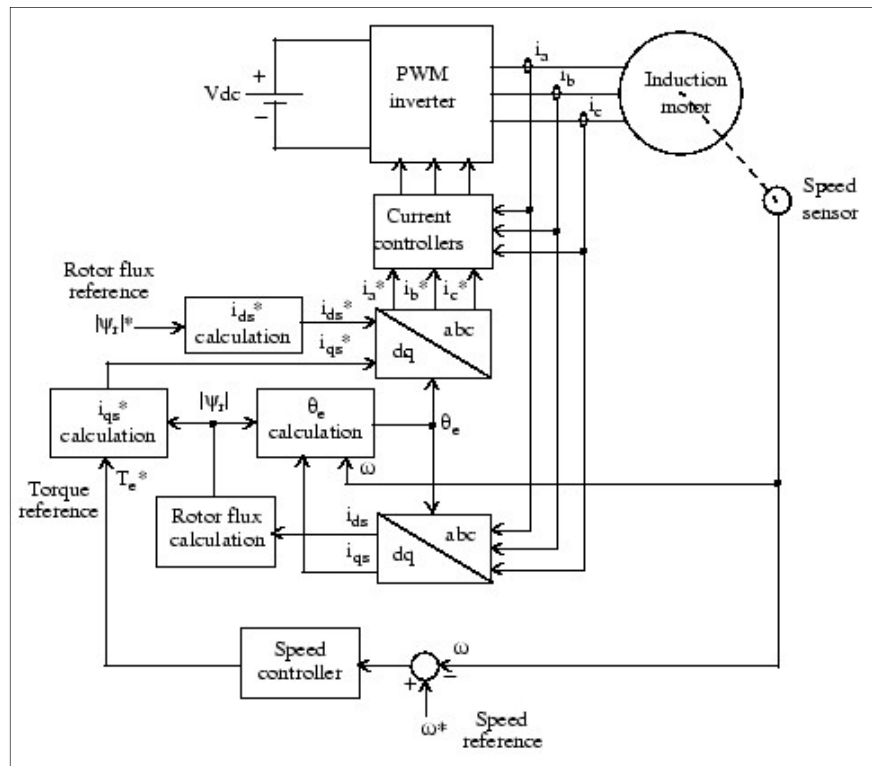


Figure 4.14 Block diagram FOC [24].

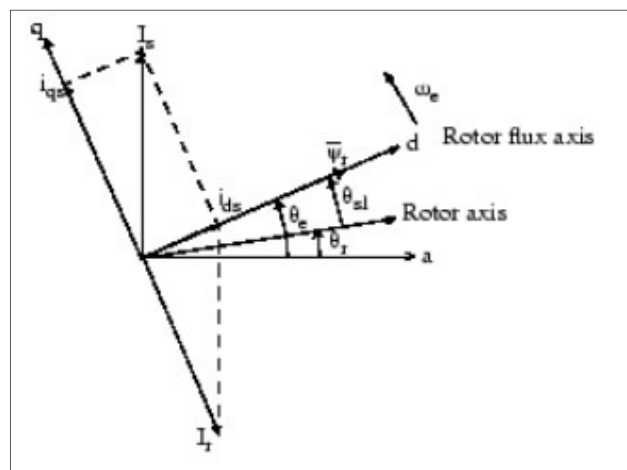


Figure 4.15 Field Oriented control principle [24]

A stator quadrature current is given by the equation 4.25, where L_r is the rotor inductance, L_m is the mutual inductance, and $|\psi_r|_{est}$ is the estimated rotor flux [24],

$$i_{qs}^* = \frac{2}{3} \frac{L_r}{L_m} \frac{T_e^*}{|\psi_r|_{est}} \quad (4.25)$$

On the other hand, the estimated rotor flux value is calculated by the following relation, where $\tau_{rS} = L_r/R_r$ defines the time constant

$$|\psi_r|_{est} = \frac{L_m i_{ds}}{1 + \tau_{rS}} \quad (4.26)$$

The direct axis current reference i_{ds}^* is solved from the rotor flux reference input $|\psi_r|^*$

$$i_{ds}^* = \frac{|\psi_r|^*}{L_m} \quad (4.27)$$

The rotor position seen in Figure 4.15 θ_e is needed to apply the correspondent coordinate transformation. This angle is solved by integrating the rotor speed ω_m and slip frequency ω_{sl}

$$\theta_e = \int (\omega_m + \omega_{sl}) dt \quad (4.28)$$

In turn, the slip frequency is obtained using the motor parameters and quadrature current component i_{qs}^*

$$\omega_{sl} = \frac{L_m}{|\psi_r|_{est}} \frac{R_r}{L_r} i_{qs}^* \quad (4.29)$$

The dq -current references should be transformed back to phase quantities, which are compared to the phase measured quantities. The error signal is fed into a current regulator; in this case, a hysteresis type regulator is used. A PI controller is another possibility.

4.16.5 Control of back-to-back VSD: Test Case

An induction motor with a front-end active rectifier and an inverter with field-oriented control is tested in this section to validate the theory discussed. The motor response is illustrated in Figure 4.16. The starting up current is roughly three times the nominal current. This result is better compared to the results obtained in the specialization project [12], when the starting current was five times the nominal value. Then it can be said that an improved soft starting is achieved by controlling the rectifier and the dc link voltage.

Different reference speeds are applied to the drive. It has been demonstrated in [12], that a decoupled torque and speed control can be applied. However, the mechanical load from the pumps are expressed in terms of a quadratic function of the rotational speed as described by equation 4.24. Consequently, the only control variable is the motor mechanical speed.

The first speed step of 0.4pu is applied at 0.001s. The first graph of Figure 4.16 has two curves, the magenta curve is the reference speed value and the blue curve is the measured speed. At 1.5s, another speed step of 0.8pu is given; the electromagnetic torque experiences an increase up to 2pu to accelerate the machine to the new desired speed value. On the other hand, the mechanical torque of the pump follows the new reference but it changes in a quadratic dependency in relation to the new speed and it has a smoother response compare to peaks shown in the electromagnetic torque. Next, a deceleration at 3s is introduced to 0.66pu. The system reacts with a negative electromagnetic torque of -1.7pu to decelerate the machine. At the same time, stator currents are reduced from 0.55pu to 0.45pu due to a slower speed and mechanical torque. Finally, at 5s the motor is set to reach nominal speed of 1.05pu, under a slip value of 5%. One second after at 6s, the machine reaches the nominal values. The electromechanical torque 1.13pu is slightly higher than the mechanical value 1.06pu to account for friction losses. The motor drive active and reactive power in Figure 4.17 illustrates the system response under different operating conditions. The active and reactive power during the first cycles is large and corresponds to the system energization and start-up period. Large active and reactive power are withdrawn from the supply source as expected during this period, but it is smaller than a direct line start-up given a soft-starting situation. Another observation is that at low speeds the reactive power is larger during the first second while the system is establishing its initial state

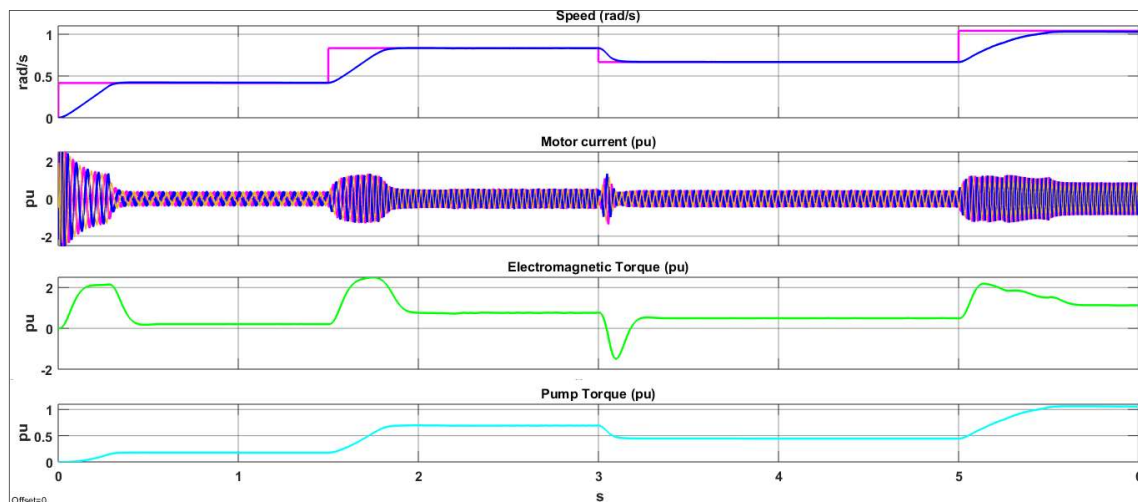


Figure 4.16 VSD Dynamic Performance FOC

During the second speed step of 0.8pu at 1.5s an active peak demand is experienced, also the reactive power rises. At 3s the system decelerates to 0.66pu, this excess of energy instead of being burnt by a chopper resistor is it sent back to the supply source, a regenerative braking can be useful to avoid high temperatures in a resistor bank. This point is important under the

assumption of frequent changes given the fluctuating nature of the wind profiles. Finally, at 5s the system is tested under nominal conditions the active power is 2.5MW and the reactive power is 0 MVar, which coincides with the control strategy of no-reactive power or current reference of $I_{sqref} = 0$.

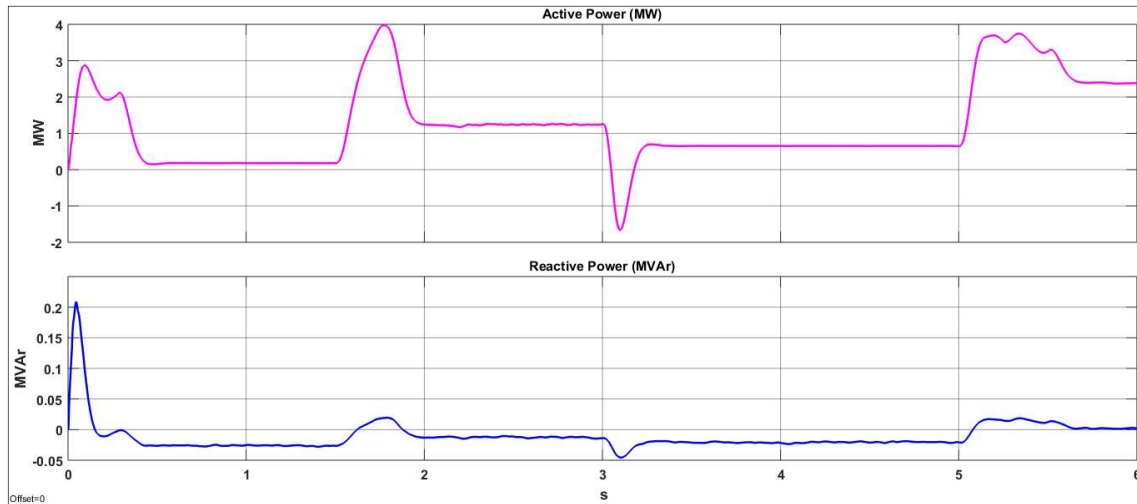


Figure 4.17 VSD Active and Reactive Power

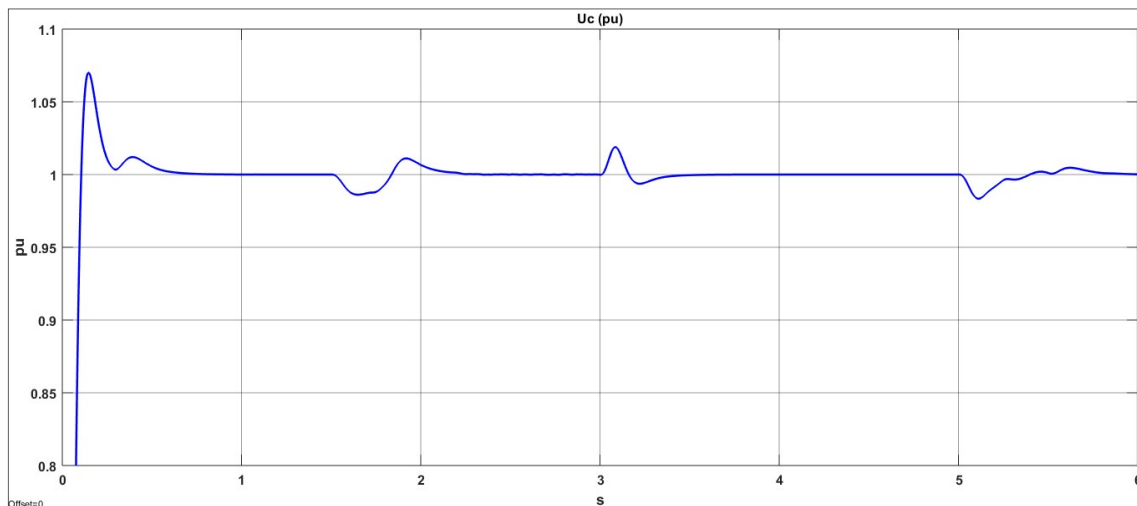


Figure 4.18 VSD back-to-back DC Link

On the other hand, a different circuit part to be investigated is the DC link in the VSD. The direct voltage at the output of the active-front rectifier, Figure 4.18 shows a stable operation under the different operating conditions. The disturbances displayed correspond to speed alterations. For example, the second and last valley at 1.5s and 5s are voltage drops due to increased power absorption during accelerations. On the other hand, the voltage peak at 3s is a

deceleration case, and energy is delivered to the source. It is important to notice that under all circumstances the dc link control is effective and displays a fast recovery.

5 STUDY CASES: HYBRID WIS MODEL

This section investigates the control and performance of the test hybrid-topology, see Figure 5.1. The system was developed in Simulink™ SimPowerSystems. As mentioned before, the system is fed by a gas turbine in parallel with a wind turbine. Offshore platforms serve priority and flexible loads. The flexible loads can minimize the negative effects of wind power fluctuations by controlling their demand.

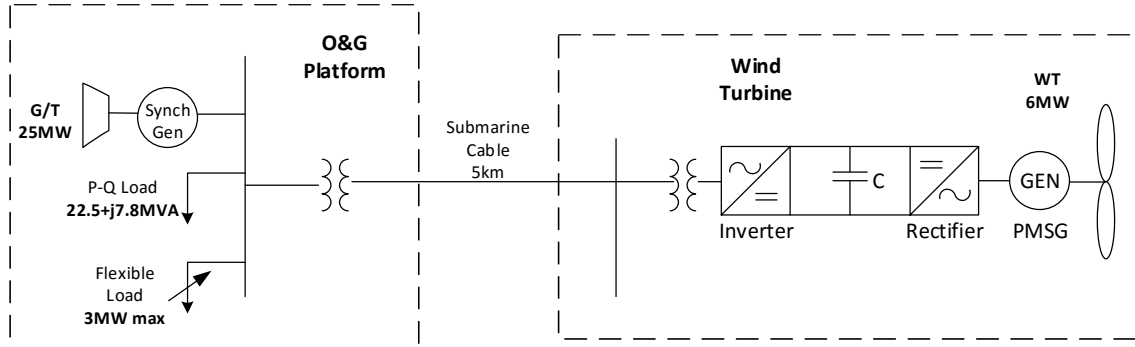


Figure 5.1 Hybrid Topology for WIS

Two study cases will be presented in the sections 5.1 and 5.2 as a generalization of a hybrid system. The first case refers to an O&G platform with a 20MW gas turbine, a 6MW wind turbine, and a 19MW fixed load. The second case will consider a mixed load, composed of a fixed load of 16MW and a flexible load of 3MW. The objective in this second case is to review a system behavior, under a flexible load situation. The aim is to demonstrate how load control can effectively contribute to a feasible operation in a scenario of high wind capacity and to understand how it can contribute to smooth out the power fluctuations of the system.

5.1 CASE 1: FIXED LOAD

The system is tested under different wind conditions. The goal is to verify the system dynamics under high and low wind scenarios, and to understand how the contribution of a 6MW wind turbine affects the system stability of a 20MW gas turbine that feeds a fixed 19MW load. The regulation function is mainly performed by the gas synchronous generator as will be shown later in this section.

5.1.1 Wind Turbine (WT): Hybrid WIS

The stator currents $I_{abc\text{stator}}$ are proportional to the electromagnetic torque according to the equation (4.13), where $i_d = 0$. The rotor speed is controlled depending on the wind speed, for best performance, a different speed reference ω_{ref} must be calculated. Changing the rotor

reference speed allows changes on tip blade speed λ_{tip} for maximum power extraction. The pitching mechanism is set to act at 1.33pu of the rotor speed by a proportional controller, limiting mechanical stress and power output.

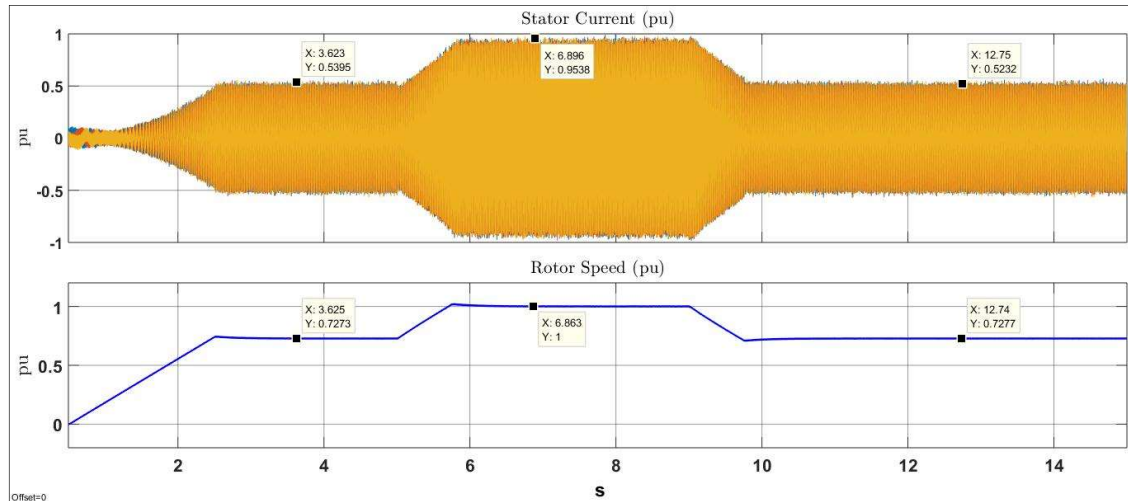


Figure 5.2 PMSG stator currents and rotor speed

The first wind speed step 8m/s occurs at 0.5s, which takes the turbine to nearly 0.72pu in rotor speed. The second step 11m/s is at 5s. The registered rotor speed is 1.0pu as expected, the stator current is slightly lower than 0.95pu. At 9s the wind speed is decreased again to 8m/s, resulting in 0.72pu in rotor speed as observed in more detail in Figure 5.2.

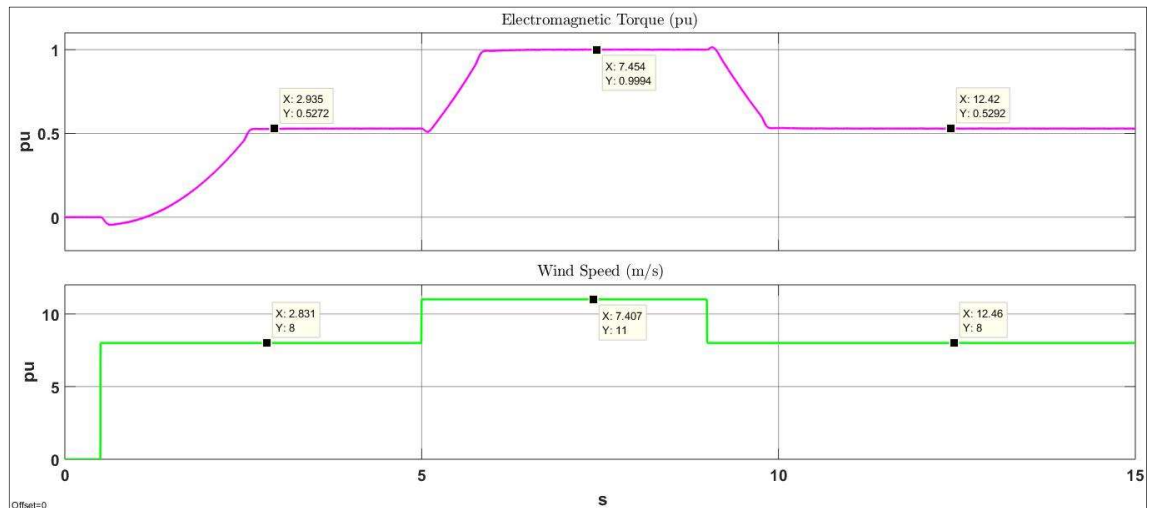


Figure 5.3 PMSG electromagnetic torque and wind speed

Figure 5.3 illustrates the PMSG torque output at various wind speeds. Naturally, the torque is increased by the wind speed according to equation (4.14). The relationship is clearly not proportional, with a wind speed of 8m/s the electromagnetic torque is 0.52pu. When wind

speed is increased at 5s to the rated wind speed of 11m/s, the electromagnetic torque reaches 0.99pu as expected. It is important to emphasize that the control on the rotor speed optimizes the generated power.

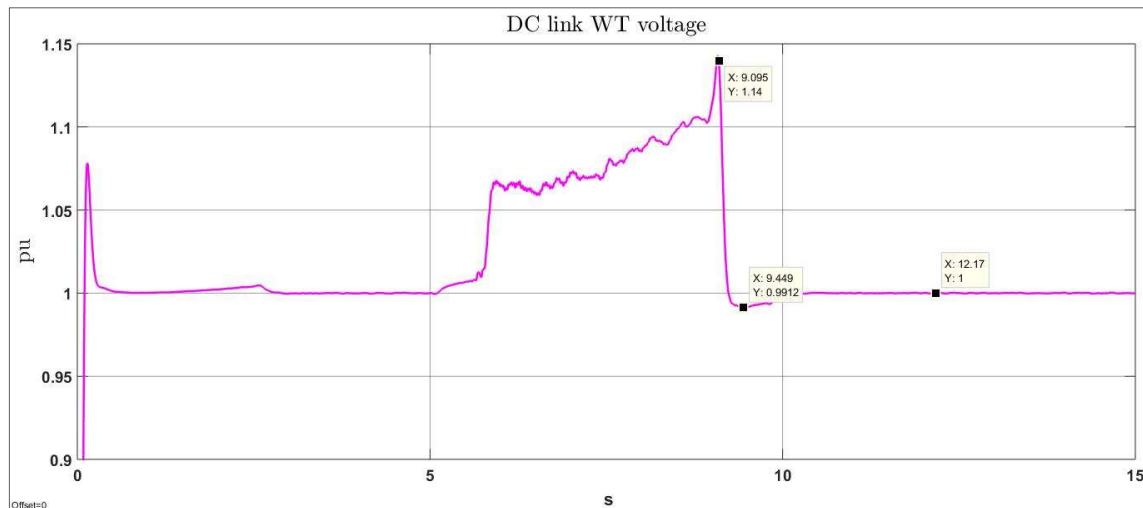


Figure 5.4 Wind turbine DC link voltage and control signal.

The DC link voltage in the wind turbine must be kept within a permissible range. Protection resistors are placed in parallel to the DC capacitor. The objective is to protect the system of overvoltages that could deteriorate the solid-state components. The control scheme is referred to as crowbar protection in section 4.12, described by a simple tolerance band. The band is modeled as relay with a threshold, with a switch on point at $U_{dc} = 1.15V_{dc}$ and a switch off point below this value. This indicates that the overvoltage allowed is 15% in continuous operation. When the voltage surpasses the region, the switch is activated and the resistor bank is connected in parallel to the capacitor introducing a voltage drop on the DC link. At 9s, the system experiences a low energy injection from the wind turbine (8m/s), then the DC voltage experiences a peak of 1.14pu followed by slightly drop falling to approximately 0.99pu. The voltage controller corrects the value restoring the nominal value to 1pu.

5.1.2 Gas Synchronous Generator (GT)

The gas turbine has two control subsystems: field voltage (excitation) and mechanical power (gas turbine). The dynamics presented in Figure 5.5, are the terminal $V_{terminal}(pu)$ and field $V_{field}(pu)$ voltages, magenta and blue curves respectively. The exciter is an IEEE type 1 synchronous machine voltage regulator combined to an exciter. The modelled implemented is an excitation system block integrated in Simulink® and recommended in [30]. The transients observed during first cycles are due to the magnetic field establishment. Later at 5s, the wind

turbine contribution (wind step: 11 m/s) is affecting the system voltage and the exciter seeks another stability point weakening the excitation field from $V_{field} = 2.14pu$ to $V_{field} = 1.92pu$. The terminal voltage $V_t(pu)$ must be kept close to 1.0pu regardless of the operating point.

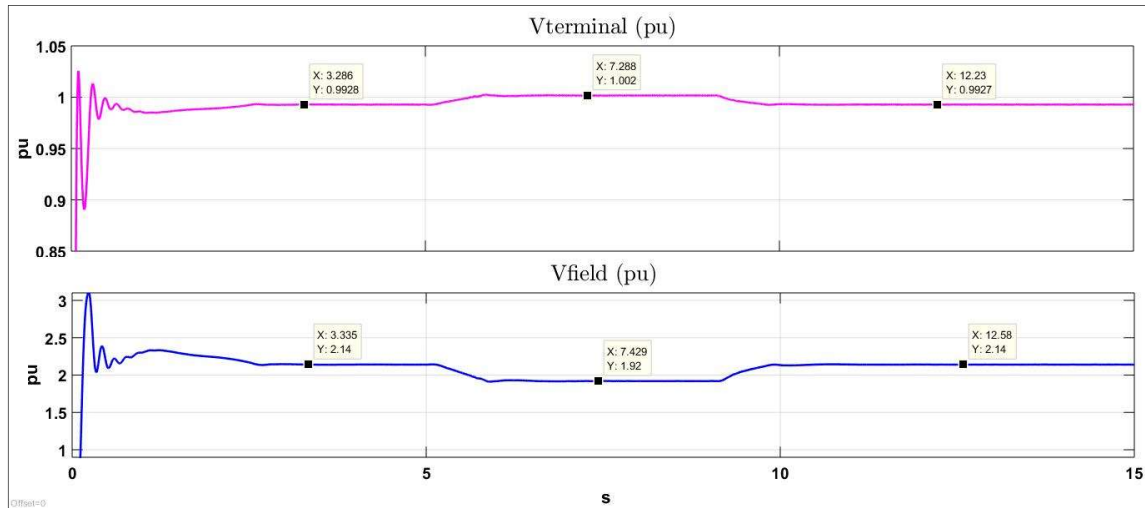


Figure 5.5 Gas synchronous generator $V_{terminal}(pu)$ and $V_{field}(pu)$ voltages. Case 1

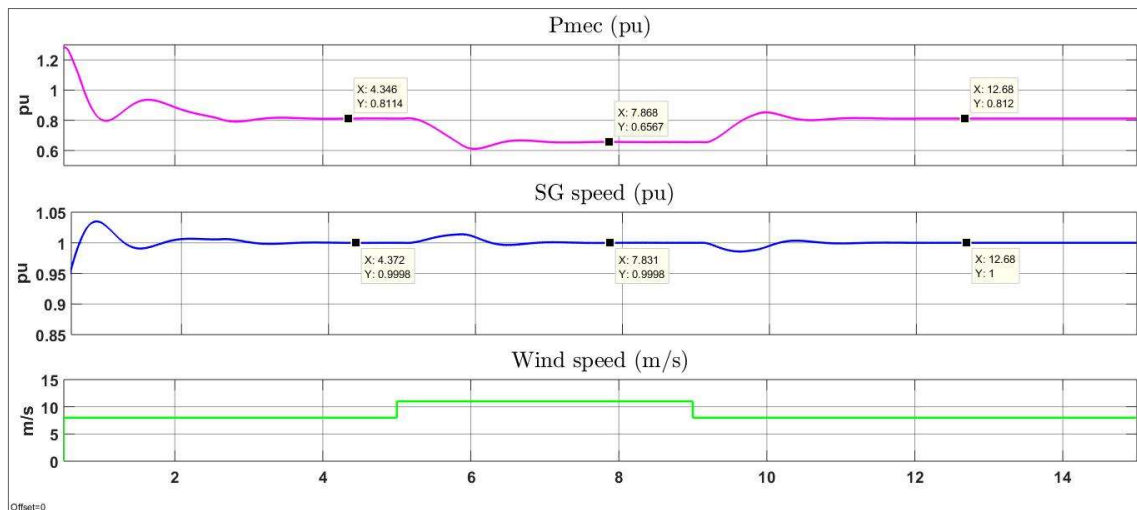


Figure 5.6 Gas synchronous generator $P_{gen}(pu)$ and $Q_{gen}(pu)$. Case 1

Figure 5.6 illustrates GT mechanical power $P_{mech}(pu)$ and rotor speed $\omega_{gen}(pu)$ for a given wind profile. The rotor speed has the same waveform as the system frequency. On the other hand, the mechanical power experiences changes along the 15s interval studied depending on the wind speed. The mechanical power output is of 0.81pu for 8m/s and of 0.65pu for 11m/s. This indicates that the wind power is high and it has priority over the gas turbine power. Lower

power output is required from the gas turbine when the wind speed is high. In contrast, higher power output is needed when the wind speed is low as to satisfy the load demand.

5.1.3 Active and reactive power

Wind Turbine (WT)

The WT active and reactive power are measured after the filtering inductance, located at the output of the WT inverter. As can be seen from the Figure 5.7, the back-to-back converter works properly and there is not net reactive injection Q_{wind} into the network as indicated. The reactive power control was achieved by using an additional control loop over the WT grid-side converter.

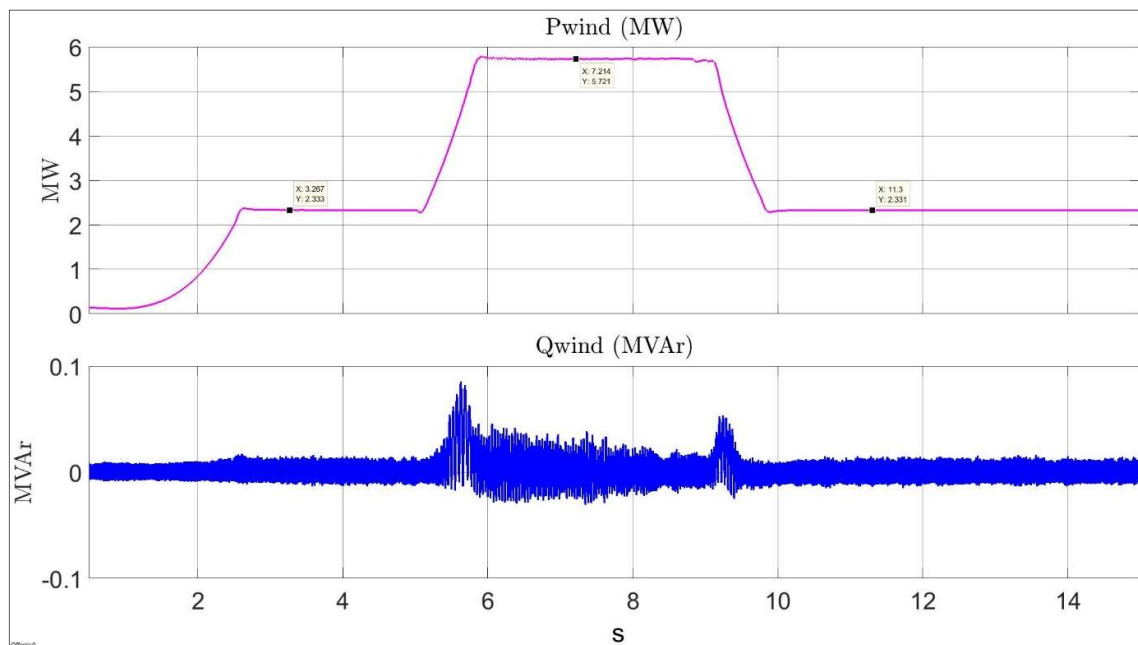


Figure 5.7 Active and reactive power wind turbine

Gas turbine (GT). Case 1

Both active and reactive power balance is achieved through the adequate control of both sources. As indicated in Figure 5.7 and 5.8, the load $S_{load} = 19MW + 4MVar$, is supplied by complementing both units. Notice also that the synchronous GT feeds the reactive load needs, since not contribution is taken from the WT. On the other hand, the GT active power is initially $P_{gt} = 16.4MW$ with 8m/s, and later drops to $P_{gt} = 13.3MW$ when the WT power is $P_{wind} = 5.7MW$ for 11m/s. Later at 10s, the initial contribution is restored after a new wind step of 8m/s.

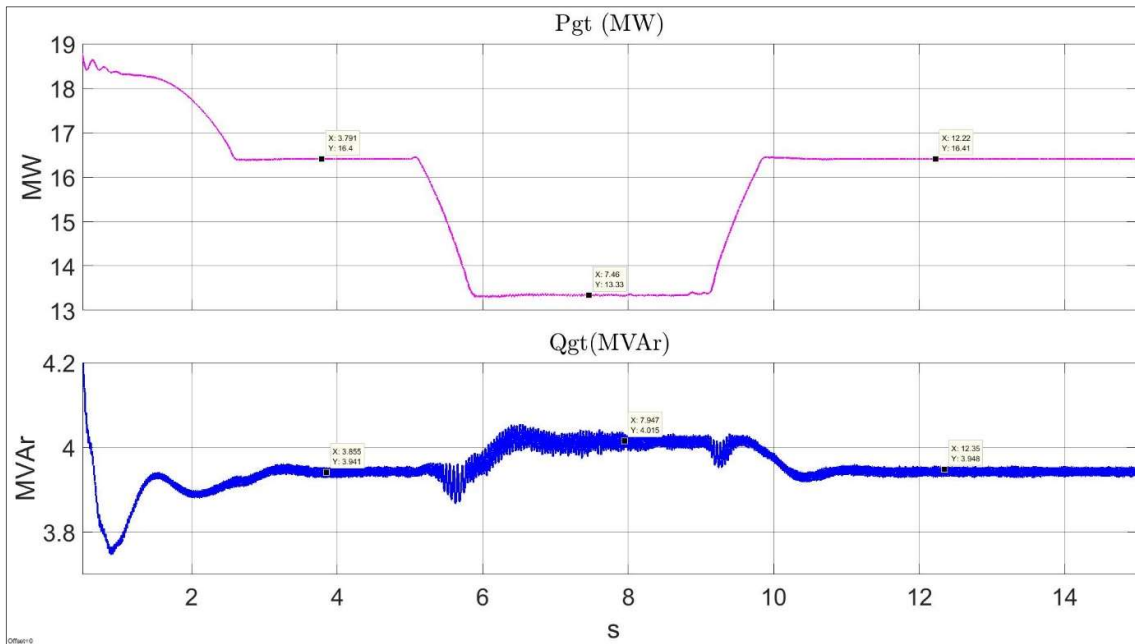


Figure 5.8 Active and reactive gas turbine. Case1

5.1.4 Overall Stand-Alone System. Case 1

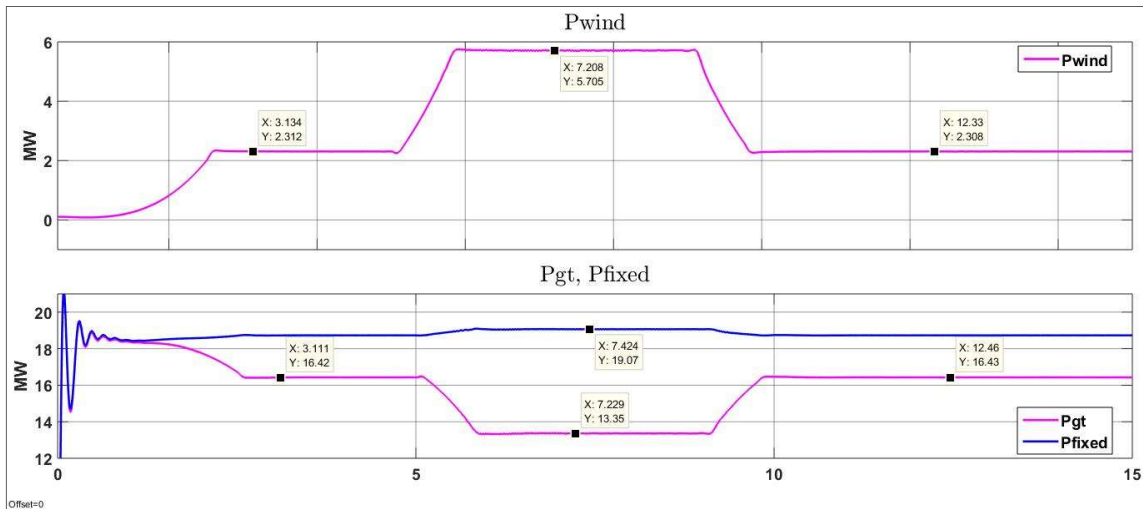


Figure 5.9 Power Curves with Fixed Load. Case 1

The general system waveforms for fixed load are indicated in Figure 5.9. The system is a representation of a conventional O&G platform with fixed loads. A fluctuating wind power has an impact on the system performance; here the wind penetration is 31.57%. The power quantities for WT, GT and FL (fixed load) represented by P_{wind} , P_{gt} and P_{fixed} , respectively. The GT takes the variations, and it is the main responsible for the system stability. After 5s, the

gas turbine reduces generation from $P_{gt} = 16.42 \text{ MW}$ to $P_{gt} = 13.35 \text{ MW}$ or 66.75% of its capacity (20MW), due to an increase of wind power $P_{wind} = 5.70 \text{ MW}$. The GT restores its initial power output at 12.46s, once the initial wind speed is reached. Even though, GTs are flexible units, constant variations might affect their performance, efficiency and higher maintenance requirements. Furthermore, the system frequency is impacted as shown in Figure 5.10, the peaks and valleys are natural response during high and low wind power conditions, respectively. The frequency dynamics depends on the wind power fluctuations to a degree given by the wind penetration or load management. The highest frequency is 50.72Hz at 5.844s after the second wind step of 11m/s and the lowest is 49.28Hz following a wind step of 8m/s.

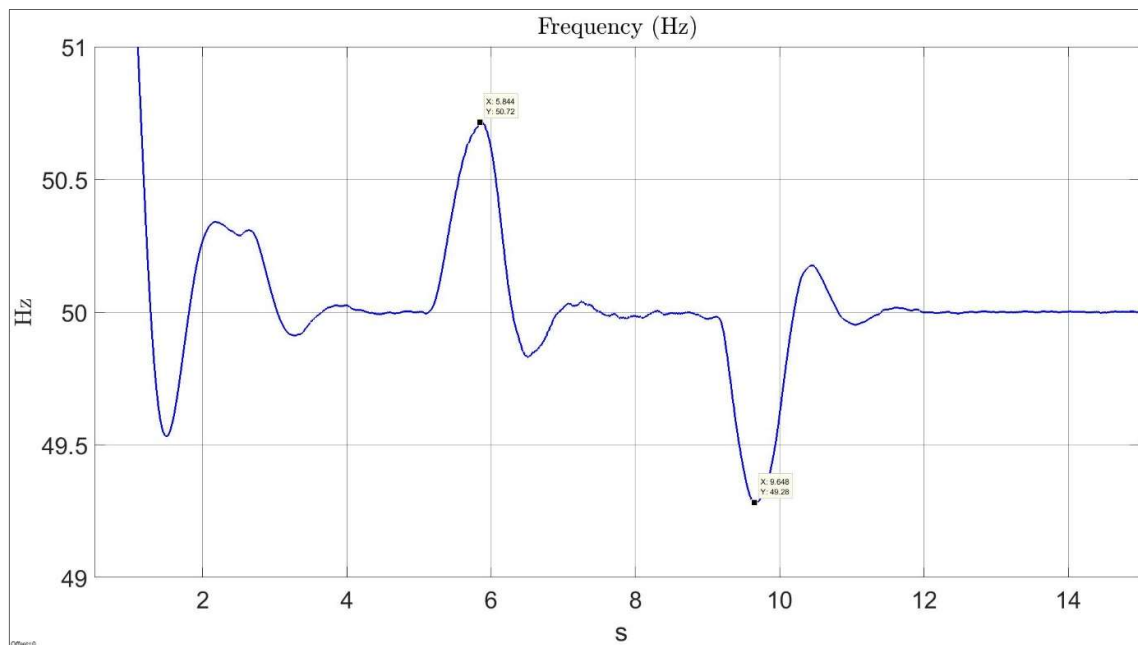


Figure 5.10 System Frequency. Case 1

5.2 CASE 2: FIXED AND FLEXIBLE LOAD

A new approach is studied in this case, the load is divided between fixed component of 16MW and flexible component of 3MW, called flexible load. The inductive load remains in 4MVar. This flexible load represents an idealization of a water injection pump. Since the wind profile and the turbine characteristics are the same, the wind turbine dynamics are not explained in this section. The emphasis is made on the gas turbine response under the condition of a flexible load component, representing the water injection pump.

5.2.1 Gas Synchronous Generator

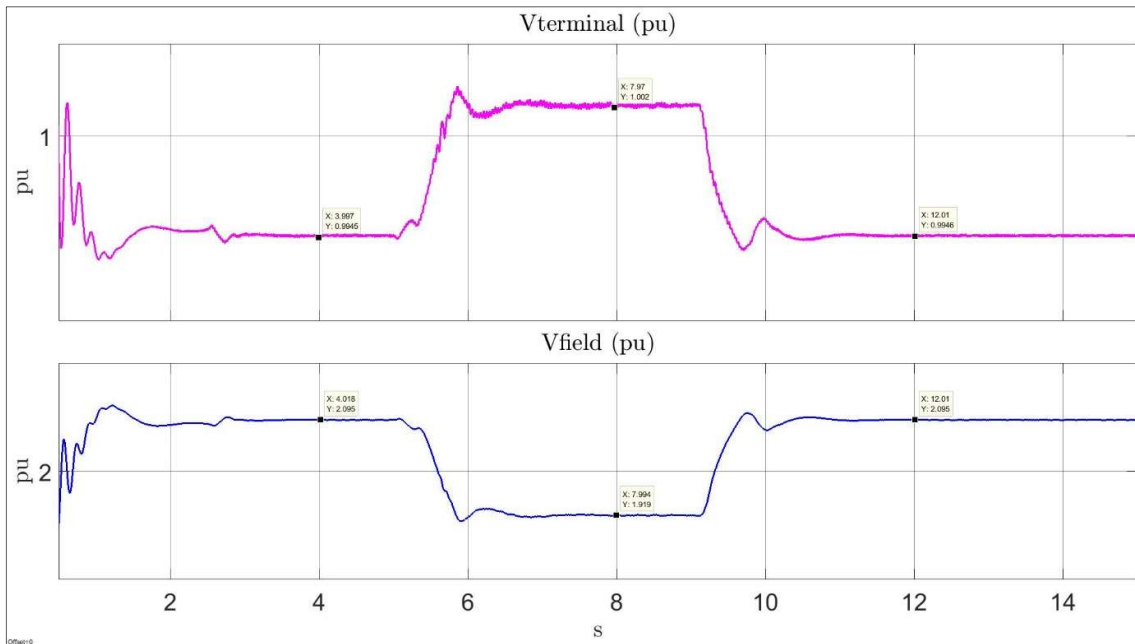


Figure 5.11 Gas synchronous Generator $V_{terminal}$ (pu) and V_{field} (pu) voltages. Case 2

Figure 5.11 and 5.12 illustrate the waveforms for the gas synchronous generator. The elasticity of the flexible load has an impact in the mechanical output. The flexible load is not consuming reactive power. However, there is a slight affectation in the V_{field} compared to Figure 5.5 in case 1.

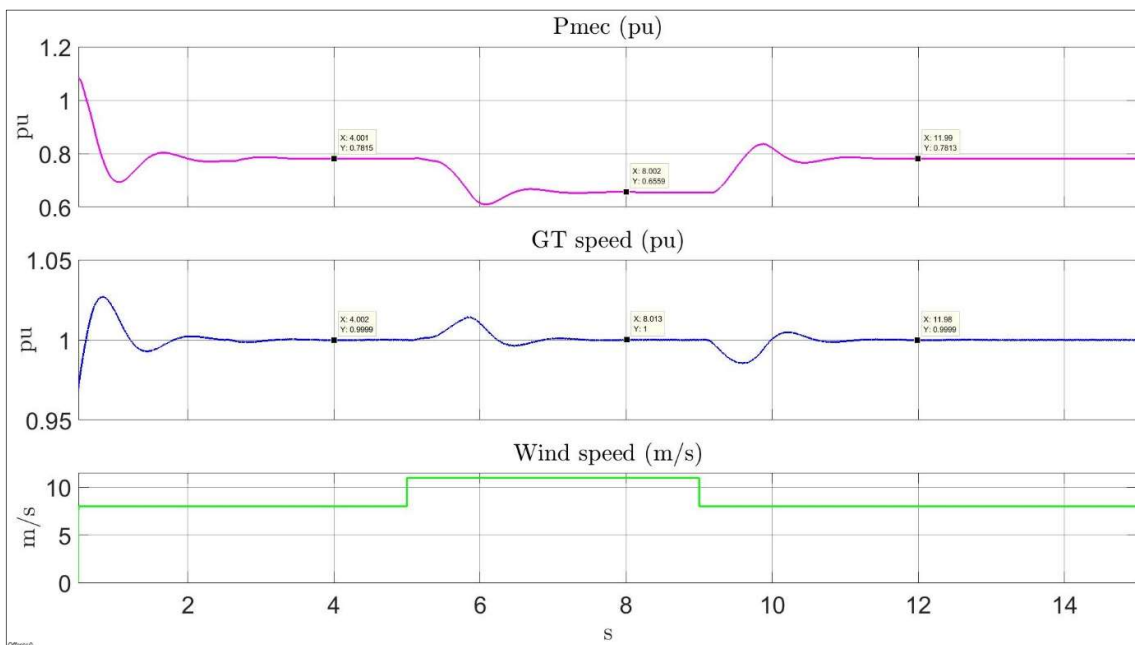


Figure 5.12 Gas synchronous generator P_{gen} (pu) and Q_{gen} (pu). Case 2

The rotor speed associated with the active power is affected for the load control, here the oscillations on the rotor are dampened compared with the previous case, which is better observed in system frequency in Figure 5.15.

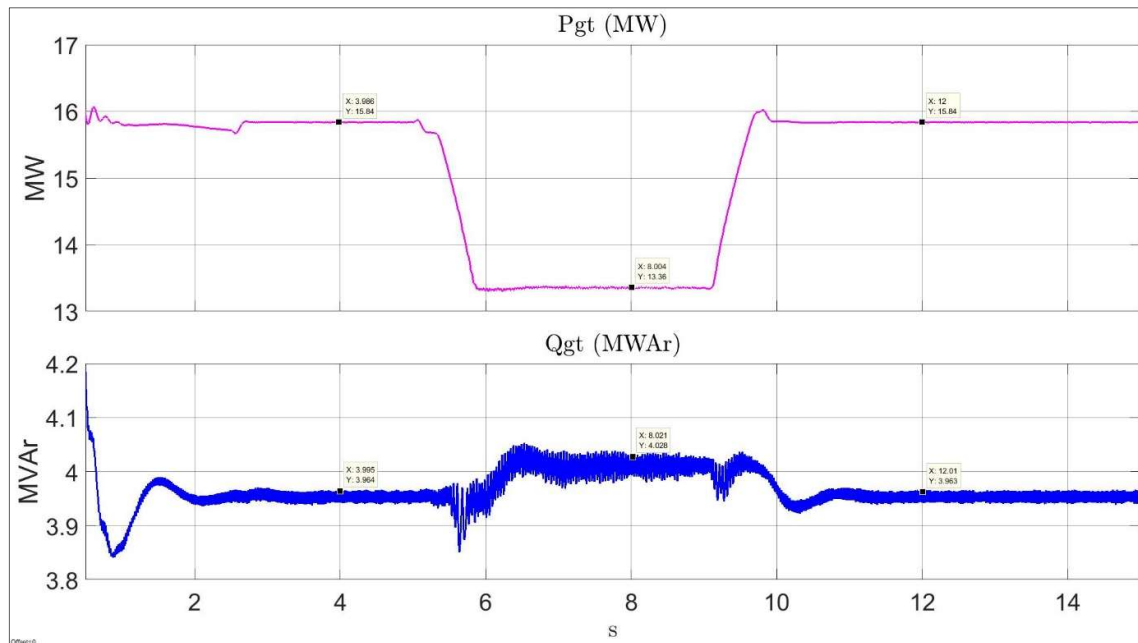


Figure 5.13 Active and Reactive Power Gas Turbine. Case 2

Active and reactive power from the GT are shown in Figure 5.13. Since, the flexible load follows the wind generated, the GT is not providing extra power output when there is a low wind condition, instead the flexible load demand is reduced. Since, there is not reactive component in the flexible load, the reactive power does not present any changes. This assumption is because the load ideally will not consume reactive power. However, an induction motor in a real case will influence the reactive power when it is controlled.

5.2.2 Overall Stand-Alone System. Case 2

The flexible load follows the energy generated by the WT. The GT produces energy for the fixed load. The power waveforms have a perfect match between generation and consumption. Since the flexible load has a maximum limit of 3MW, an excess of 2.71MW is integrated into the system, resulting in a reduced power output from the gas turbine as shown in the valley form in Figure 5.14 to $P_{wind} = 13.36MW$. A more realistic situation, will consider a shifted flexible load curve between the generation and the demand, given that the actuators and the controllers have a finite actuation time.

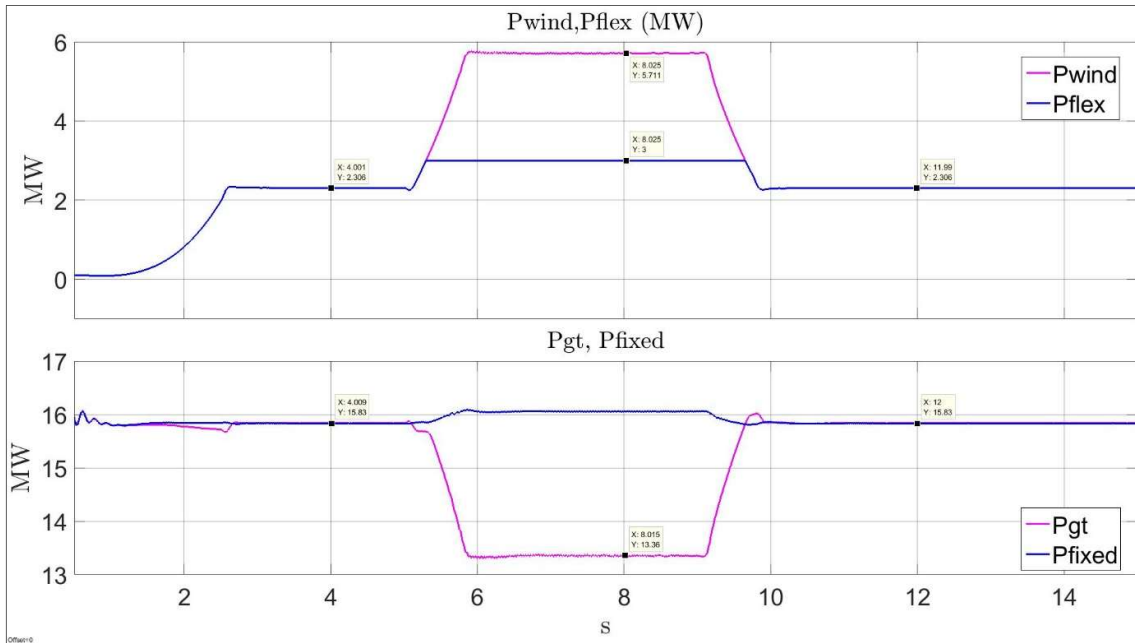


Figure 5.14 Power Curves with Fixed Load. Case 2

The system frequency can be examined in Figure 5.15. The frequency swings from a maximum peak of 50.7Hz to a minimum of 49.25Hz. The disturbances observed coincide with the highest wind step (13m/s) and the lowest wind step (5m/s), which is part of natural response of a synchronous generator.

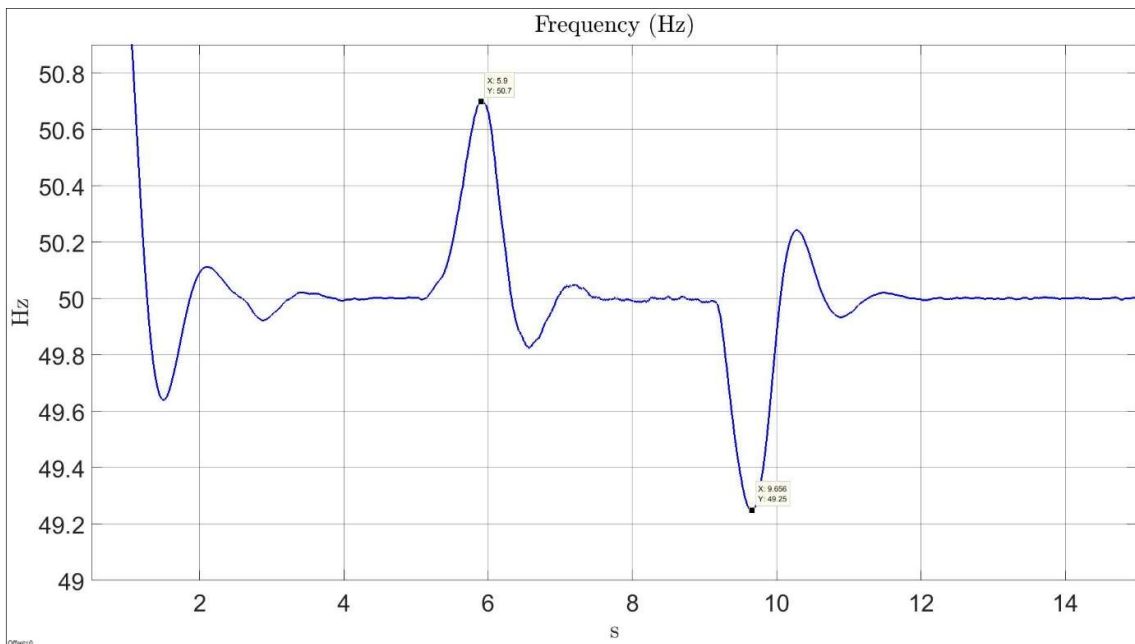


Figure 5.15 System Frequency. Case 2

5.3 DISCUSSION OF RESULTS

Comparison between both studies is understood by revising Figures 5.9 and 5.14. An O&G platform that integrates wind power to its system will exhibit power and frequency fluctuations as indicated in Figures 5.9 and 5.13. The wind penetration index is limited to the capacity of the synchronous machines that have to keep the system stable. The approach presented in Case 2, adds a different degree of freedom to the problem by controlling the load. The flexible part considered is 3MW out of 19MW, which represents a 15.78%. Even though, this percentage is conservative considering that the system can have a large component of controlled pumps. It is clearly demonstrated that suitable control strategy on the induction motors can improve the system performance. For example, there is a “decoupling” effect between the wind power and thermal power. In other words, the system seems to be unaffected by the wind fluctuations as long as the energy is absorbed by the flexible load (pumps). When this load reaches its maximum nominal value, the GT starts to reduce its power output. In fact, comparing the frequency in both scenarios Figure 5.10 and 5.15, the fixed load case presents larger frequency oscillations compared to the flexible load case. Considering a case with multiple turbines and a larger proportion of controllable load, it is possible to deduct that the system will be less impacted by the wind intermittency. Consequently, larger proportion of wind power could be integrated to the O&G facilities in a more efficient and stable manner. On the other hand, it is worth mentioning that a gas turbine working close to its nominal value has a better efficiency. Additionally, avoiding turn-on and off cycles due to wind fluctuations implies less intensive maintenance on the gas turbines.

6 STUDY CASES: STAND-ALONE WIS TOPOLOGY

6.1 CASE 1: FIXED LOAD AND FLEXIBLE LOAD

The system has the following characteristics,

Wind Turbine: 6MW

Fixed load: 1 MW

Flexible load: 3MW

Additionally, a 5MVA synchronous flywheel is defined. The system configuration is presented in Figure 3.3.

6.1.1 Wind Turbine Stand-Alone

The *abc* stator currents, rotor speed and wind speed are presented in Figure 6.1. Here the system is started up with at 0.02s with a wind step of 9 m/s. In this case, the energization depends exclusively on the WT; this wind step takes the machine to a speed of 0.81pu and a current of 0.66pu. The stator current reaches 0.95pu during rated wind speed of 11m/s and a rated rotor speed of 1.0pu at 7.54s. This follows at 9s a wind step of 7m/s, decelerating the WT to 0.62pu and reducing the stator current to 0.43pu. Finally, a wind step of 8m/s accelerates the WT to 0.73pu and a current of 0.50pu. the system behaves as expected.

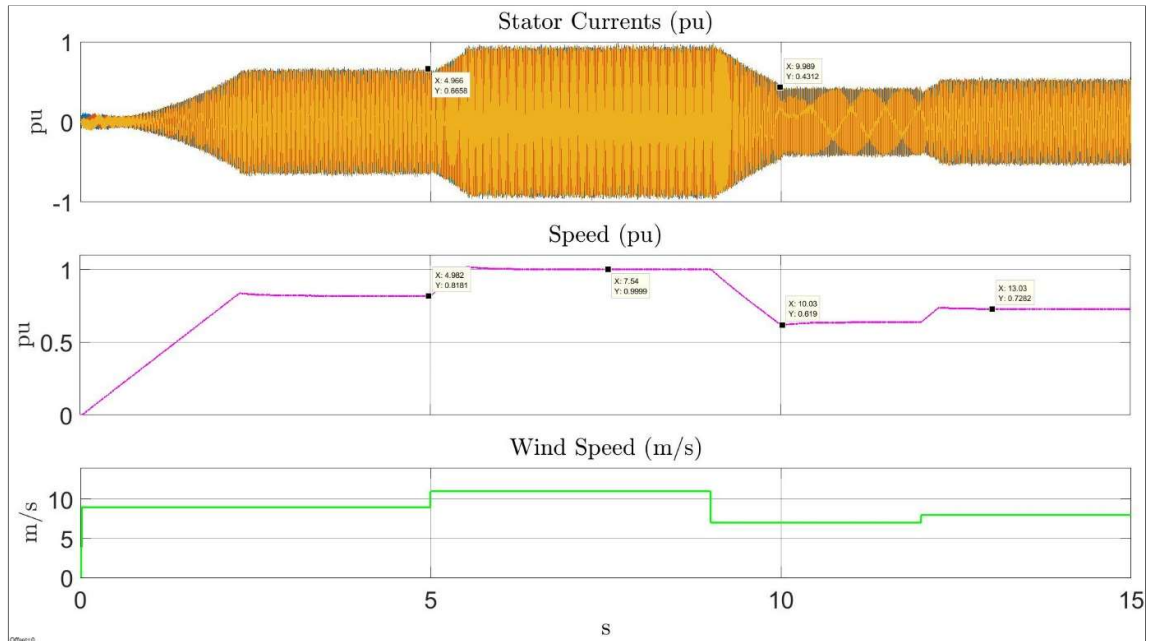


Figure 6.1 PMSG stator currents and rotor speed

Figure 6.2 indicates all the different torque operating points, demonstrating the relationship between speed and torque, it is worth mentioning that the generator speed is set for maximum power extraction. The first torque for 9m/s is 0.67pu, and as expected a torque of 1pu for rated speed. Then two more steps of 0.41pu and 0.53pu for 7m/s and 8m/s respectively.

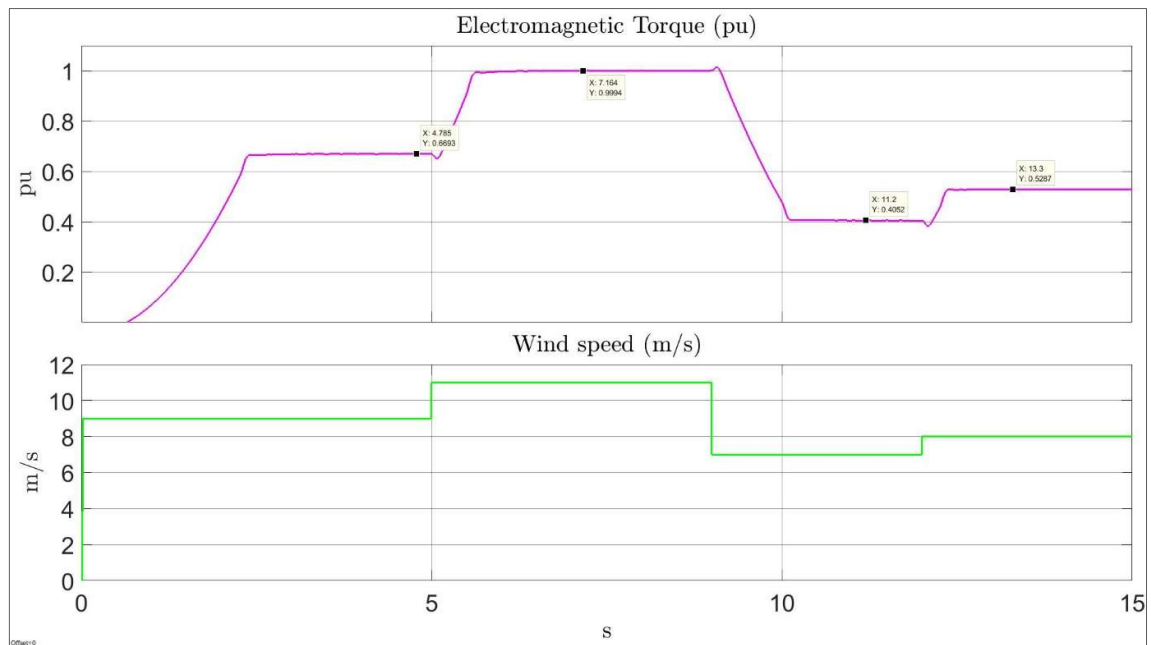


Figure 6.2 PMSG electromagnetic torque and wind speed.

The curve shown in Figure 6.3 represents the U_{dc} link WT voltage. At 5s the wind speed increases to 11 m/s and the voltage magnitude jumps to above the 10%. However, the crowbar protection is activated when the voltage is above 15%, which is not the case. At 9s the wind changes to 7m/s, which is a large fluctuation. The WT reacts trying to keep the DC link voltage avoiding a large voltage drop. The peak value registered is 1.13pu at 9.35s, and it is not enough to activate the crowbar. In other tests, not shown here, the crowbar was activated for wind speeds above the rated speed and during transients where DC link was superior to 15% of nominal voltage.

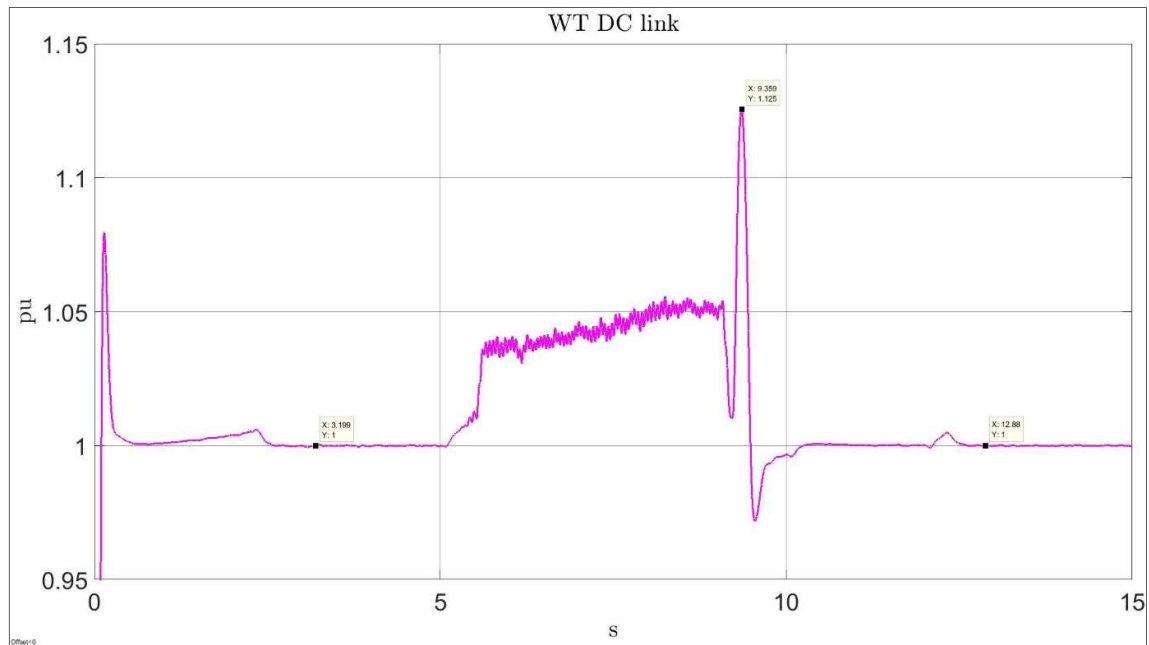


Figure 6.3 Wind turbine DC link voltage

6.1.2 Synchronous Flywheel Stand-Alone

The 5MW synchronous flywheel (FW) has an inertia coefficient of $H = 6.9s$. This inertia helps the system to accumulate energy in kinetic form. As illustrated in Figure 6.4, the FW power P_{fw} is absorbed and released to the system. The flywheel accelerates and decelerates as a function of the system energy balance. At 5s the wind speed is increased to 11m/s, producing more power than the required by the loads leading to a consumption in the FW in form of kinetic energy. The negative peak observed after 5s is the converted kinetic energy absorbed by the rotating masses with a peak value of -1.69MW at 7.54s. The dump load (DL) controls the FW. Once the DL finds a frequency deviation beyond 0.2Hz; it increases the resistor load to reestablish a valid frequency range. At 9s, a negative wind step from 12m/s to 7 m/s, makes the FW decelerate faster and it swings to a low value. The actuation of the DL and low wind situation are relative close events.

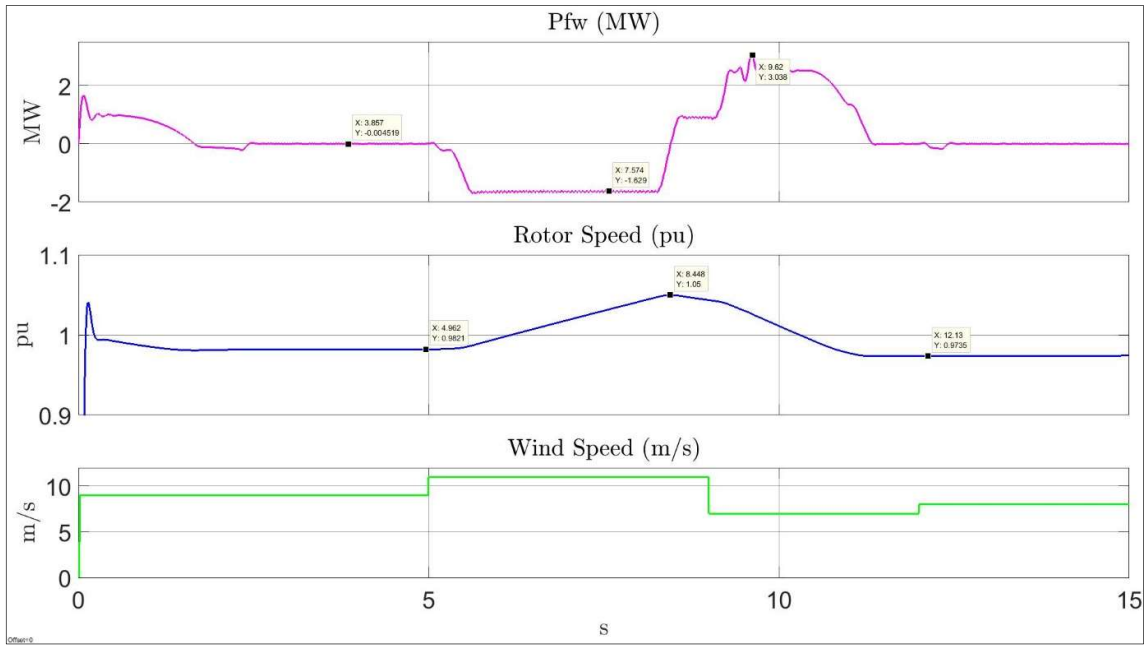


Figure 6.4 Synchronous flywheel P_{sg} (pu), ω_{sg} (pu) and wind speed. Case 1

6.1.3 Active and reactive power

Wind Turbine (WT)

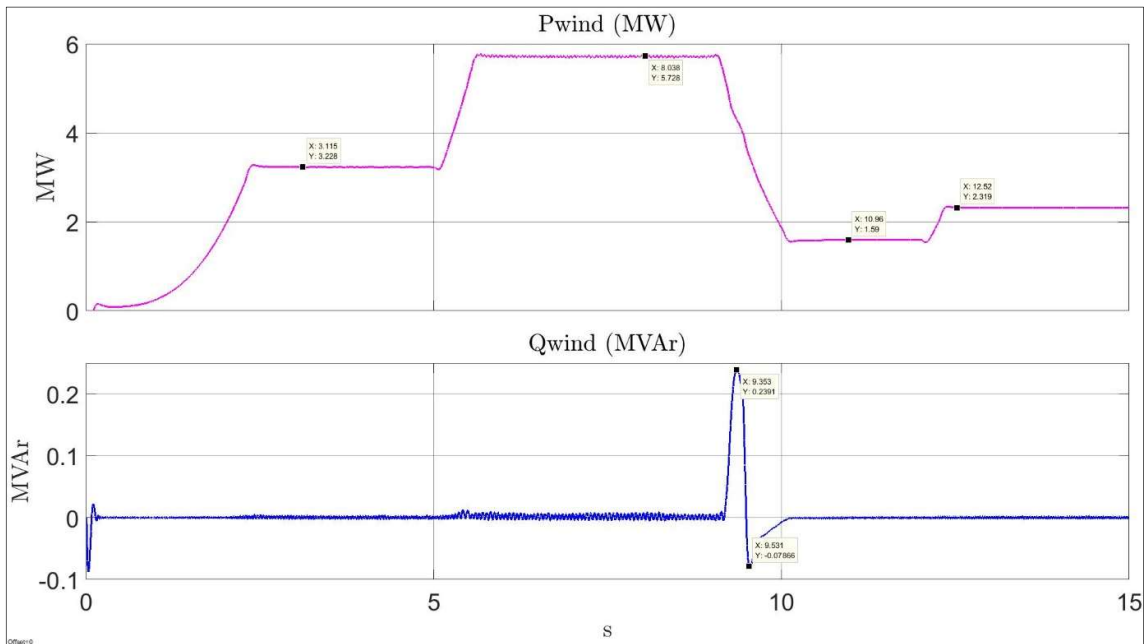


Figure 6.5 Wind Turbine active and reactive power. Case 1

The active and reactive power is observed in Figure 6.5. The active power profile shown has several changes corresponding to the different wind steps, with a maximum of 5.78MW and a minimum of 1.59MW corresponding to 11m/s to 7m/s. An event to notice occurs during this

large fluctuation. As shown before, the DC reacts to keep the voltage and there is an injection of reactive power as indicated in the peak illustrated in the figure at 9.53s. However, the control loop on Q_{wind} actuates and takes the system back to its normal condition, which implies a zero reactive power injection.

Flywheel (FW)

The field voltage V_{field} results from the exciter controls over reactive power. As appreciated in the Figure 6.6, during the event discussed before, the terminal voltage drops in the entire system and the field voltage injects reactive to help restoring the nominal terminal voltage.

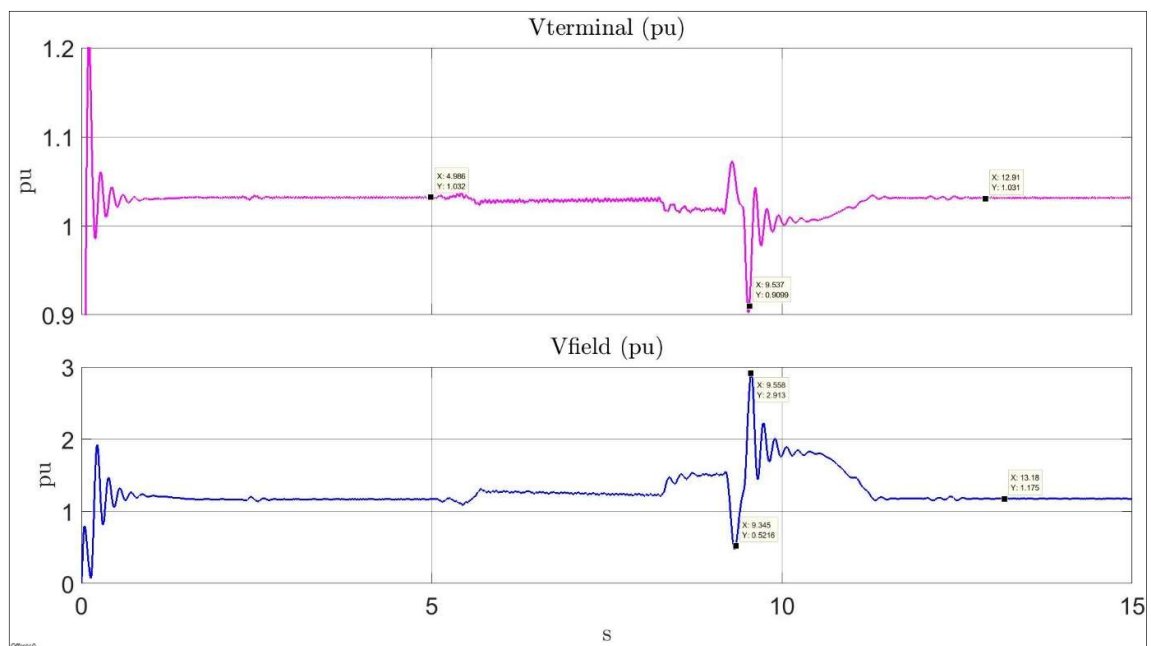


Figure 6.6 Flywheel $V_{terminal}(pu)$ terminal and field $V_{field}(pu)$ voltages. Case 1

The dump load and flywheel maintain the power balance. The flywheel works, whether absorbing or releasing active or reactive power as observed in Figure 6.7. The dump load is a passive element and only burns energy. The active power in the FW was discussed before, when analyzing the acceleration and deceleration of this unit. On the other side, the reactive power behaves as expected similarly to the field voltage of the FW, an acute voltage drop implies reactive power injection. Once the equilibrium is achieved by the actuation of the wind turbine controller and exciter, the system regains nominal voltage.

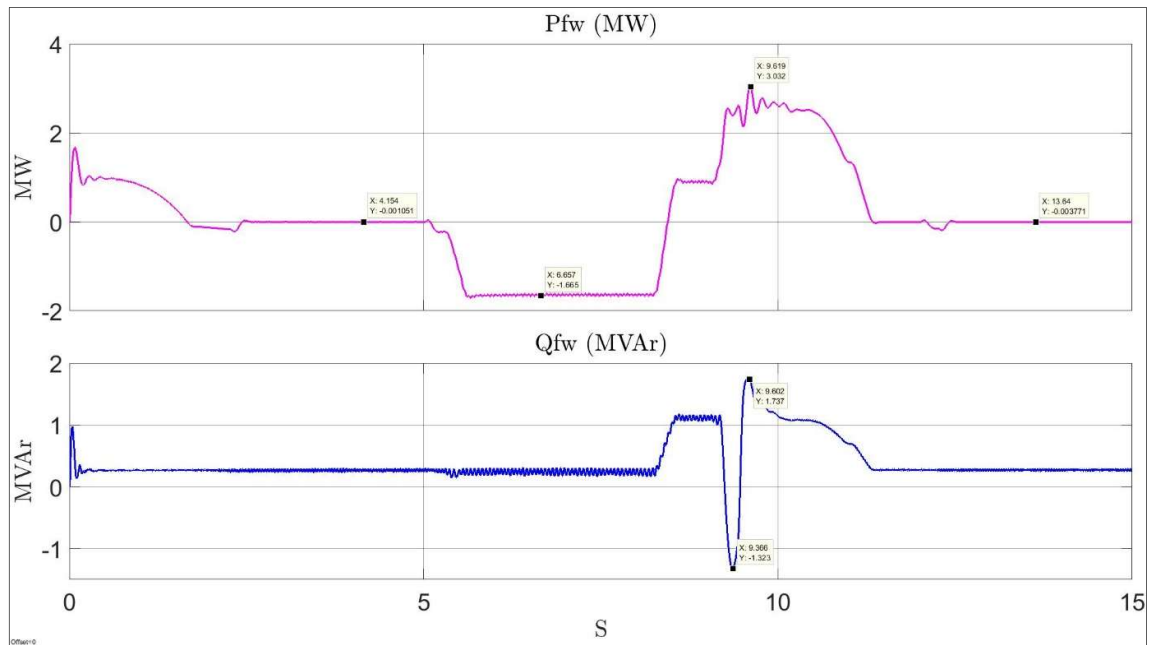


Figure 6.7 Flywheel active and reactive power. Case 1

The energy accumulated in the flywheel can be estimated by integrating the area under the FW power curve P_{fw} . They can be either the positive or the negative area shown in Figure 6.9, in the overall system response, both of which cancel out each other. The negative area is easier to make such estimation, which amounts approximately to 5MWs, that indicates that it can reserve its own power rating during one second. It is then understood that the dynamics have not been transferred from the GT to the FW, since it is a rather small quantity.

Dump load (DL)

The dump load waveforms are illustrated in Figure 6.8. The FW starts to accelerate beyond permissible range right after a wind speed of 11m/s and this is detected by a PLL synchronized to the system frequency. Under this condition, the DL triggering signal is sent to the resistor bank to increase its value. The control is made through a discrete time integrator, which accumulates or integrates the input signal with a range from 0 to 1, being 1 the maximum value for maximum power in the resistor bank. The dump power has a peak value of 2.92MW. Once the wind speed falls to 7m/s, implying a frequency reduction, the DL is deactivated and the triggering signal is suppressed at approximately 11s.

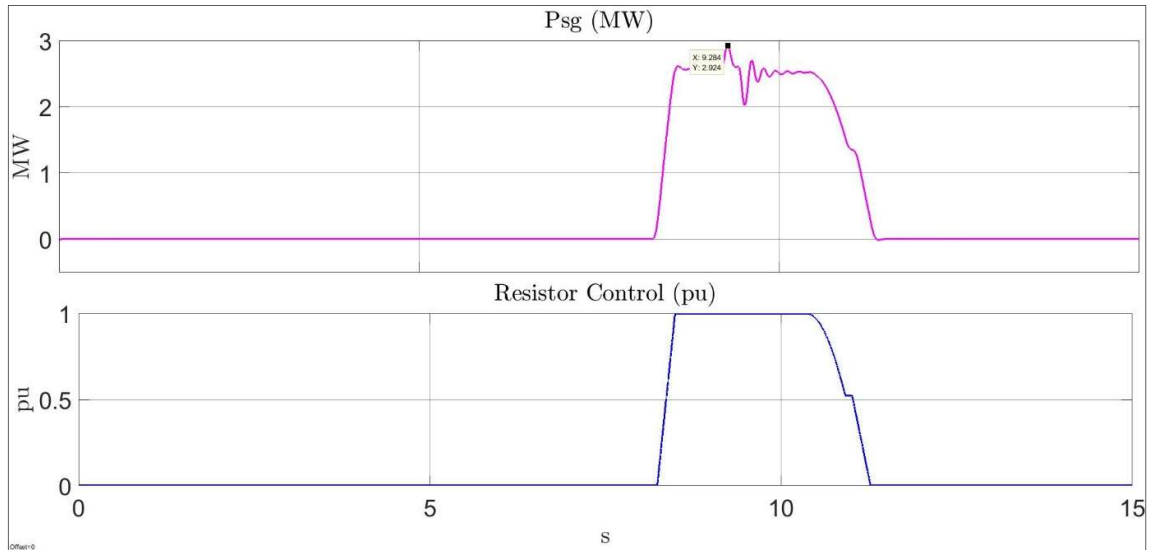


Figure 6.8 Dump load power and control. Case 1

6.1.4 Overall Stand-Alone System. Case 1

The system waveforms for the fixed load case are shown in Figure 6.9. The first set of power curves are P_{wind} and P_{flex} , which are a representation of the wind power and flexible load. As can be observed, the flexible load follows the power generation up to 3MW, which is its maximum value. The difference observed between the magenta and blue curve is the energy absorbed by the 1 MW fixed load, in blue in the second set of curves.

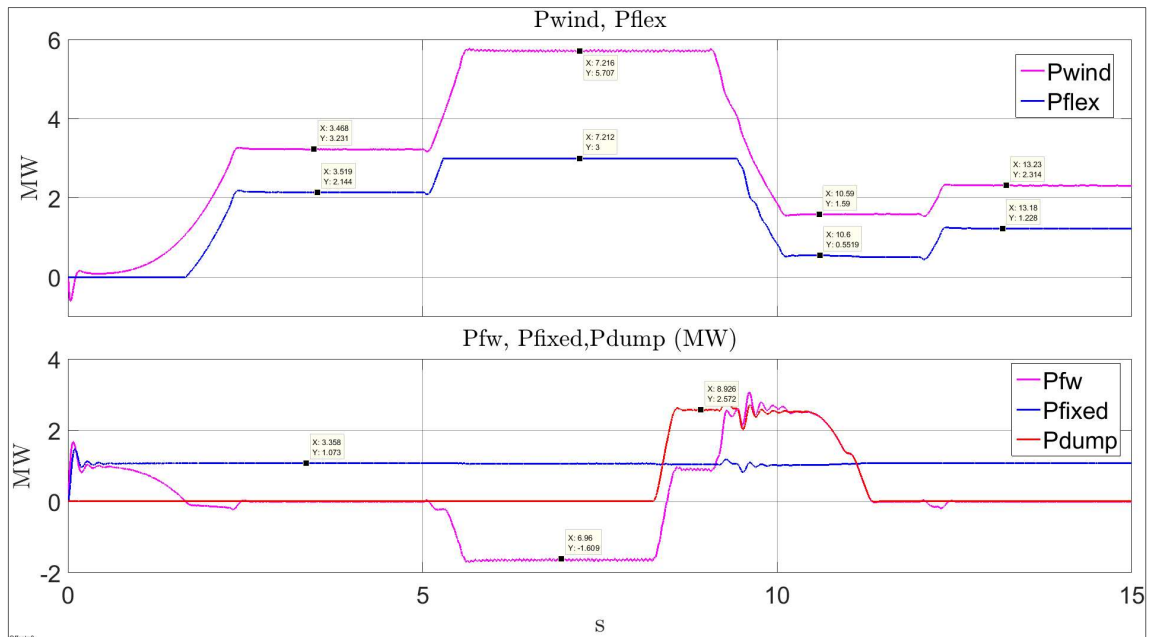


Figure 6.9 Power curves with flexible load. Case 1

The red curve represents the dump load. The dump load acts when the frequency on the synchronous generator is above 50.2 Hz. As illustrated, this happens when the wind rises to 11m/s at 5s. The generation surplus is partially absorbed by the rotating masses, and later it is dissipated by the dump load. At 9s the wind speed goes to 7 m/s from 11m/s and 2s later the DL decreases, since now the condition has inversed due to a lower wind power injection. It is important to notice that the fixed load is always served. Additionally, the total system load is adjusted by the flexible load, which follows the wind generation.

6.2 CASE 2: FIXED LOAD AND VSD PUMP

The complete double back-to-back system response is studied in this section. The model is the non-ideal system representing the dynamics for all the subsystems previously described, including the VSD that replaces the flexible load, which is an idealization. The variable speed drive receives as input a speed signal. Before creating this reference, the wind power available must be converted into a speed signal. There is not a linear relationship between torque and speed. On the other hand, the mechanical pump load is as explained before given by,

$$T_m = k\omega_m^2, \quad (6.1)$$

The mechanical power is calculated using the expression,

$$P_m = T_m\omega_m \quad (6.2)$$

The combination of 6.1 and 6.2, yields.

$$P_m = k\omega_m^3 \quad (6.3)$$

Equation 6.3 describes a cubic relationship between mechanical power P_m and ω_m .

6.2.1 Variable Speed Drive (VSD)

Figure 6.10, illustrates the VSD curves including, motor speed, stator current and mechanical and electromagnetic torque, all quantities are in per unit. The first curves shown are the reference speed in blue and the measured mechanical speed ω_m in magenta. The speed has a saturation block, which independently of energy available it cannot go above the maximum slip of 5%. Therefore, there is a difference between the reference and actual speed during high wind condition after 5s with the wind speed of 11m/s. Later at 9s, the rotor speed goes to 0.69pu for 7m/s and 0.88pu for 8m/s at 12s.

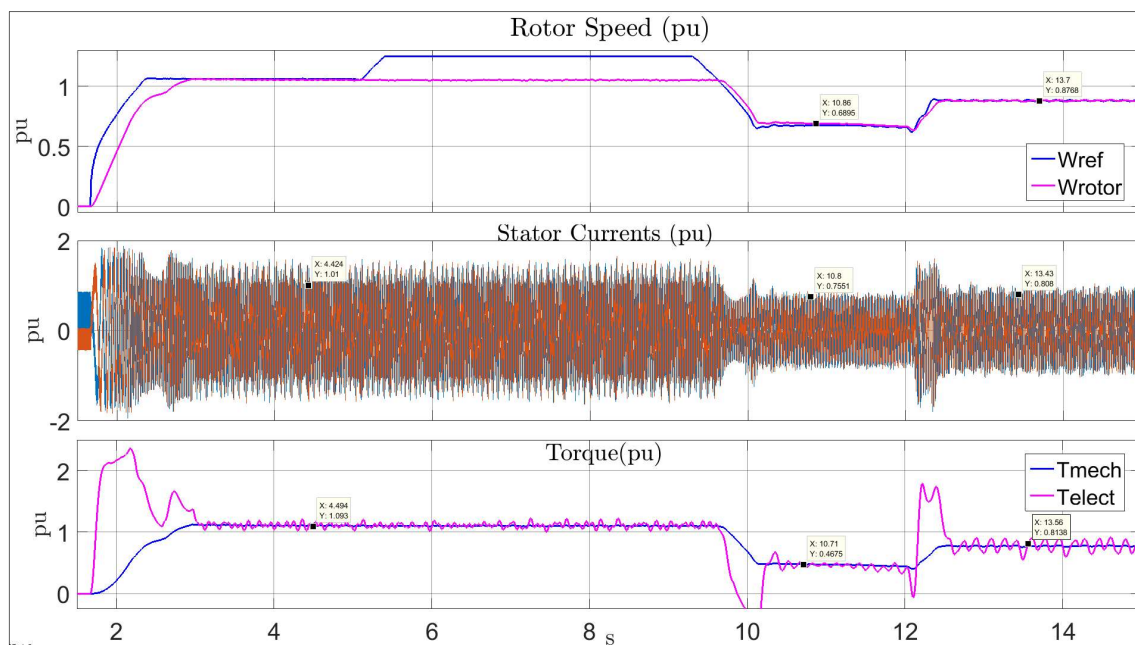


Figure 6.10 Variable Speed Drive curves

The reference speed calculated follows the energy available from the source as explained before. The second graph illustrates the *abc* stator currents in per unit. The startup current during the first cycles gets to a magnitude of 2.2pu, which indicates a motor soft starting compared to the typical starting current of 6-6.5pu [23]. The oscillations on the current curve are produced by changes in the nonlinear reference speed, which in turn affects the electromagnetic torque, as seen on the last set of curves. The magnitude of the stator current is 1.01pu for wind speed of 9m/s and it is kept constant until there is a decrease to 0.75pu after 7m/s and 0.81pu for 8m/s. On the other hand, the mechanical torque presented in blue does not present oscillations compared to the electromagnetic torque, indicating low mechanical pulsations.

The variable speed drive active and reactive power are displayed in Figure 6.11. As observed, the active power P_{vsd} presents fluctuations similar to the stator current or electromagnetic torque in Figure 6.10. The best response is obtained close to the nominal value 2.6MW, with smaller oscillations. The VSD is fully controlled, and it is possible to have negative power values, as the one detected at 10.12s. A steep deceleration forces the system to reverse the energy flow, injecting energy back to the grid with a peak of -1.18MW. The reactive power Q_{vsd} is inductive 0.06 MVar during the period studied, which indicates a proper control

defined by ideally by $i_d = 0$. Keeping a low reactive power improves the motor performance, since most of the energy consumed is in useful work and lower energy losses.

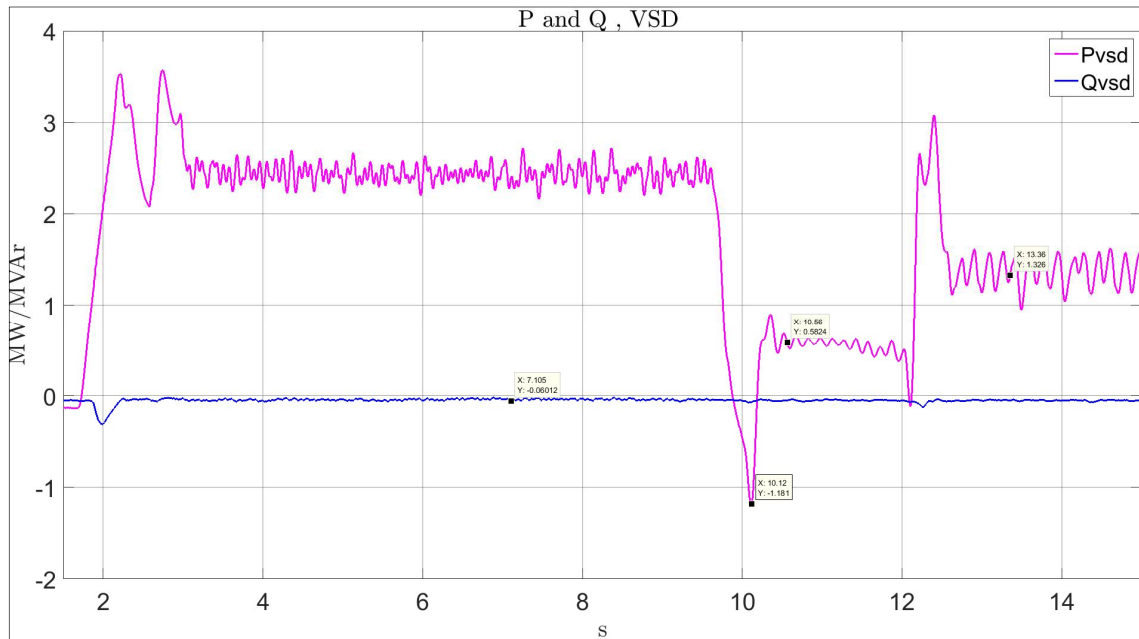


Figure 6.11 VSD Power curves

6.2.2 Overall Stand-Alone back-to-back System. Case 2

The system power curves are presented in Figure 6.12. The non-linear expression introduces oscillations to the VSD input, which is reflected in the entire system.

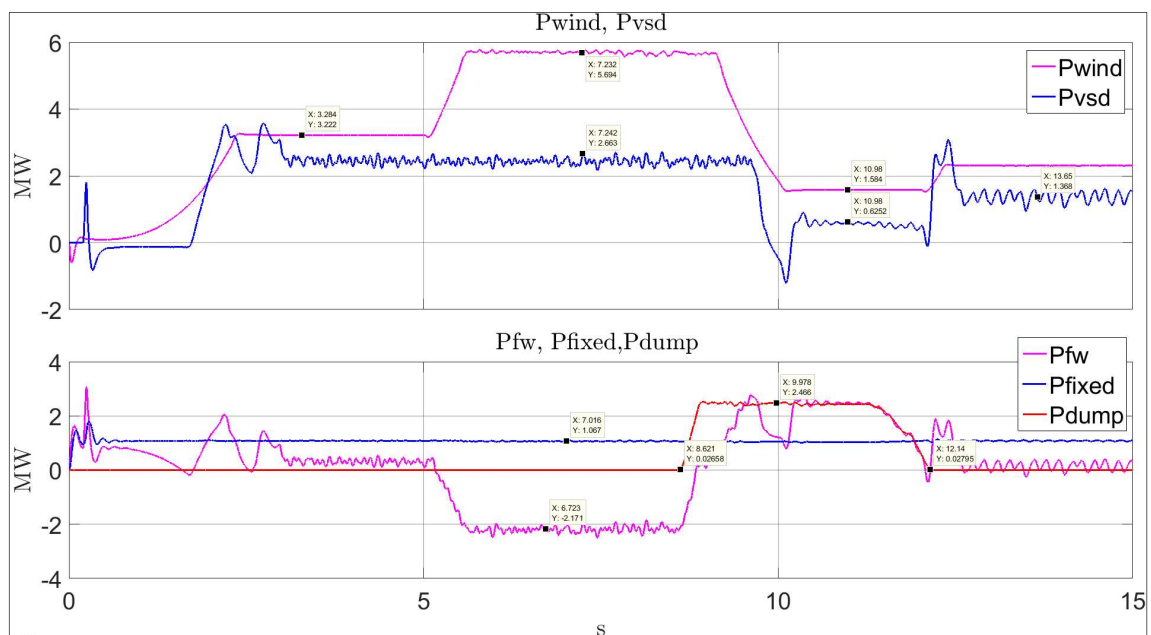


Figure 6.12 Power curves with VSD implementation. Case 2

As can be observed the pump active power has smaller oscillations in the region of nominal value, where the expression and constant were deduced. As the energy available starts to decrease, the pump follows the general behavior as the ideal case 1 with the flexible load, but there are larger oscillations that can be attributed to the non-linearity of the reference speed. The first peak is attributed to the system start-up to feed the fixed load, the second and third peak corresponds to the VSD start-up, keeping its nominal value even with 11m/s at 5s. The third event is related to the wind change from 11m/s to 7m/s, the power observed is negative since the VSD can send back power to the system while is it decelerating. Finally, there is acceleration for an increase in power injection due to a wind power of 8m/s. However, the maximum real power consumed by the pump is 2.66MW and the ideal case was 3MW. Different operating points are 0.63 MW and 1.37MW for 7m/s and 8m/s respectively. The dump load takes the excess of power until it starts to burn at 8.61s, during 3.52s having a peak value of 2.47MW.

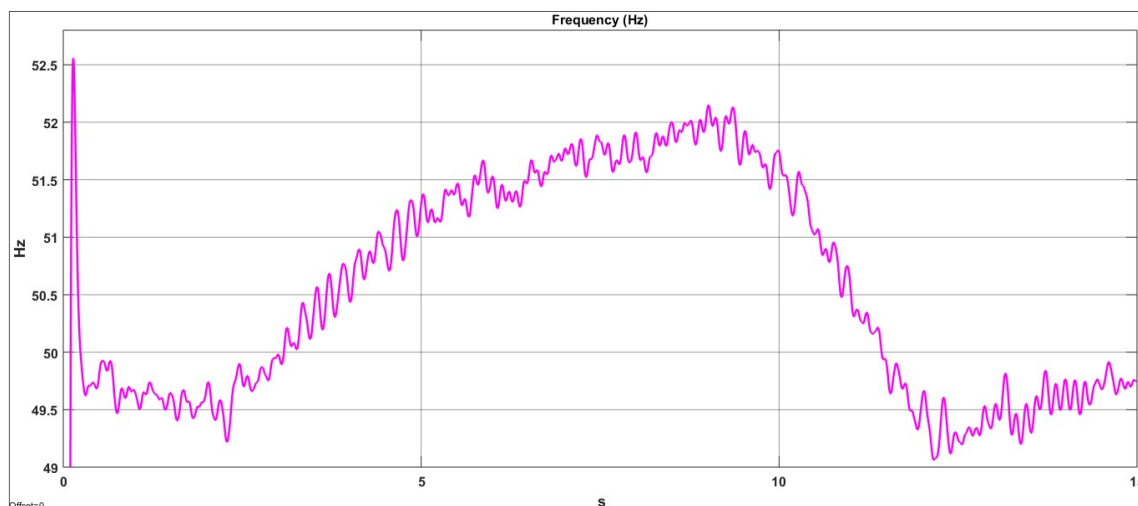


Figure 6.13 System frequency with VSD implementation. Case 2

The frequency curve in Figure 6.13 reflects the energy balance in the system. During the first cycles a peak in frequency of 52.5Hz is observed, which is explained by the initial system start-up and acceleration of the different rotating masses in the system. A wind step of 11 m/s at 5s, brings the frequency to a peak of 52Hz, which is counteracted by the activation of dump load. Later, a lower wind step of 8m/s, takes down the frequency to 49Hz. However, at 12s, the frequency starts to recover to its nominal value.

6.3 DISCUSSION OF RESULTS

The stand-alone WIS cases 1 and 2 present the same general behavior. Case 1 is an idealization with controllable load, a dump load and a synchronous flywheel. In both cases, the synchronous flywheel functions as a balancing element supplying active and reactive power during transients. Case 2 is more realistic, because it also takes into account the dynamics of the variable speed drive and the calculation of the reference speed. Figures 6.9 and 6.12 illustrate the general power curves for case 1 and 2 respectively. Firstly, it is worth noticing that the motor load in case 2 is not 3MW is 2.66MW maximum, since there is reactive power associated which is not modelled in case 1. Secondly, the speed reference calculated for the VSD is non-linear as previously discussed which introduces undesired oscillations to the system, which are amplified when the pump is not close to the nominal operating point. An improved method to calculate the reference speed is suggested for future implementations. For example, if the motor speed and power curves are known a look-up table can be implemented, generating a speed reference signal depending on the power available. This solution could soften the oscillations, and it could exhibit improved dynamic performance. Finally, it can be concluded that both stand-alone cases modelled are theoretically feasible, which coincides with the conclusions drawn for the DNV-GL independent technical assessment in [10].

7 ENERGY WIS MODEL

7.1 SYSTEM OVERVIEW

The objective of this study is to evaluate the functioning of a stand-alone WIS system in a long time scale perspective. The previous chapters focused on the dynamic response of the hybrid and stand-alone configuration. Long-term energy assessment is required in order to make energy estimations and build a feasibility case, to estimate the energy generation, consumption and to calculate different electrical parameters for an economic revision. The study addressed wind resource estimation, wind turbine generation and synthetization of load track strategy for WIS energy model. The wind resource is assessed in terms of daily, monthly averages, annual profile and speed histogram. Considering the wind as input, it is important to determine the WT power curves, daily, monthly and cumulative frequency generation. The generation is the starting point to synthetize the load demand, optimizing the wind power available and dumping the excess of energy.

The energy model evaluated, is located off the north coast of Trondheim, see Figure 7.1. This location is arbitrary and tries to evaluate the wind resource potential and the region wind characteristics.



Figure 7.1 Project Location

The general overview of the WIS stand-alone system is shown Figure 7.2. It consists of a generic 6MW wind turbine and an electric peak demand of 3.5MW. This load corresponds to a lumped load summing up a 2.5MW pump and 1MW water treatment plant.

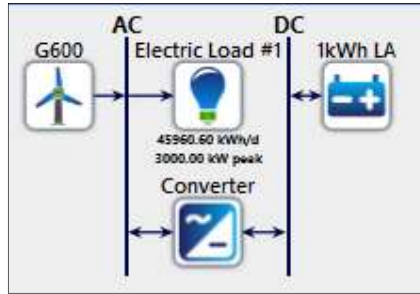


Figure 7.2 System components

The converter and the battery bank are rated to 250kW representing the auxiliary load whose values are taken from [1]. The battery bank does not work as the flywheel, and does not have an effect in the normal system operation; therefore, it is not further treated. The storage can be used to smooth out the power output to the load, but it was not conceived this way because it would have required a large capacity, which is no viable due to space and weight constraints. The storage purpose is to feed the emergency load needed for system restoration, controls and communication unit. The following sections explain with detail the system components.

7.2 WIND TURBINE

A generic power curve of a 6MW wind turbine was estimated. The rated output power happens when the wind speed is 12-14 m/s as shown in Figure 7.3. The power curve is an extrapolation from an existent 3MW wind turbine included in the HOMER software. A real power curve will offer results that are more accurate, for this theoretical assessment, it is considered a good approximation.

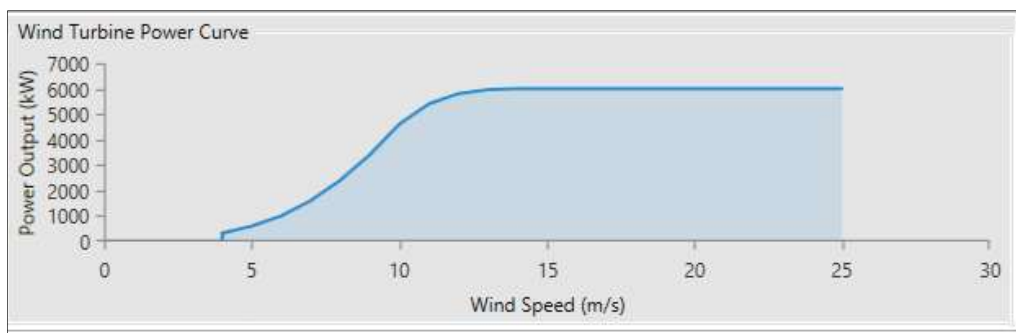


Figure 7.3 Wind turbine power curve

7.3 WIND PROFILE

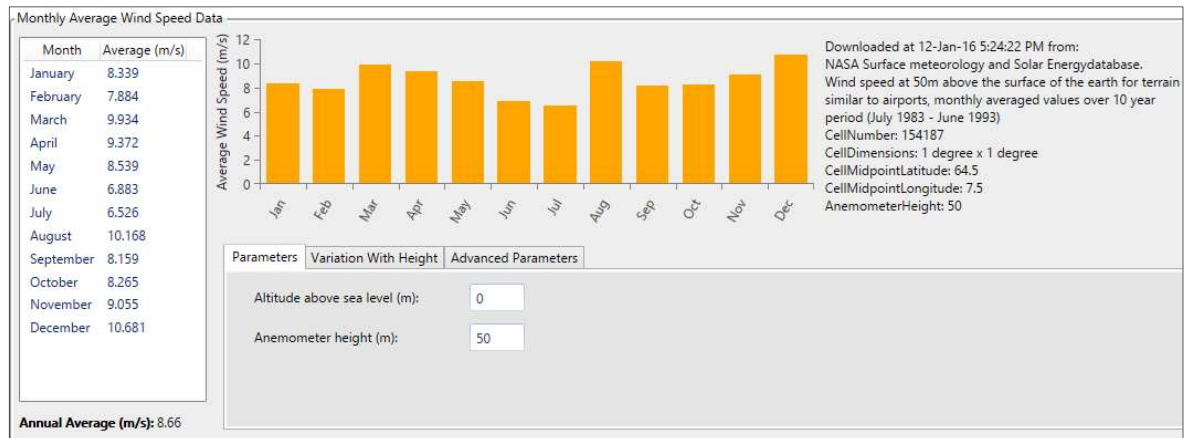


Figure 7.4 Monthly average wind speed data

Figure 7.4 shows the input data values downloaded from NASA Surface meteorology and Solar Energy database through HOMER Energy software [2]. The wind speed was measured at 50m above the earth surface. The measurements are monthly averages values in a 10-year period (July 1983- June 1993). The histogram displays the monthly average, and the table besides the numerical values.

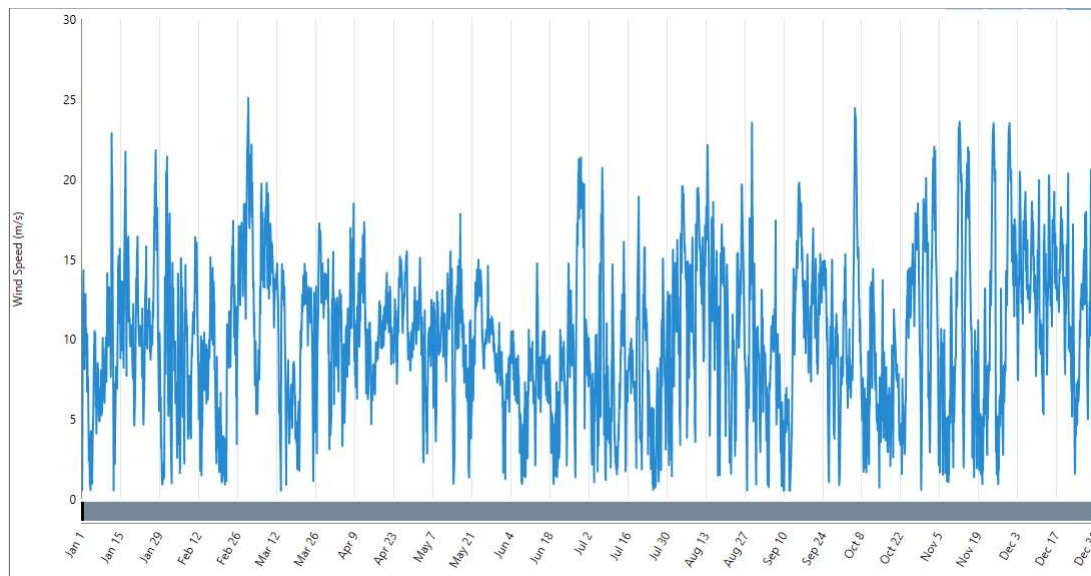


Figure 7.5 Wind annual profile

Figure 7.5 contains the annual wind profile. The values are hourly average during a complete year, i.e. it has 8760 values, over 10 years of historical data as mentioned before. The annual wind profile used is an average year over a 10-year-period.

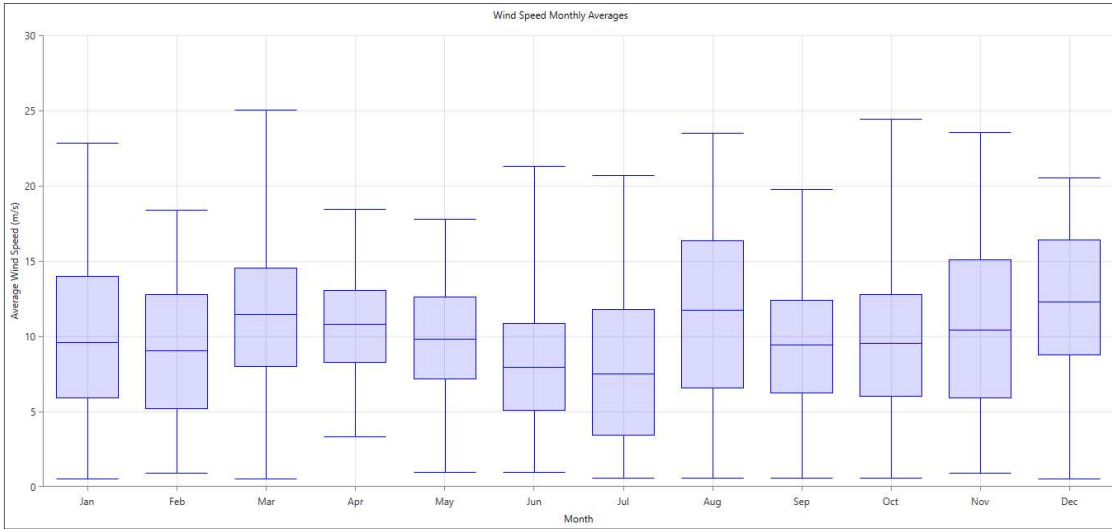


Figure 7.6 Wind speed monthly averages

Figure 7.6 indicates the monthly wind average, maximum, minimum and wind speeds registered in horizontal bars. Dispersion along the bands depends on the wind intermittency over the average. June and July are the months with smallest average values. The higher the blue bar then the more fluctuating the month results.

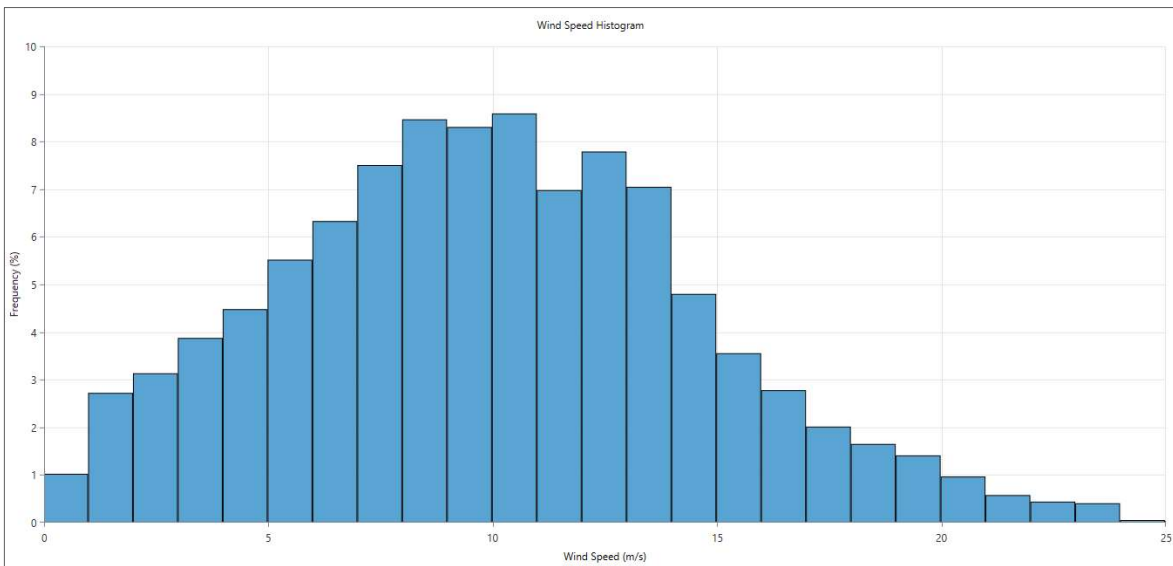


Figure 7.7 Wind speed histogram

Figure 7.7, shows the wind speed frequency. The best and most stable wind will result in a high frequency close to the mean value (8.66m/s).

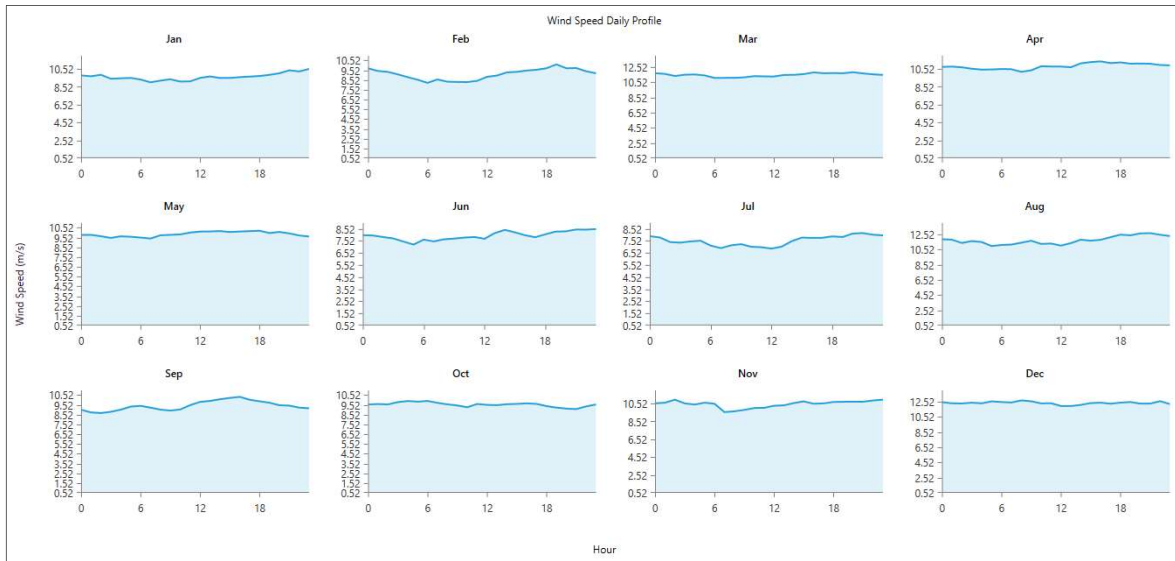


Figure 7.8 Wind speed daily profile

The smooth curves in Figure 7.8 demonstrate daily fluctuations within a month are not large. This is a good indication that the wind blows constantly with little daily variations.

7.4 LOAD PROFILE

The load has been synthesized artificially, with a peak value of 3.5MW. The main characteristics are summarized in Table 7-1. The data was imported from an array of 8760 wind speeds taken from HOMER, which is connected to NASA wind measurement database. Each value represents an hourly average demand. The load has a daily noise of 38% and an hourly noise of 71%, a higher noise content indicates a more variable demand.

Load	
Data source	Imported
Daily noise	38%
Hourly noise	71%
Scaled annual average	63,095.352 kWh/d
Scaled peak load	3,500.0000 kW
Load factor	0.7511

Table 7-1 Load main characteristics

The load, see Figure 7.9, was synthesized by using the wind turbine out-put production presented. This is possible due to the possibility of controlling the load by means of a variable speed drive (VSD) connected to the pump as demonstrated in the previous chapter. The profile consists of 8760 hourly average values, having a peak of 3.5MW and a load factor of 0.7511. The load factor is a dimensionless number equal to the average load divided by the peak load.

The scaled annual average is 63095.36 kWh/day or can be interpreted as the annual average energy consumption per day.

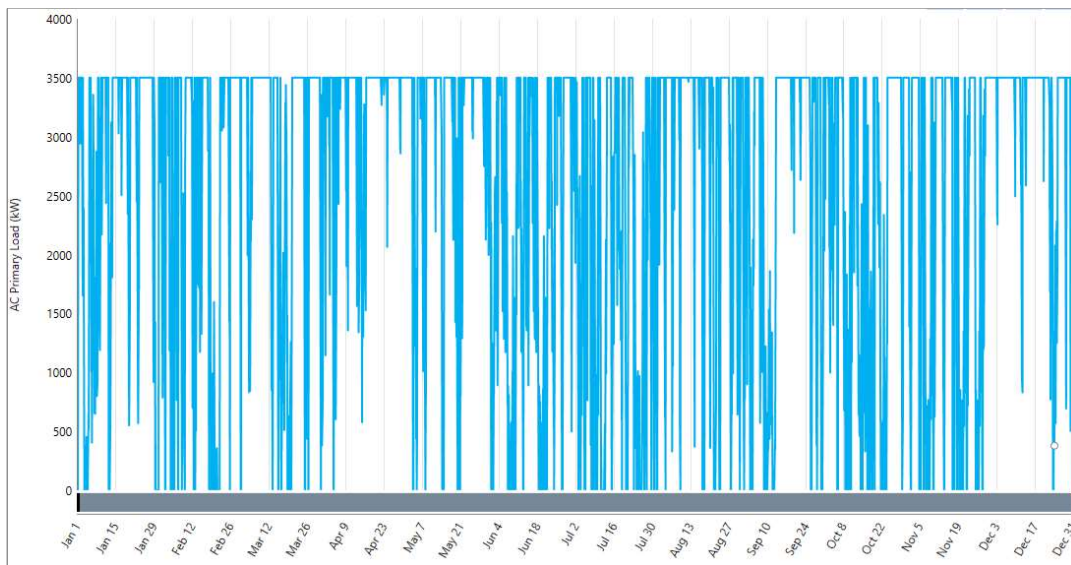


Figure 7.9 Annual Load Profile

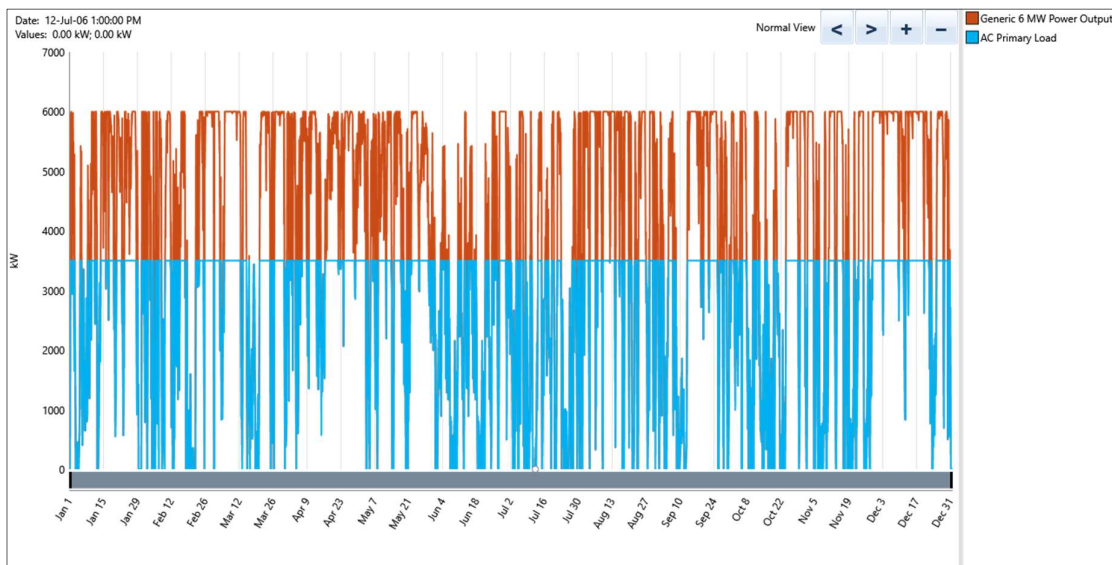


Figure 7.10 Generation-load tracking

Figure 7.10 shows how the pump load profile *follows* the energy generation available. The AC load profile is managed depending on the energy available as shown in graph. The red curve belongs to the 6MW turbine power output and the blue demand curve fits perfectly the power generation with the limited peak value of 3.5MW given that it is the maximum demand permissible.

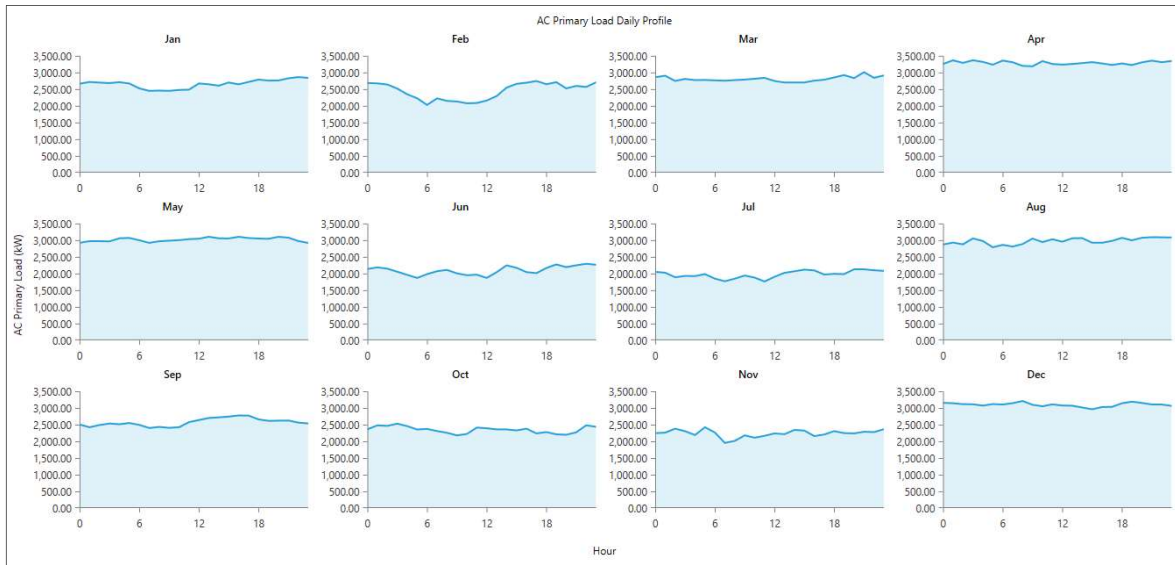


Figure 7.11 AC primary load daily profile

The average AC load (kW) is shown in Figure 7.11, the months where the load profile has approximately 2MW average are June and July belonging to the least windy months.

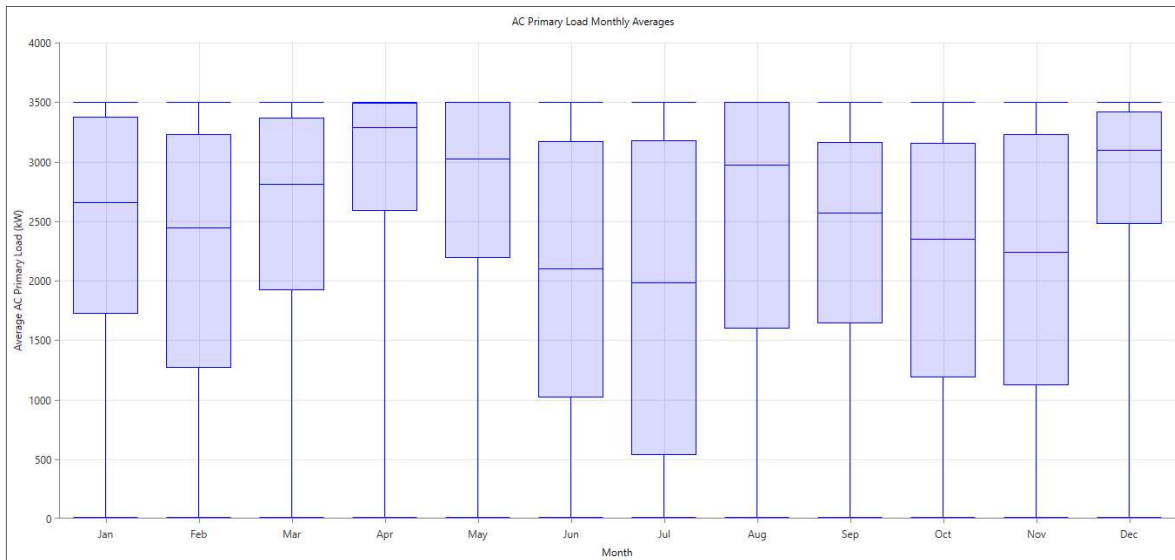


Figure 7.12 AC primary load monthly averages

The average AC primary load monthly averages are marked in Figure 7.12 by horizontal lines, in the middle of the bars, maximum and minimum loads are indicated as well. The longer the bars are the more scattered the values are as well. This indicates that the larger the bars are, the more power fluctuations are found. When the generation is over 3MW in average, typically in the windiest months, the load power fluctuations are smaller.

8 ENERGY WIS STUDY CASES

The WIS stand-alone system Figure 8.2, has been solved for two different wind scenarios. The first case considers an annual average value of 12m/s and the second case takes 8.66m/s as average wind speed. This software is suitable for analyzing the complexities of building cost effective and reliable microgrids. Usually microgrids combine traditional power and renewable sources, storage and load management [31]. Economic studies can be carried out, but investments costs and economic variables are required, which are out of the scope here.

8.1 CASE 1: HIGH WIND SCENARIO (12M/S)

8.1.1 Wind Turbine

The mean output is 4.3MW, which means that on average this configuration is above the assigned load demand of 3.5MW for this wind scenario. The base case is 8.66m/s, but this case has been scaled to 12m/s to analyze a windier case.

Quantity	Value	Units
Total rated capacity	6.0	MW
Mean output	4.3	MW
Total production	37.662	GWh/yr
Minimum output	0.00	kW
Maximum output	6.0	MW
Wind energy penetration	169.0*	%
Hours of operation	7897	hrs/yr

Table 8-1 Wind turbine simulation summary. Case1

*The wind penetration looks at the percentage of demand covered by wind energy in a certain region per year defined according to [32] as,

$$\text{Wind energy penetration (\%)} = \frac{\text{Total amount of wind energy (annually)(GWh)}}{\text{Gross annual electricity demand (GWh)}} \quad 8.1$$

In a situation with energy excess, it can be more than 100%, in this case 169%.

A different concept is the instantaneous wind power penetration, which is defined [32] as,

$$\text{Instantaneous power penetration (\%)} = \frac{P_{\text{wind}}(\text{MW})}{P_{\text{load}}(\text{MW})} \quad 8.2$$

8.1.2 Wind power output

The energy production from the wind turbine is 37.662GWh/yr. and the total annual load is 22.241GWh/yr, which implies that 40.9% of energy should be burnt or never capture by pitching the blades of the wind turbine. Energy storage for more operating hours does not seem to offer advantages considering that there is a small value of unmet energy in this high wind scenario. The windier months of the region are April, May, August while the less windy are June and July, by developing a follow-up load strategy the unmet electrical load is scarcely 3.4%, as seen from the electrical case summary Figure 8.1

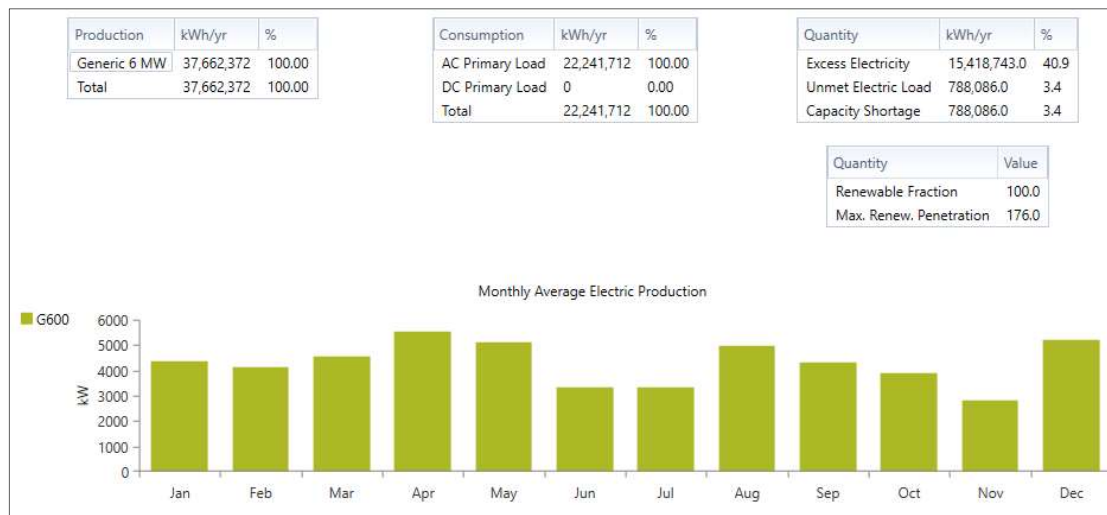


Figure 8.1 Electrical summary. Case 1

Figure 8.2 shows the monthly power output averages, maxima and minima. This graph shows how the energy production fluctuates. The fluctuations are larger coincidentally in the less windy months.

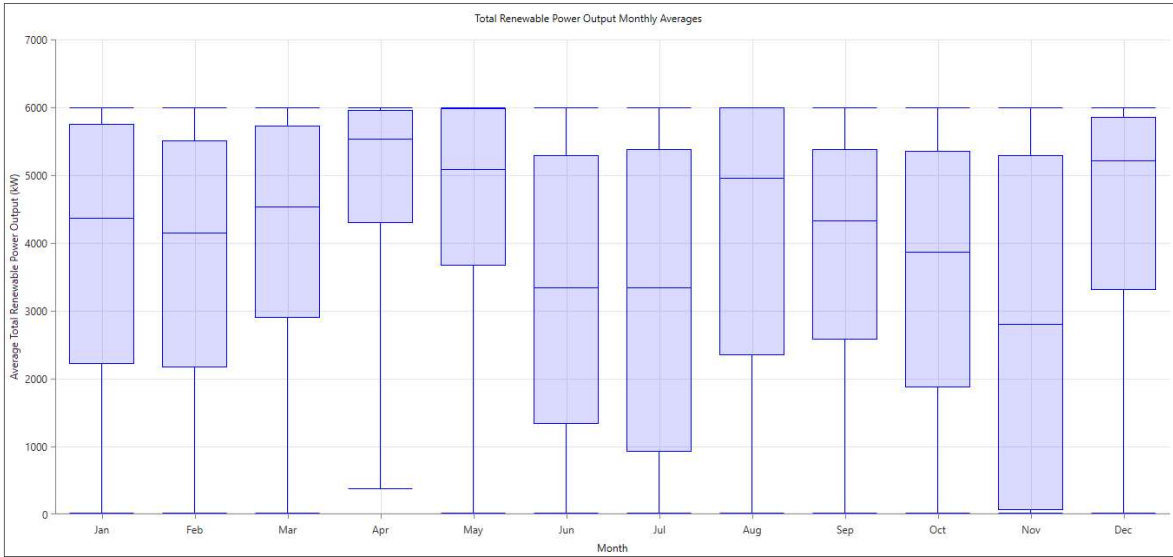


Figure 8.2 Monthly power output. Case 1

Figure 8.3 considers the daily output profile. An indication of power fluctuation within hours can be identified from this graph. Smooth curves demonstrates a more constant energy production. November and February are the more variable months and when the pump is supposed to be more electrically stressed due to different set points (reference speed) within a day.

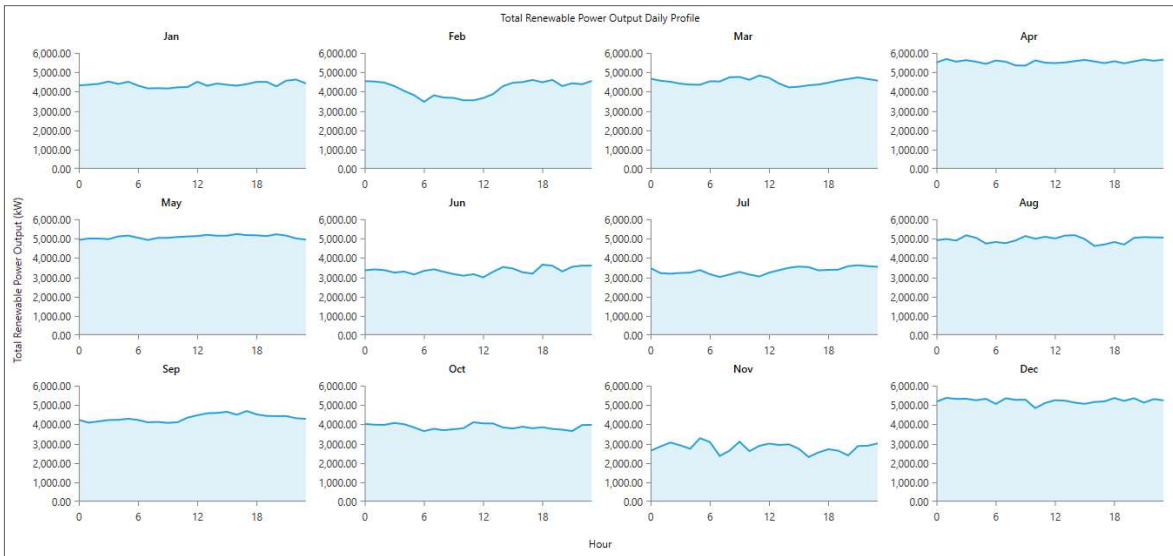


Figure 8.3 Power Output daily profile. Case 1

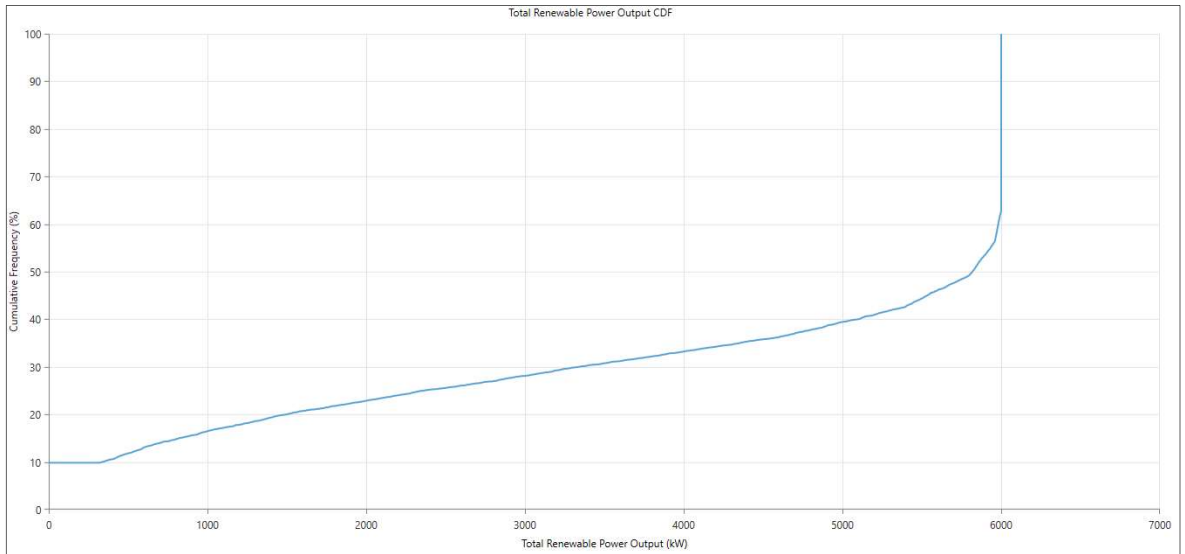


Figure 8.4 Power Output Cumulative Frequency. Case 1

According to Figure 8.4, only 30% of the time the energy production would be below the nominal value 3.5MW and by effective load management, the unmet demand is 3.4% as stated before. Effective load control is important to make the water injection system feasible and not affecting oil production targets.

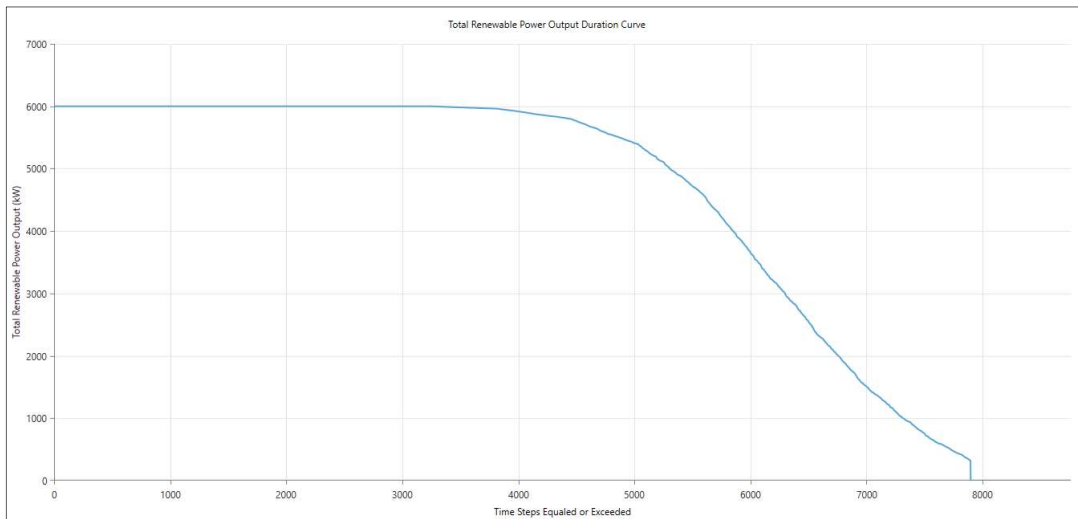


Figure 8.5 Power Output Duration curve. Case 1

A different look at the power output is reflected on Figure 8.5, under this high wind scenario, the energy generation is excellent and approximately 6000hrs or 68.8% of the year satisfying the target demand. This is consistent with the previous analysis.

8.1.3 Dumped Load (Excess Energy)

The excess of energy has a peak value of 2.5MW, as shown in Figure 8.6. Therefore, the resistors bank should be designed to withstand this demand at least or pitch de blades to capture less energy. For protection purposes, in case of a short circuit, the resistors banks can be oversized but a trade-off is required. An interesting fact to highlight here is that the most fluctuating months also displays the highest variation in load dumping.

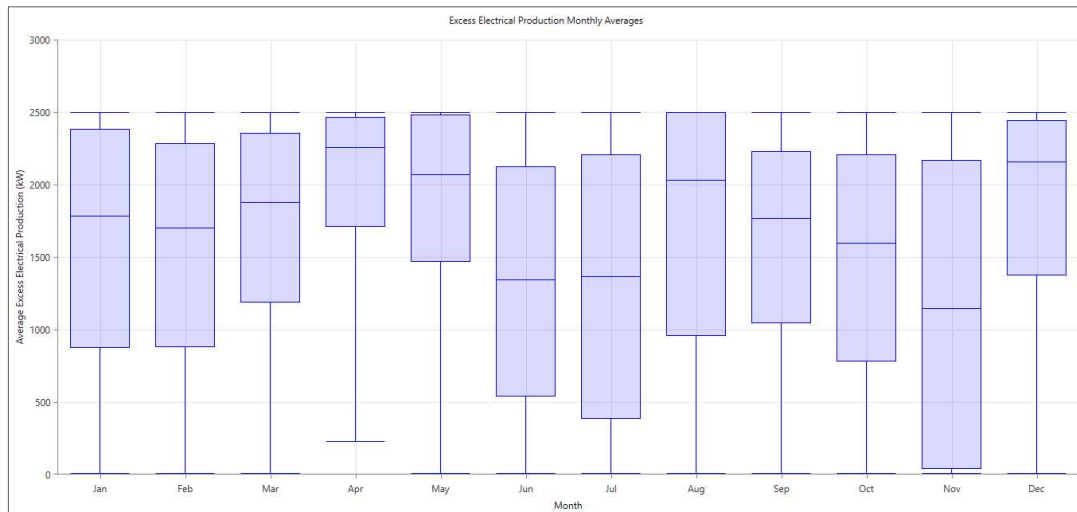


Figure 8.6 Excess electrical production monthly averages. Case 1

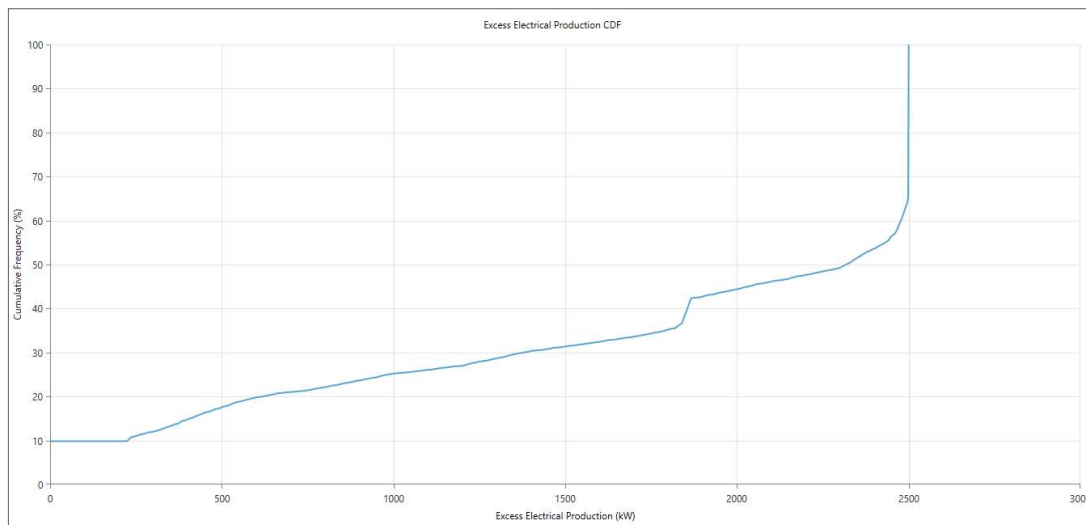


Figure 8.7 Excess electrical production cumulative frequency. Case 1

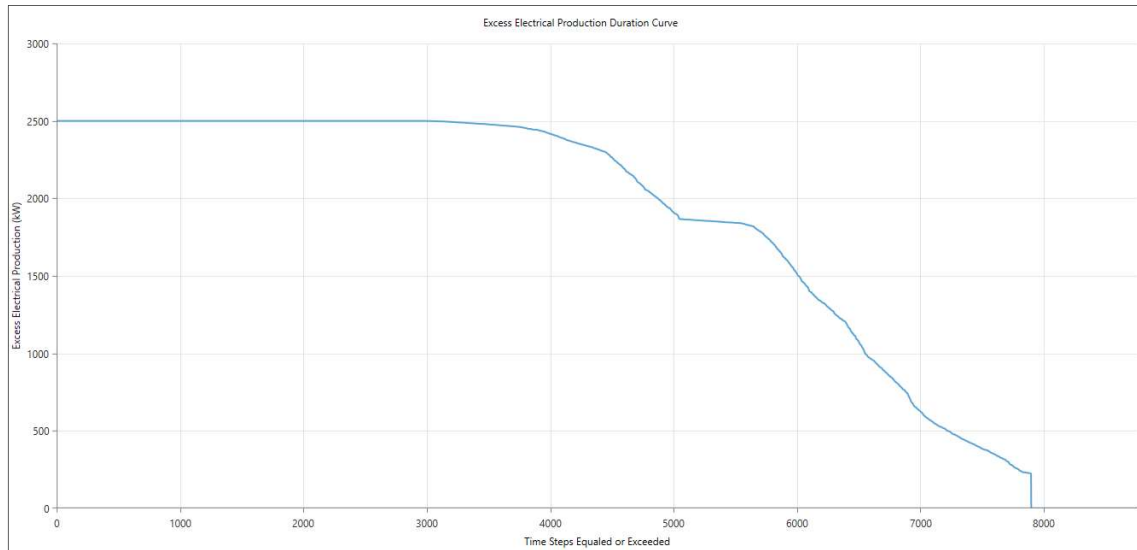


Figure 8.8 Excess electrical production duration curve. Case 1

Figures 8.7 and 8.8 indicate that over 3500hr or the 40% in cumulative frequency the energy dumped is 2.5MW. Generally, the dump load will be always acting as the energy balance element. On the other hand, dimensioning of the wind turbine is recommended for future studies in a high wind scenario, avoiding an unnecessary system oversizing.

8.1.4 System overall results

The power curves in Figure 8.9 shows the magnitudes of the power output from the wind turbine, the main load profile and the excess electrical production. The electrical energy dumped is 40.9% in this high wind 12m/s scenario. This might not be the case when there is a lower wind scenario. When the wind measurements are available, it is possible to determine an optimized size for the wind turbine and dump load. However, the idea behind an oversized turbine is to capture energy even under low wind conditions and reaching the annual injection target.

For example, June is one of the least windy months and coincidentally the values are more fluctuating. The injection pump and the dump load are subjected to larger daily variations. Emphasis should be made on the follow-up strategy to preserve the energy balance between generation and consumption. Observation of the power curves show a close fitting between them, ensuring the energy equilibrium.

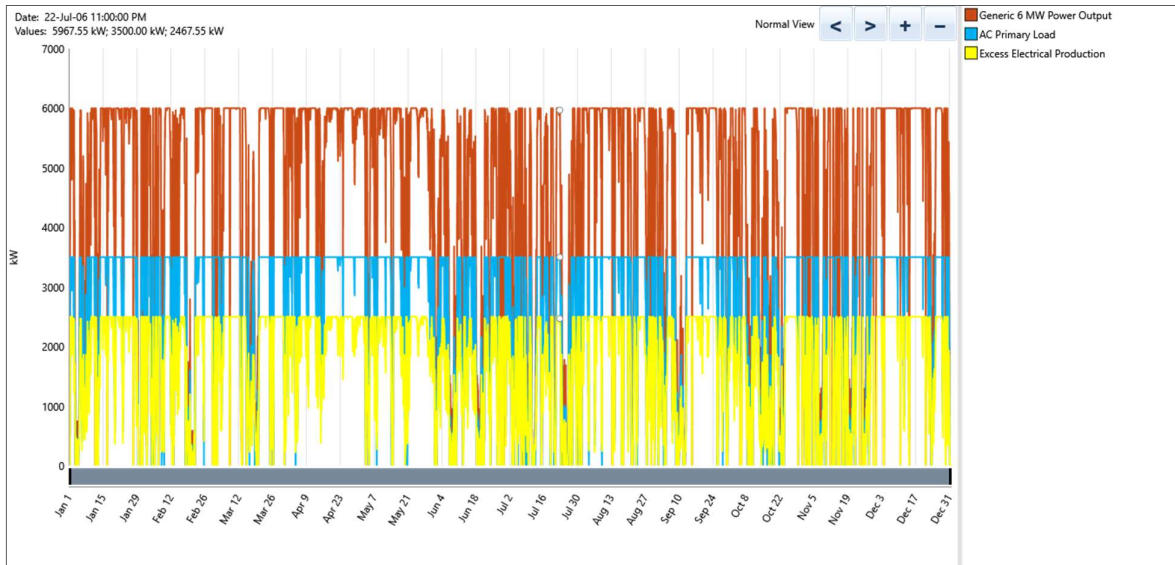


Figure 8.9 Yearly power curves: power output, load and dump load. Case 1

8.2 CASE 2: NORMAL WIND SCENARIO (8.66M/S)

8.2.1 Wind Turbine

Quantity	Value	Units
Total rated capacity	6.0	MW
Mean output	3.422	MW
Total production	30.065	GWh/yr
Minimum output	0.00	MW
Maximum output	6.0	MW
Wind Energy penetration	130.55	%
Hours of operation	7734	hrs/yr

Table 8-2 Wind turbine simulation summary. Case 2

The mean output is 3.422MW, which means that on average this configuration is slightly smaller than the rated demand of 3.5MW. This case has percentage of wind energy penetration of 130.55%, indicating less excess of energy compared to case 1. The hours of operation are

7734hrs compared to 7897 from the previous case. Therefore, the downtime is higher up to 1026hrs/year or 11.7%, indicating a higher number of restoration events or black-stars.



Figure 8.10 Electrical summary. Case 2

Under this scenario, the energy generated is 30.065GWh/yr. This amount is naturally 24.78% smaller than the case of high wind conditions. Interesting values are the unmet energy which increased to 7.6% compared to 3.4% and the excess of energy that fell from 40.9% to 29.1%. Having an unmet load below 7.6% under low wind conditions gives good indication of the system good performance, even under this conservative wind profile.

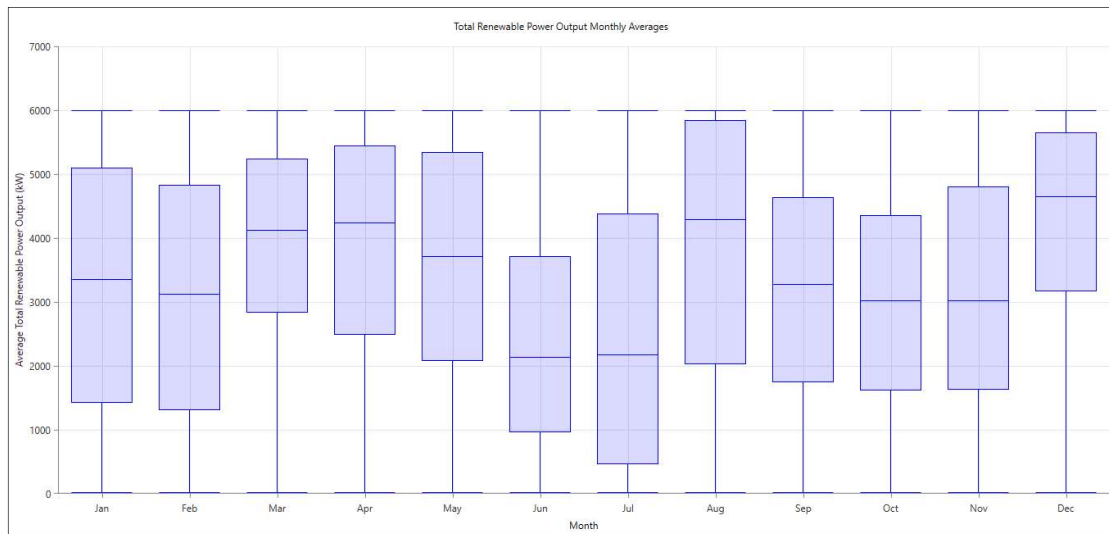


Figure 8.11 Monthly power output. Case 2

Figure 8.11 has the same trend as Figure 8.2, in terms of power output behavior. The difference is that the wind data has is now “scaled” to 12m/s as annual average and the power output is naturally bigger.

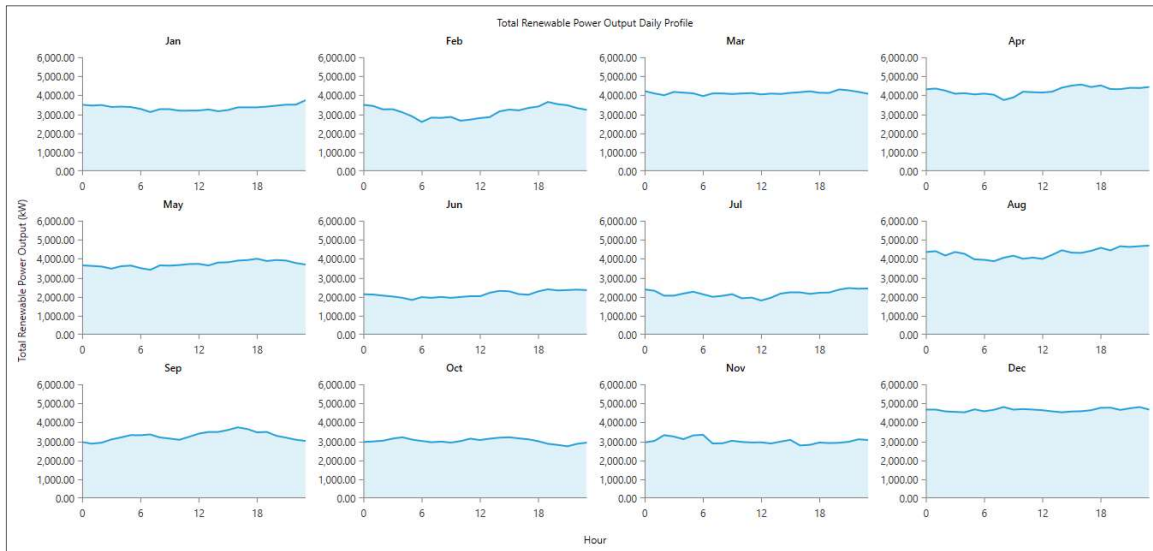


Figure 8.12 Power Output daily profile. Case 2

The same considerations are valid for Figure 8.12 where the average daily fluctuations per month are illustrated. The load power supply is more stable as long as the curves are flat. This does not consider the dynamic changes in the second timeframe since these are hourly averages, but indicates that the supply is stable.

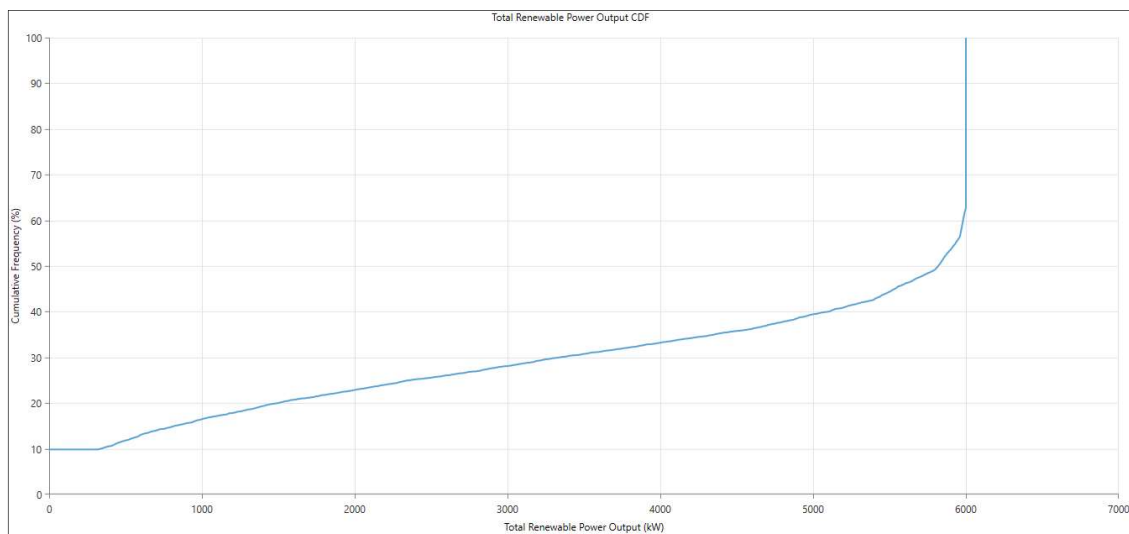


Figure 8.13 Power Output Cumulative Frequency. Case 2

The cumulative frequency from graph in Figure 8.13 is below 3.5 MW is only 30% of the hourly measurements. This indicates that theoretically 70% of the time the pump is working at its nominal point. Furthermore, below this point by adequately controlling the pump it is possible to keep the pump operating at a lower injection rate and contribute to the target volume.

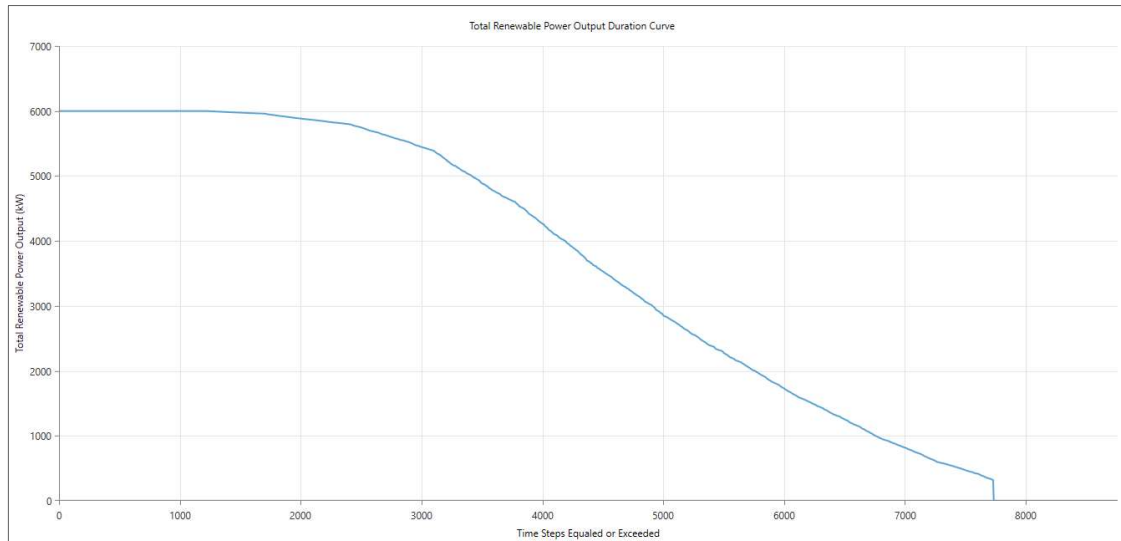


Figure 8.14 Power Output Duration curve. Case 2

Figure 8.14 is an alternative way of interpreting the system operation, during 4500hr in a year the power over 3.5MW out of 7734hrs of normal operation. This scenario is as expected, lower than the high wind scenario with a total of 6000hrs above rated demand.

8.2.2 Dump Load (Excess Energy)

The total dumped energy is 8.763GWh/yr., which represents 29.1% of the total energy output. Compared to the previous case where the excess energy turned to be 40.9%, this value is more conservative. As before, the months with higher electricity generation are April, March and December, which correspond to the months with higher dumped energy as naturally expected.

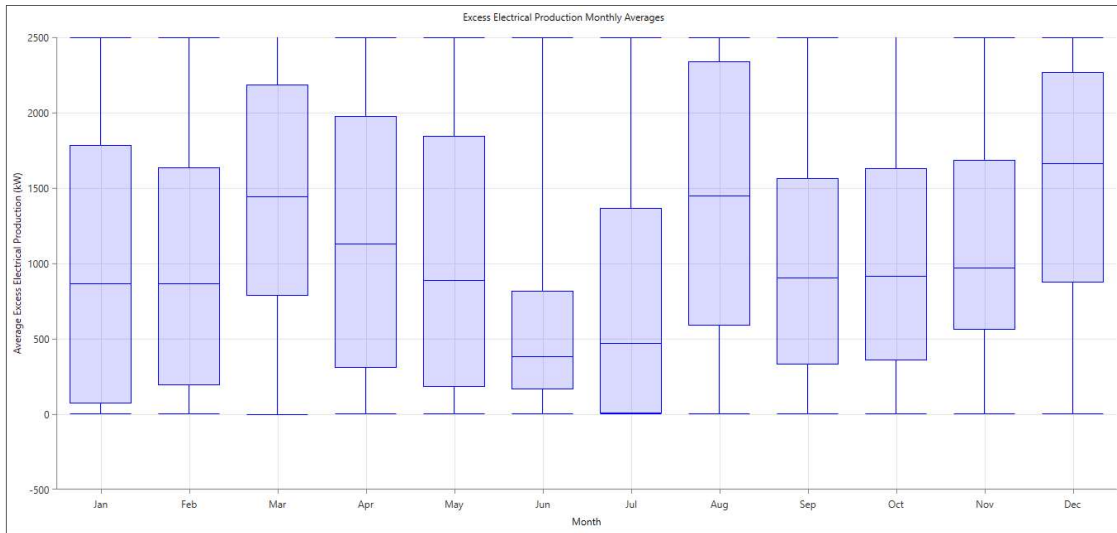


Figure 8.15 Excess electrical production monthly averages. Case 2

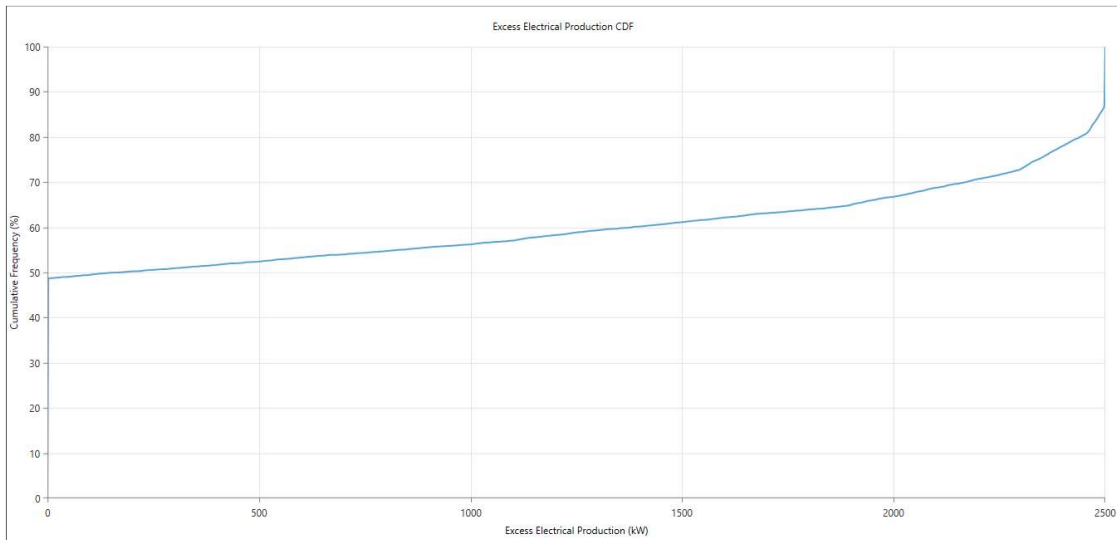


Figure 8.16 Excess electrical production cumulative frequency. Case 2

The excess electrical energy according to Figure 8.16 is 50% below 500kW. Figure 8.17 points out that during 4500hr the dump load is burning the excess of energy. This figure is 43.75% lower respect to 8000hr in the first case. When a component is less stressed, as it is case for the resistor banks under this scenario the system reliability can be positively affected. Here, no consideration is taken regarding the pitch control. Pitching blades in the wind turbine will have an important impact on the energy capture and eventually on energy burnt to sustain the system stability.

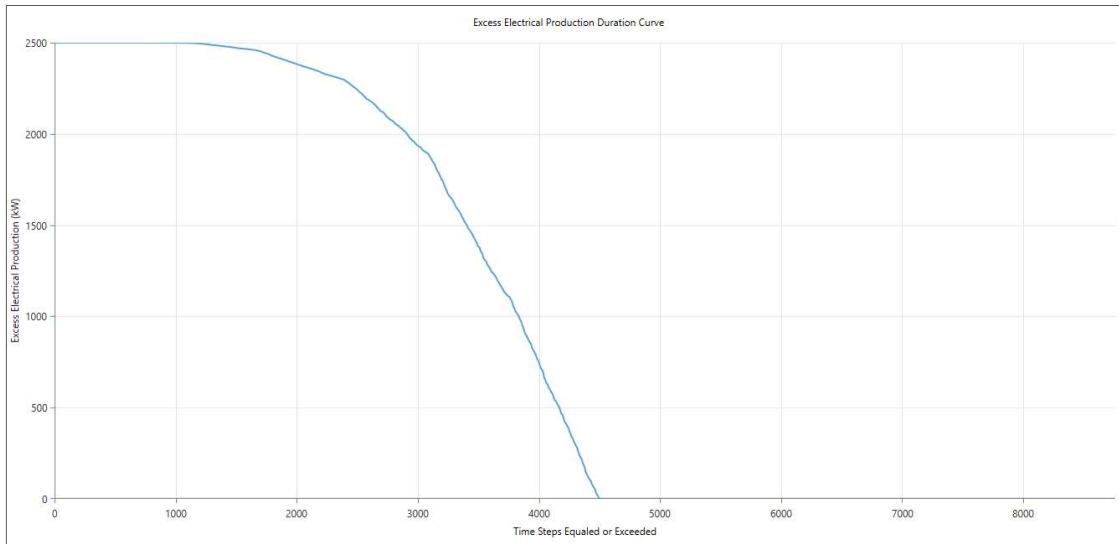


Figure 8.17 Excess electrical production duration curve. Case 2

8.2.3 System overall results:

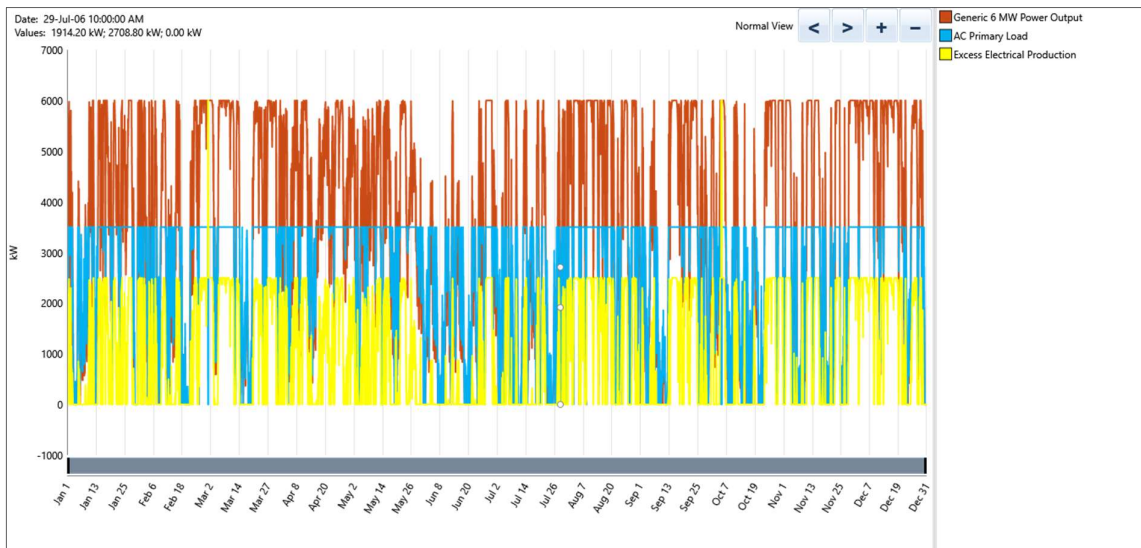


Figure 8.18 Yearly power curves: power output, load and dump load. Case 2

The system annual overview can be observed in Figure 8.18, comparison between the power output, load and dump load are displayed. The wasted energy is 29.1% and the unmet load power is 7.6%, for this wind scenario of 8.66 m/s. Even under this conservative wind profile, the results are satisfactory for the case studied.

Load demand management is a key concept for the realization of this idea. The blue line or the load curve has as maximum demand at its rated value of 3.5MW, as can be observed for this detailed week overview. The wind turbine generation is balanced out by the dump energy in

yellow. It is worth noticing that during some of less windy hours, the load failed to follow up the generation. An alternative for a better follow up strategy can be to execute a predictive method or algorithm that help keeping an improved track between generation and consumption.

9 CONCLUSIONS AND FURTHER WORK

9.1 HYBRID WIS MODEL

The hybrid WIS model consisted of a 25 MW O&G platform connected in parallel to a 6MW wind to a suitable combination of fixed and flexible load. Two study cases were developed. The first case had a fixed load of $P_{fixed} = 19\text{MW}$ and $Q_{fixed} = 4\text{MVAR}$. The second case the load was divided in two parts a fixed $P_{fixed} = 16\text{MW}$ and $P_{dyn} = 3\text{MW}$ the reactive component was not altered. The same wind conditions were applied to both cases. As expected, the dynamic behavior in the second case showed a better performance. First, the wind variations had a minor impact, since the flexible load was managed to increased and decreased according to the wind power available. In other words, despite of the fact that the manageable active load represented only a small fraction of the total (18.75%), it worked as it were a “decoupled” load. This indicates that more wind power can be integrate to the system, as long as there is more potential loads to be controllable. Second, the frequency in the second case experienced less oscillations compared to the first case. The effect is understood given that the load demand was adapted to the energy available. However, this was an ideal case with an instantaneous response in terms of load adaptation. This should not be the case for a real system, due to the time delays. For example, those associated to actuators and mechanical equipment, or time constants related to the water injection processes. Another consideration, was the impact on the gas turbine since there was this “decoupling effect” in the second case, the gas turbine does not experimented changes within the regulating range of the flexible load. When the wind power production was larger than 3MW, the gas turbine started to decrease its power output. This could allow it to have less turn on and off cycles or work in a more efficient operating point.

9.2 STAND-ALONE WIS MODEL

The stand-alone cases were successfully simulated according to the initial premises. The first case consisted of a 6MW wind turbine connected to a load combination of $P_{fixed} = 1\text{MW}$ and $P_{dyn} = 3\text{MW}$, a variable dump load, and finally a 5MW flywheel. For the second case, instead of an ideal flexible load, a $P_{motor} = 2.5\text{MW}$ induction motor controlled by a VSD was implemented for a more realistic approach. The flywheel in both cases acted as an energy balance element, delivering active and reactive power depending on the system requirements,

additionally it was responsible for fixing the voltage and system frequency. Another advantage identified with its implementation was the incorporation of inertia to the system. An inertialess system or virtual inertia as the one modelled in the specialization project could also be a different alternative. However, a modular, off-the-self solution proposed by DNV-GL with a wind turbine, mechanical package (including flywheel) and VSD was taken as reference for development in this project. The first case, obtained good performance results both fixed and flexible loads were fed with 100% renewable energy. As the energy available started to increase the flexible load followed by increasing its demand, keeping the system balance up to its nominal power. On the contrary, less energy available was counteracted by a smaller demand. The excess of energy was taken by the flywheel in form of kinetic energy. The system frequency was affected by the speed increase in the flywheel but it can speed up to a certain limit. Above of this limit, the dump load was activated to drain or burn the excess of energy, when the frequency was restored the dump load was deactivated. The second case followed the same general functioning as the first case. However, the introduction of the VSD controlling the injection motor, introduced another degree of freedom to the system and a higher complexity. A different control loop was required represented by the VSD speed to adjust the power consumption. The conversion of a speed control signal from a power measurement used a nonlinear relation, whose estimation was acceptable within the nominal point. However, out of this range the system started to show unwanted oscillations. An improved method suggested for future work, would include a look up table considering the induction motor curves and mechanical load against speed.

9.3 ENERGY WIS MODEL

Energy studies are important to have a more accurate assessment of wind resources and long-term system evaluation. The wind resources are time and space dependent. An arbitrary location was chosen off the north coast from Trondheim ($65^{\circ}27'35''N$; $01^{\circ}11'26''E$). The system implemented consisted of a generic 6MW wind turbine, a flexible load with an average daily consumption of 63.095MWh/day, average power of 2.6MW and 3.5MW as peak demand. Additionally a lead-acid battery bank of 250kW and a converter same rating was added. The wind input data values was downloaded from NASA Surface meteorology and Solar Energy database. The wind speed was measured at 50m above the earth surface. The measurements are monthly averages values in 10-year period (July 1983- June 1993). The load profile was synthetized. The synthetization technique consisted of estimating the energy production first from the wind turbine. Once the energy profile was deduced, the load was spread along the year

with a generation follow-up strategy. This was possible due to the assumption of load control by means of a variable speed drive connected to the pumps.

In this report, a wind resource assessment was elaborated. The simulations were performed on Homer (Hybrid Optimization of Multiple Energy Resources) Energy software from National Renewable Energy Laboratory (NREL) in the United States. A generic 6MW wind turbine curve was calculated with nominal output for 12-14m/s. Two study cases were developed. The first case consider an annual scaled-average wind speed of 12m/s and the second case is 8.66m/s. The referred wind speeds were annual values. The evaluation included annual wind profile, daily and monthly distribution, and finally a wind speed histograms. Extensive curve elaborations were introduced including: monthly, daily power output, cumulative frequency and power output duration curves. Additionally, an assessment on the electric energy excess was made. Load curves followed same behavior as generation were also introduced.

In summary, the first case revealed an excellent performance satisfying the rated demand 68.8% of the time, with an excess of energy 40.9% and an unmet load of 3.4%. On the other hand, the second case or normal scenario exhibited larger downtimes, the system run during 7734hr/yr. However, the unmet load was 7.9% and the dumped energy amounted to 29.1%. In absolute terms, the energy satisfied in the first case was 22.241GWh/yr. compared to 21.289GWh/yr. implying a difference of 4.28%. Adequate load demand management is key for the studied system and even under low wind scenarios, the target annual energy production is reached within reasonable deviations. For further work, economic studies can be carried out, but investments costs and economic variables are required as inputs and they are usually difficult to have access to due to the project innovative nature.

9.4 FURTHER WORK

This thesis is a preliminary investigation on the use of wind power for water injection systems in O&G facilities. For the hybrid WIS model it is necessary to make further research in two different aspects. First, the amount of wind penetration must be increased, which can be achieved through the connection of multiple wind turbines, in the condition of inflexible and flexible load in order to revise the system response in terms of power and frequency stability for both situations. The system should be capable of admitting more wind power fluctuations if the load is adequately managed. Studies on the impact of the gas turbine related to efficiency, emissions and maintenance for both cases are also interesting to investigate. In addition,

contingency analysis in the occurrence of events like sudden wind power disconnection and short circuit analyses.

For the stand-alone WIS model run 100% in wind power, investigation should be made on a system with not physical inertia. Improved control protocol between the wind power available and the reference speed for the VSD should be defined, in order to avoid undesired torque oscillations. An automatic pitching mechanism limiting the wind power output should be studied and reduce the dimension and influence of the dump load. Furthermore, contingency and short circuit analysis should be carried out to evaluate these dynamic phenomena.

Finally, the energy WIS model must include for future work the economic analysis, which were not executed here. Measurements on potential sites to calculate the power curves, and optimization of sizing of components, since preliminary the system is over dimensioned considering the dumped energy. All three models and simulations should be verified and supported by laboratory experiments.

10 BIBLIOGRAPHY

- [1] D. G. S. research & innovation position paper 2-2015. H. G. T. a H. A. Transmission, “DNV GL Strategic research,” 2015.
- [2] A. Grynning, S. V. Larsen, and I. Skaale, “Tyrihans Raw Seawater Injection,” *Proc. Offshore Technol. Conf.*, no. May, pp. 4–7, 2009.
- [3] E. Gavenas, K. E. Rosendahl, and T. Skjerpen, “CO₂-emissions from Norwegian oil and gas extraction,” no. 806.
- [4] M. Korpås, L. Warland, W. He, and J. O. G. Tande, “A case-study on offshore wind power supply to oil and gas rigs,” *Energy Procedia*, vol. 24, no. 1876, pp. 18–26, 2012.
- [5] E. Øyslebø and M. Korpås, “Electrification of offshore petroleum installations with offshore wind integration,” 2011.
- [6] G. Shi, S. Peng, X. Cai, and Z. Chen, “Grid Integration of Offshore Wind Farms and Offshore Oil / Gas Platforms,” pp. 1301–1305, 2012.
- [7] H. Svendsen and M. Hadiya, “Integration of offshore wind farm with multiple oil and gas platforms,” ... *2011 IEEE Trondheim*, pp. 1–3, 2011.
- [8] A. R. Ardal, K. Sharifabadi, O. Bergvoll, and V. Berge, “Challenges with integration and operation of offshore oil & gas platforms connected to an offshore wind power plant,” *2014 Pet. Chem. Ind. Conf. Eur.*, pp. 1–9, 2014.
- [9] “Hywind Power 2015 status.pdf.” [Online]. Available: <http://www.tu.no/petroleum/2015/11/26/statoil-vil-bruke-hywind-til-a-levere-strom-til-kvitebjorn-og-valemon>. [Accessed: 17-Dec-2015].
- [10] DNV GL, “WIN WIN Technical Assessment Power System,” 2015.
- [11] J. Slätte, D. N. V. Gl, J. Sandberg, T. Flach, G. Dekker, and C. Sixtensson, “OTC 25284-MS Wind-powered Subsea Water Injection Pumping: Technical and Economic Feasibility,” 2014.
- [12] J. Silva, “Islanded wind power solutions for water injection facilities,” 2015.
- [13] EWEA, “Wind European Statistics,” 2015.
- [14] “Foundation Deep Water.” NTNU Specialization Course Wind Power.

- [15] “Statoil.com,” 2016. [Online]. Available: <http://www.statoil.com/en/TechnologyInnovation/NewEnergy/RenewablePowerProduction/Offshore/HywindScotland/Pages/default.aspx?redirectShortUrl=http://www.statoil.com/HywindScotland>. [Accessed: 30-May-2016].
- [16] “Norwea,” 2016. [Online]. Available: <http://www.norwea.no/nyhetsarkiv/visning-nyheter/oil-gas--offshore-wind-joint-industry-project-leads-to-win-win-situation.aspx?PID=1145&Action=1>. [Accessed: 30-May-2016].
- [17] “Petrowiki,” 2016. [Online]. Available: http://petrowiki.org/Gas_lift. [Accessed: 09-May-2016].
- [18] “Rigzone.” [Online]. Available: http://www.rigzone.com/training/insight.asp?insight_id=341&c_id=4. [Accessed: 01-Dec-2015].
- [19] D. Nilsson and A. Westin, “Floating wind power in Norway: Analysis of future opportunities and challenges,” *M.S. thesis, Dept. Ind. Electr. Eng. Autom. Fac. Eng., Lund Univ.*, 2014.
- [20] Offshore Magazine, “2015 worldwide survey of subsea processing: separation, compression and pumping systems.,” 2015.
- [21] K. M. Høvik, “Control of Offshore Passive Platform System Voltage and Frequency through Control of Onshore Back-to-Back Voltage Source Converters,” 2011.
- [22] “Open Electrical.” [Online]. Available: http://www.openelectrical.org/wiki/index.php?title=Single-Phase_Line_Models. [Accessed: 02-Dec-2015].
- [23] P. Kundur, N. J. Balu, and M. G. Lauby, “Power system stability and control.” p. 1202, 1994.
- [24] “Mathworks Documentation Simpower,” 2016. [Online]. Available: <http://se.mathworks.com/products/simpower/>. [Accessed: 16-May-2016].
- [25] V. Perelmuter, *Electrotechnical Systems*. 2012.
- [26] A. R. Årdal, “Feasibility Studies on Integrating Offshore Wind Power with Oil Platforms,” no. June, 2011.
- [27] D. Mehrzad, J. Luque, and M. Capella C, “Institute of Energy Technology Vector Control of Pmsg for Wind Turbine Applications. Aalborg Universitet,” 2008.

- [28] “Regenpowertech,” *Regenpowertech.com*, 2016. [Online]. Available: <http://www.regenpowertech.com/42/technology>. [Accessed: 14-May-2016].
- [29] L. Carlos and G. Vasquez, “Control of a Variable Speed Drive with a Multilevel Inverter for subsea applications,” *Sci. Technol.*, no. June, 2010.
- [30] IEEE Standard 421.5-2005, “{IEEE} Recommended Practice for Excitation System Models for Power System Stability Studies,” *IEEE Power Eng. Soc.*, vol. 2005, no. April, pp. 1–85, 2005.
- [31] “HomerEnergy.” [Online]. Available: <http://homerenergy.com/documents/MicropowerSystemModelingWithHOMER.pdf>. [Accessed: 30-Jan-2016].
- [32] T. Ackermann, *Wind Power in Power Systems* *Wind Power in Power Systems Edited by*, vol. 8. 2005.
- [33] M. O. Malley, “Power Systems Design.” [Online]. Available: <http://www.powersystemsdesign.com/mcu-with-fpu-allows-advanced-motor-control-solutions>. [Accessed: 11-Oct-2015].
- [34] C. Bajracharya and M. Molinas, “Control of VSC-HVDC for wind power,” *Dep. Electr. Power Eng.*, vol. MSs Thesis, no. June, p. 75, 2008.

11 APPENDICES

11.1 Voltage Oriented Control

Vector control is based on the Clarke and Parks transformations that allows time varying quantities to be represented as DC quantities in the dq reference frame and independent control of active and reactive power, which simplifies the control of the converters.

The sequence of mathematical transformations are shown in Figure 11.1 [6], firstly a Clarke transformation on the abc quantities and to the stationary $\alpha\beta$ coordinate system and secondly a Park transformation to a rotating dq reference frame at synchronous speed ω with respect to stationary $\alpha\beta$.

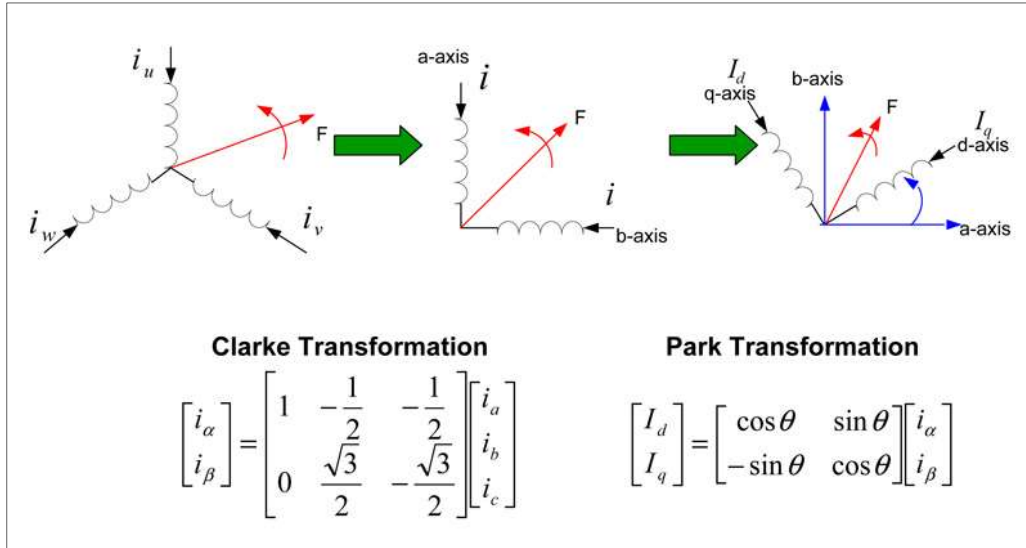


Figure 11.1 Clarke and Park Transformations [33]

A generic Voltage Source Converter is shown in Figure 11.2, consisting of a voltage source, resistor and inductance. Applying the suggested transformation above, the matrix representation in the dq frame is given by [34],

$$\begin{bmatrix} v_d \\ v_q \end{bmatrix} = -L \frac{d}{dt} \begin{bmatrix} i_d \\ i_q \end{bmatrix} - R \begin{bmatrix} i_d \\ i_q \end{bmatrix} - \begin{bmatrix} 0 & -\omega L \\ \omega L & 0 \end{bmatrix} \begin{bmatrix} i_d \\ i_q \end{bmatrix} + \begin{bmatrix} v_{d,conv} \\ v_{q,conv} \end{bmatrix} \quad (11.1)$$

A different relationship can be calculated at the output node in Figure 11.2, applying node current law,

$$I_{dc} = C \cdot \frac{d}{dt} V_{dc} + I_L \quad (11.2)$$

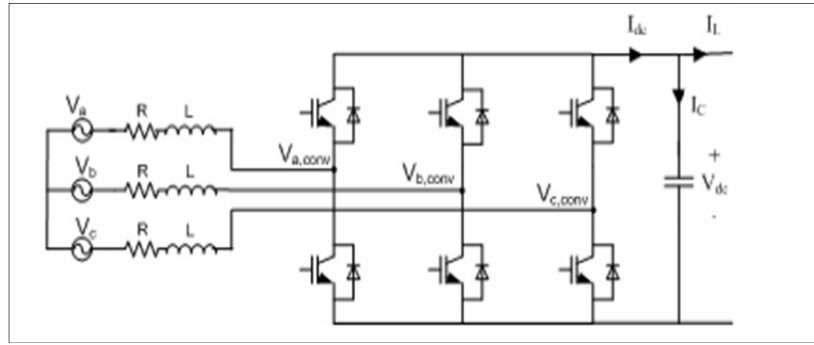


Figure 11.2 Schematic of the general system [34].

At the same time, power balance between the ac and dc quantities can be established as,

$$p = \frac{3}{2}(v_d \cdot i_d + v_q \cdot i_q) = V_{dc} \cdot I_{dc} \quad (11.3)$$

A conventional formulation is to define dq reference along the d -axis, this alignment implies $v_q = 0$. Therefore, active and reactive power are simplified to,

$$p = \frac{3}{2}v_d i_d \quad (11.4)$$

$$q = -\frac{3}{2}v_d i_q$$

The reference angle θ of the rotating d -axis, with respect to the fixed α -axis is extracted by using a phase locked loop (PLL),

$$\theta = \tan^{-1}\left(\frac{v_\beta}{v_\alpha}\right) \quad (11.5)$$

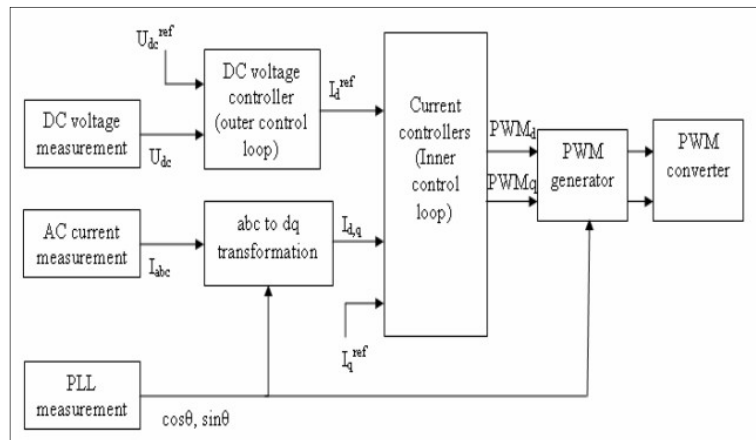


Figure 11.3 Vector control principle [34].

Since the matrix (11.1) has two coupling terms, compensating terms are introduced to eliminate this cross coupling effect. These feed-forward terms allows independent control of active and reactive power. A block diagram of the vector control principle is shown in Figure 11.3 [34]. The block diagram is composed of two cascaded control loops; the first is an outer voltage controller loop and an inner but faster current PI controller.

11.2 Matlab Model Diagram

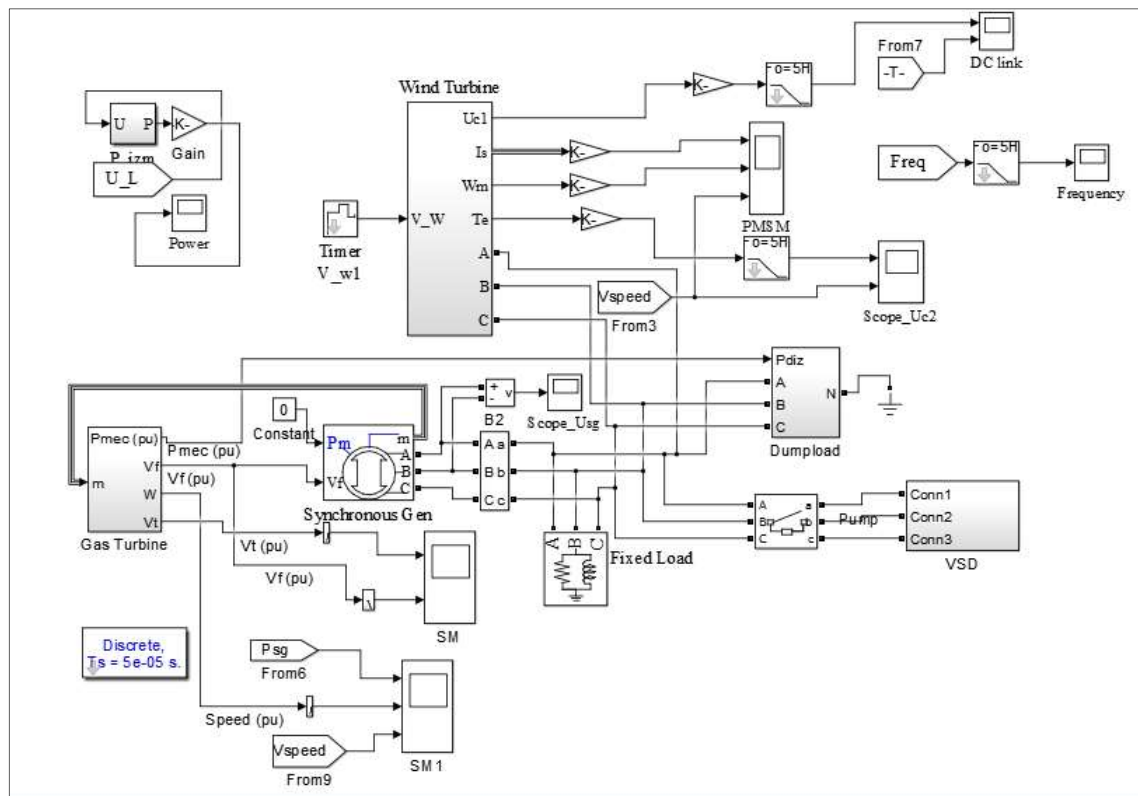


Figure 11.4 Stand Alone Complete Model

11.3 Paper Abstract to be presented in Offshore Energy & Storage Symposium

Malta-July 2016



Topic: Offshore renewable energy generation

Integration of Wind Power to Supply Water Injection Systems in Offshore O&G

University of Science and Technology, Norway

***Jesus Silva**, e-mail: jesuses@stud.ntnu.no

#**Elisabetta Tedeschi**, e-mail: elisabetta.tedeschi@ntnu.no

Introduction

The need of increased sustainability at global level encourages the implementation of greener solutions, especially in the most polluting industrial sectors. The will of reducing CO_2/NO_x emissions from Oil and Gas (O&G) installations, as well as the difficulty of deploying new gas turbines to supply increasing loads due to space and structural constraints on the platforms, makes the idea of integrating wind turbine power to O&G facilities attractive [1][2]. This paper, in particular investigates the possibility of using wind power to supply the platform water-injection systems, similarly to the concept proposed by DNV-GL in the WinWin project [3].

The objective of the water injection system (WIS) is to inject raw salt or processed water in order to pressurize the well and consequently increase the oil recovery rate using the energy produced locally by the wind turbines. The wind turbine works in parallel to the gas turbine and it supplies a generic load, representing a water injection pump. However, there are several challenges associated to wind power integration that might affect the secure and stable operation of the O&G power system: those of main interest in this work are the system dynamics due to the wind intermittency, which causes power and frequency fluctuations to the O&G platforms.

Water injection motors can play an active role in counteracting the wind intermittency and help maintaining the system energy balance. This type of motors are equipped with variable speed

drives, which are flexible units adjustable to different operating points or injection rates, and consequently adaptable to multiple demand levels. The idea proposed here exploits the load flexibility of the WIS to sustain a stable and efficient system operation, ensuring the minimum impact possible to the existing system and actuating mainly on controllable loads.

Methodology:

The presented test cases are developed in MATLAB Simulink environment, with use of the SimPowerSystem tool. A standard O&G platform that consists of a gas turbine driving a synchronous machine supplies power to typical a water injection motor and an accumulated PQ load, additionally an AC submarine cable connection is made through to a wind turbine as seen in Figure 1. Advantages and disadvantages of the different control solutions implemented for the selected application will be evaluated and discussed in the paper.

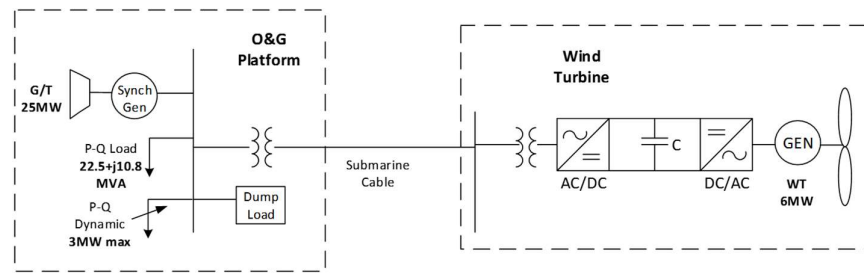


Fig. 1 WT and O&G integrated system

Preliminary results:

The load flexibility on a generic platform installation is investigated as a counteracting strategy to the intermittent nature of the wind, easing the integration of wind power to the platform. The water injection system operation does not require a fixed injection rate, thus in this configuration it is considered a fully elastic load and that it can be managed according to the wind generation available. Therefore, the demand can follow the generation. As seen from the preliminary simulation results shown in Figure 2, the energy produced by the wind turbine P_{wind} , is absorbed by the water injection pump, $P_{dynamic}$, until it reaches its maximum value of 3MW at 4s. The second graph represents the fixed or priority load of the O&G platform, P_{fixed} . The excess of energy from P_{wind} is counteracted by the adequate control of the gas turbine P_{sg} , which reduces its power output to balance out the energy in the system.

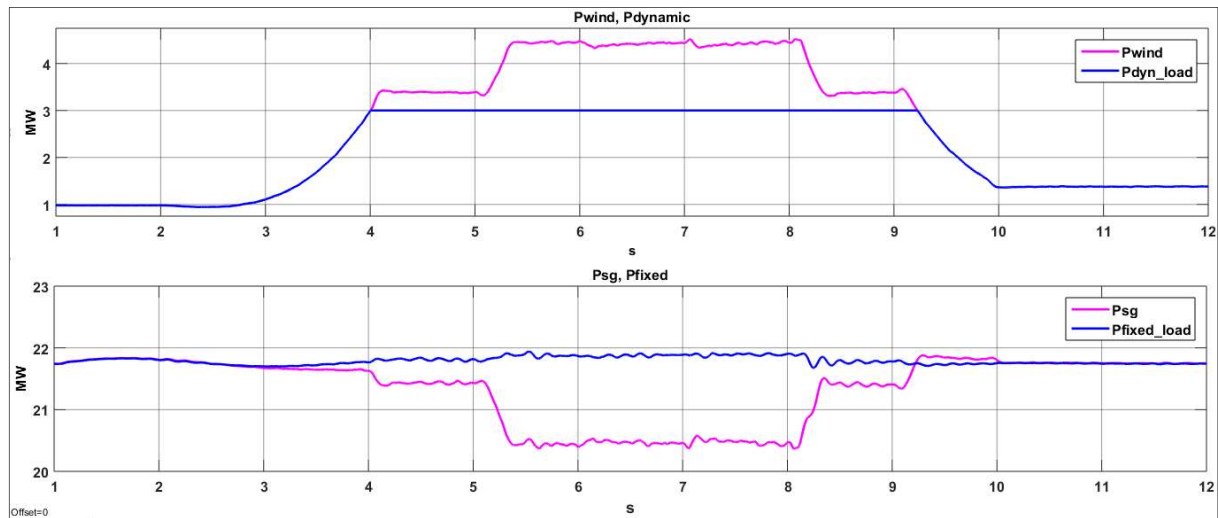


Figure 2 O&G, WT and load power curves.

Summary of the work

Offshore O&G facilities are facing increased energy demands in order to keep production levels and at the same time avoid pollution from gas. The potential use of wind turbines to power O&G platforms thanks to development of large turbine technology and floating structures is driving the interests of the sector to integrate them with conventional gas generation units. In general, the existence of large motors equipped with variable speed drives with flexible loads, as is the case for water injection systems, can help to meet some challenges, related to wind intermittency and frequency stability. Additionally, non-essential load control strategies and load segregation can be implemented to reduce the effect of wind power fluctuations, and help maintaining optimal gas turbine loading for improved efficiency. The basic assumption is that the WIS follows the generation available from the wind turbines, which is valid for this kind of systems that do not require fixed injection rate. This work will investigate the system dynamics in the event of power fluctuations, when integrating wind power to O&G platforms and how an adequate load control can smooth out these variations.

References

- [1] H. Svendsen and M. Hadiya, "Integration of offshore wind farm with multiple oil and gas platforms," 2011 IEEE Trondheim, pp. 1–3, 2011.
- [2] A. R. Årdal, "Feasibility Studies on Integrating Offshore Wind Power with Oil Platforms," no. June, 2011.
- [3] D. G. S. research & innovation position paper 2-2015. H. G. T. a H. A. Transmission, "DNV GL Strategic research," 2015.